Thor Offshore Wind Farm

Metocean Hindcast Data and Validation Report

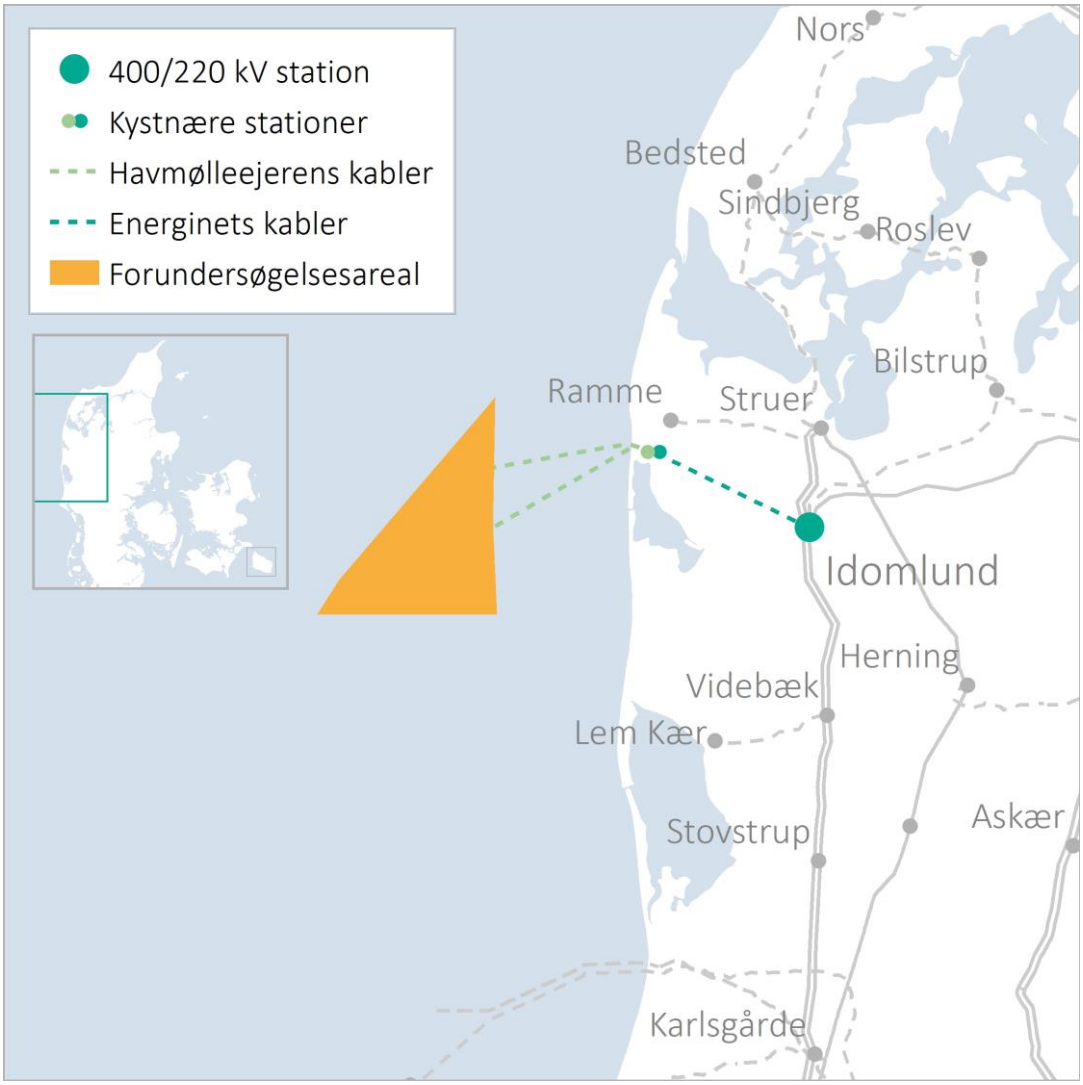

Energinet.dk

ENERGINET

Report

November 2020

This report has been prepared under the DHI Business Management System certified by Bureau Veritas to comply with ISO 9001 (Quality Management)

Thor Offshore Wind Farm

Metocean Hindcast Data and Validation Report

Prepared for Energinet.dk

Represented by Jan Havsager

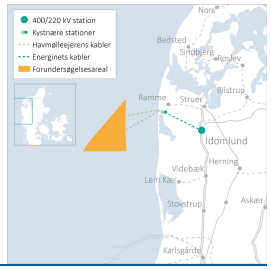

Frontpage illustration: Thor Offshore Wind Farm

Project manager	Jacob Berg Jørgensen
Quality supervisor	Maziar Golestani

Project number	11824164
Approval date	19-11-2020
Revision	Final 2.0
Classification	**Public**

DHI A/S • Agern Allé 5 • • DK-2970 Hørsholm • Denmark
Telephone: +45 4516 9200 • Telefax: +45 4516 9292 • dhi@dhigroup.com • www.dhigroup.com
Company Reg. No.: 3646681

CONTENTS

FIGURES

TABLES

APPENDICES

Nomenclature

Abbreviations	
CFSR	Climate Forecast System Reanalysis model
CREA6	Cosmo Reanalysis data
CDF	Cumulative distribution function
DEA	Danish Energy Agency (DK: Energistyrelsen)
DVR90	Vertical coordinate reference system used in Denmark (Dansk Vertikal Reference 1990)
EVA	Extreme Value Analysis
HAT	Highest Astronomical Tide
HRL	Highest Residual Level
HSWL	High Still Water Level
HWL	High Water Level
JPA	Joint Probability Analysis
LAT	Lowest Astronomical Tide
LRL	Lowest Residual Level
LSWL	Low Still Water Level
LWL	Low Water Level
mAGL	Meters Above Ground Level
MHHW	Mean Higher High Water
MHW	Mean High Water
MHWS	Mean High Water Spring
MHWN	Mean High Water Neap
MLLW	Mean Lower Low Water
MLW	Mean Low Water
MLWN	Mean Low Water Neap
MLWS	Mean Low Water Spring
mMSL	Meters above Mean Sea Level
MWD	Mean Wave Direction
MSL	Mean Sea Level
MSLP	Mean Sea Level Pressure
NCAR	National Center of Atmospheric Research
NCEP	National Centers for Environmental Prediction
OWF	Offshore Wind Farm
PDF	Probability density function
PWD	Peak Wave Direction
STD	Standard deviation
SWL	Still Water Level
Tr	Return Period
WL	Water Level

Symbols	
Latin characters	
A	Weibull scale parameter for wind speed
c	Wave celerity
C	Wave crest elevation
CD	Current direction
CS	Current speed. Depth-averaged, if not otherwise noted
C_{max}	Maximum wave crest elevation
d	Water depth
H	Individual wave height
H_{m0}	Significant wave height (spectral based)
H_{max}	Maximum wave height
k	Weibull shape parameter for wind speed
N	Number (of discrete value, number of waves, etc.)
S_U/σ_U^2	Spectrum of wind speed normalised by variance of wind speed
T	Individual wave period (no doppler shift included due to currents)
T_a	Averaging time with a central moving average window
T_{01}	Mean wave period (spectral based)
T_{02}	Zero-crossing wave period (spectral based)
T_p	Peak wave period
T_z	Zero-up crossing wave period (time domain based)
WS	Wind speed
WD	Wind direction
WS_{10}	Wind speed at 10 metres above MSL
WS_{100}	Wind speed at 100 metres above MSL
WD_{10}	Wind direction at 10 metres above MSL
WD_{100}	Wind direction at 100 metres above MSL
Z_ψ	Crest elevation from stream function theory
Greek characters	
γ	Threshold
λ	Rate (events/year)
η	Surface elevation
θ	Direction (°N)

Subscripts	
CFSR	Climate Forecast System Reanalysis model
HD	Hydrodynamic model
P	Peak value
Sea or W	Wind-sea partition of a sea state
SW	Spectral Wave model
Swell or S	Swell partition of a sea state
Z	Vertical coordinate

Definitions	
Time	Times are relative to UTC
Level/Height/Elevation	Level is used in water levels, height is used in wave height, and elevation in crest elevation. Levels/Heights/Elevations are relative to MSL (if not specified otherwise). It is assumed in this report that 0 mMSL=0 mDVR90.
Coordinate system	Long/Lat WGS84 (if not specified otherwise)
Direction	Direction Wind: °N coming from Current: °N going to Waves: °N coming from
Time averaging	All time averages are based on a central window averaging, for example 3 hours in the case of time series from Spectral wave model.

Executive Summary

This report constitutes the Metocean Hindcast Data and Validation Report for the Thor Offshore Wind Farm (OWF) project as required by Energinet, Denmark.

The metocean conditions are based on state-of-the-art numerical hydrodynamic and spectral wave models established previously by DHI and known as the DHI Danish Waters Model.

The hindcast covers 24 years (1995-2018 inclusive) of hourly sampled data. It has been forced with wind/pressure field data from the COSMO-REA6 (CREA6) dataset developed by the Hans-Ertel-Centre of the Deutscher Wetterdienst (German meteorological Office) and the University of Bonn in Germany[1]. Validations of the model results were conducted against various measurements adjacent to Thor OWF and are presented in this report. The validations showed very good model performance.

Three analysis points P1, P2, and P3 have been chosen in agreement with Energinet within the designated Thor OWF project area (Section 1).

Both normal and extreme conditions are presented as omnidirectional statistics, i.e. independent of mean wave direction and/or peak wave direction, at the three analysis locations. A summary of the extreme value results is given in Table 0.1, Table 0.2 and Table 0.3 for points P1, P2 and P3, respectively.

Table 0.1 Extreme values for return periods of 1, 50 and 100 years at P1 for significant wave height (H_{m0}), associated periods (T_p) and (T_{02}) in the 5%-95% percentile range, maximum wave height (H_{max}) and maximum crest elevation (C_{max}) for Forristal and stream function theory. *Extreme values of depth-averaged current speed (CS) and water level (WL) are unrestricted and not associated with an extreme value of significant wave height. The estimates are based on 24 years of data.

P1	1 year	50 year	100 year
H_{m0} [m]	7.1	9.7	10.1
Associated T_p [s]	11.7-14.4	13.8-16.5	14.1-16.8
Associated T_{02} [s]	8-5-9.7	10.0-11.1	10.2-11.4
H_{max} [m]	12.8	18.3	19.2
C_{max} (Forristall) [mMSL]	9.2	13.8	14.6
C_{max} (stream function) [mMSL]	-	15.1	16.1
CS* [m/s]	0.7	0.9	1.0
WL* [mMSL]	1.4	2.0	2.1

[1] https://reanalysis.meteo.uni-bonn.de/?Download_Data___COSMO-REA6

Table 0.2 Extreme values for return periods of 1, 50 and 100 years at P2 for significant wave height (H_{m0}), associated periods (T_p) and (T_{02}) in the 5%-95% percentile range, maximum wave height (H_{max}) and maximum crest elevation (C_{max}) for Forristal and stream function theory. *Extreme values of depth-averaged current speed (CS) and water level (WL) are unrestricted and not associated with an extreme value of significant wave height. The estimates are based on 24 years of data.

P2	1 year	50 year	100 year
H_{m0} [m]	6.8	9.2	9.6
Associated T_p [s]	11.9-14.3	14.2-16.4	14.5-16.7
Associated T_{02} [s]	8.5-9.4	10.1-10.8	10.3-11.0
H_{max} [m]	12.2	17.4	18.2
C_{max} (Forristall) [mMSL]	8.9	13.3	14.0
C_{max} (stream function) [mMSL]	-	14.5	15.4
CS* [m/s]	0.7	0.9	1.0
WL* [mMSL]	1.5	2.1	2.2

Table 0.3 Extreme values for return periods of 1, 50 and 100 years at P3 for significant wave height (H_{m0}), associated periods (T_p) and (T_{02}) in the 5%-95% percentile range, maximum wave height (H_{max}) and maximum crest elevation (C_{max}) for Forristal and stream function theory. *Extreme values of depth-averaged current speed (CS) and water level (WL) are unrestricted and not associated with an extreme value of significant wave height. The estimates are based on 24 years of data.

P3	1 year	50 year	100 year
H_{m0} [m]	6.5	8.8	9.1
Associated T_p [s]	11.3-14.0	13.2-16.0	13.5-16.3
Associated T_{02} [s]	8.1-9.3	9.4-10.6	9.6-10.8
H_{max} [m]	11.7	16.5	17.2
C_{max} (Forristall) [mMSL]	8.7	12.8	13.5
C_{max} (stream function) [mMSL]	-	13.9	14.7
CS* [m/s]	0.7	0.9	1.0
WL* [mMSL]	1.6	2.2	2.3

1 Introduction

In this report, DHI has delivered the analyses and validation of metocean hindcast data for the Thor Offshore Wind Farm (OWF) for **Energinet,** who is in charge of delivering metocean data for the 440 km^2 project area appointed by the Danish Energy Agency (DEA). The area is shown in Figure 1.1. The specific content of this report follows the proposal delivered by DHI on 2020-04-20 and accepted by Energinet.

The Thor OWF is planned to have a capacity of minimum 800 MW and maximum 1000 MW and to be in full operation no later than ultimo 2027. The offshore wind farm will be established in the North Sea, west of Nissum Fjord, min. 20 km from shore and will be named “Thor” after the name of the town “Thorsminde [2].

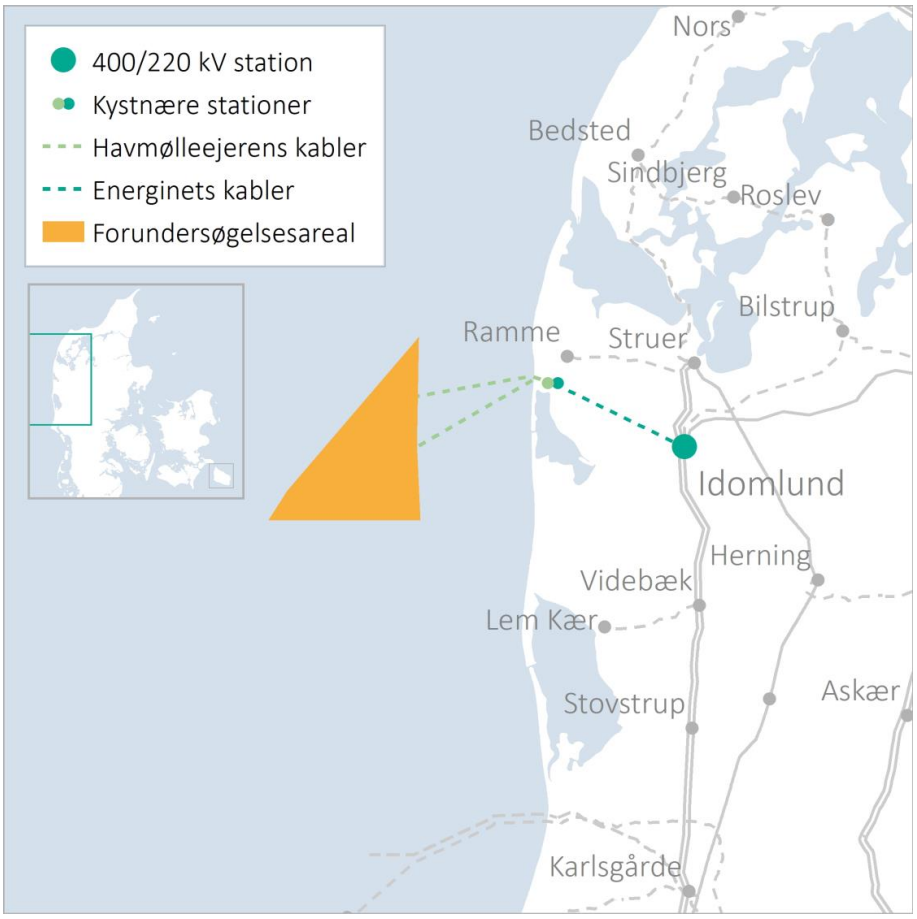

Figure 1.1 Thor OWF project area “forundersøgelsesareal” in orange. The figure is from https://en.energinet.dk/Infrastructure-Projects/Projektliste/Thor-Offshore-Wind-Farm

Three analysis points (P1, P2 and P3) inside the project area have been chosen in an agreement between Energinet and DHI for time series delivery and analyses (this report). Furthermore, a point for Directional Wave Spectrum (DWS) time series delivery has also been chosen. The three points P1, P2 and P3, together with DWS are shown in Figure 1.1. The associated coordinates and water depths are provided in Table 1.1.

[2] https://en.energinet.dk/Infrastructure-Projects/Projektliste/Thor-Offshore-Wind-Farm

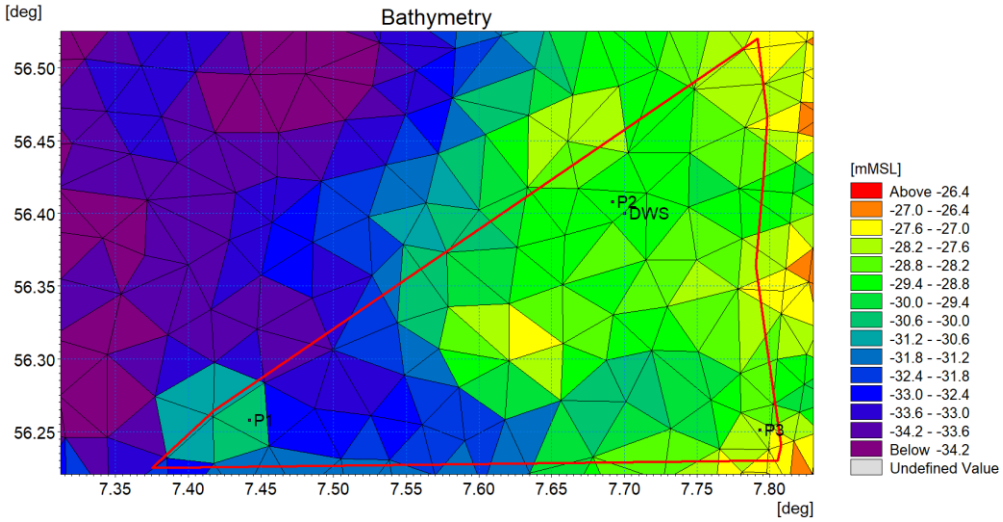

Figure 1.2 Thor OWF project area (shown in red polygon) and DHI Danish Waters Model mesh and bathymetry (mMSL). Locations of analysis points P1, P2 and P3 and the point for directional wave spectrum (DWS) are shown.

Table 1.1 Geographical location and water depth of analysis points, P1, P2 and P3, and point, DWS, for extraction of Directional Wave Spectrum.

Name	Latitude [°E]	Longitude [°N]	Depth [mMSL] Taken from the wave model
P1	7.442	56.258	30.56
P2	7.692	56.408	29.17
P3	7.793	56.251	27.84
DWS	7.700	56.400	28.90

2 Data Basis

In this section the bathymetry data, wind reanalysis data together with measurement data used for validation, are listed and presented. Only measurement data from locations of relative proximity to the Thor OWF are included. A comprehensive list of all data used in setup, calibration and validation of the DHI Danish Waters Model can be found in Section 2.2 of [1]. Locations of stations used for validation in the present report are presented in Figure 2.1.

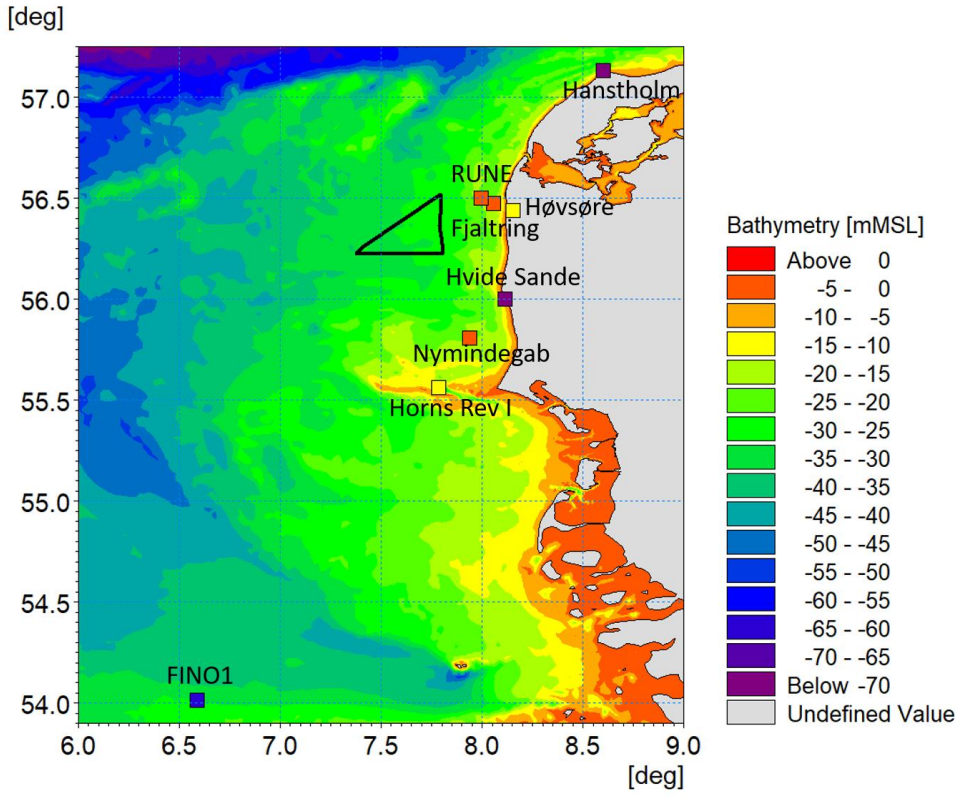

Figure 2.1 Station locations (with bathymetry – based on DHI's Danish Waters Model) used for validation in the present report.
Purple coloured markings represent stations (Hanstholm and Hvide Sande) used for Water levels only; red coloured markings represent stations (Rune, Fjaltring and Nymindegab) used for waves only; yellow coloured markings represent stations (Horns Rev 1, and Høvsøre) used for wind only, while; blue coloured markings represent stations (FINO1) used for both water level, waves and wind. Thor OWF area is represented in the plot by the polygon .

2.1 Bathymetry and vertical datum

This section describes the bathymetry data sources applied to establish a comprehensive and detailed bathymetry for the hydrodynamic (HD) and the spectral wave (SW) models of DHI's Danish Waters Model [1]. The modelled domain extends from 5°E to 16.5°E in longitude, and from 52.3°N to 59.8°N in latitude, covering Denmark as shown in Figure 2.2. The applied bathymetric data is summarised in Table 2.1. Please refer to Section 2.1 in [1] for more information.

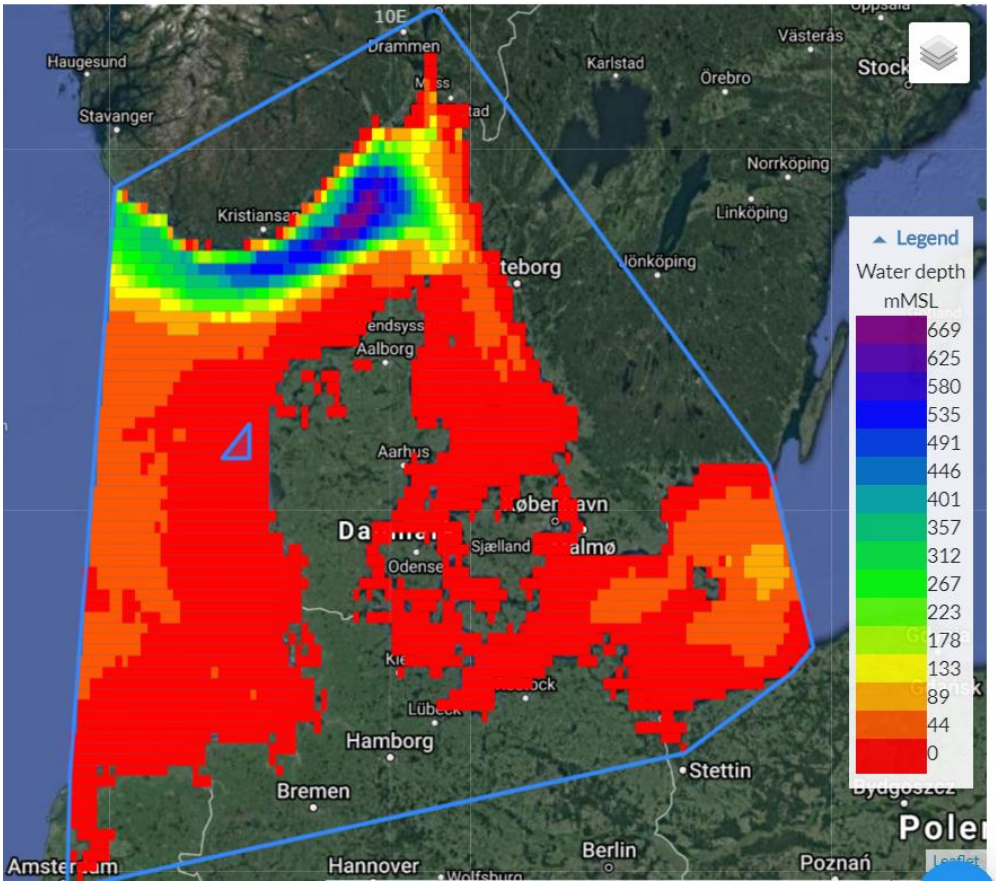

Figure 2.2 Domain of DHI Danish Waters Model with bathymetry. Thor OWF is shown as a blue polygon. Picture from https://www.metocean-on-demand.com

Table 2.1 Bathymetry datasets used in DHI Danish Waters Model. Please see Section 2.1 in [1] for more information.

Priority	Area	Data provider	Resolution [m]	Vertical reference
1	Anholt & Inner Danish Waters	DHI GRAS (satellite)	10	DRV90
2	Limfjorden	DHI	300-900	MSL
3	Remaining areas	EMOD [2]	500	LAT

The overall bathymetry was obtained from the European Marine Observation and Data Network (EMODnet) of 2018 [2][3], which generated a Digital Terrain Model (DTM) for the European Sea regions based on bathymetric survey datasets, composite DTMs and Satellite Derived Bathymetry (SDB) products. The data is provided, processed and quality-controlled at a grid resolution of 1/16 x 1/16 arc minutes (~115m x ~115m). The area surrounding the Thor OWF used data originating from the Danish Geodata Agency[4] and has a resolution of 500m. The main part of data used here was taken from the

[3] https://www.emodnet.eu/bathymetry

[4] https://eng.gst.dk/danish-hydrographic-office/

bathymetric data in LAT reference was converted to MSL by subtracting the difference between MSL and LAT (adopted from a regional model simulation by DHI) from the data.

2.2 Wind measurements

Wind measurement data used for validation of COSMO-REA6 (CREA6) wind reanalysis data (see Section 2.5 for information on CREA6 wind data) are listed in Table 2.2. Data is provided at several elevations from 10mMSL to 200mMSL. But only time series at 10mMSL and 100mMSL are delivered in with this report (see Section 4). However, the elevation closest to the measurement device was used for validation purposes, as presented in Section 2.5.

Table 2.2 Wind measurements used for validation of CREA6 data (see Section 2.5). Locations are shown in Figure 2.1.

Station	Latitude (°N)	Longitude (°E)	Elevation	Period	Provider
FINO1	54.014	6.588	102.0 (mMSL)	2004-01-01 - 2011-01-01	BSH[5]
Horns Rev 1 M2	55.562	7.786	62.0 (mMSL)	1999-05-14 - 2002-08-28	Vattenfall
Høvsøre	56.441	8.151	100.0 (mAGL, on land)	2004-05-31 - 2019-05-31	DTU[6]

2.3 Water level measurements

Water level measurement data used for the validation of Danish Waters Hydrodynamic (HD) Model (Section 3.1) are listed in Table 2.3. A comprehensive list of all data used in the setup, calibration and validation of the DHI Danish Waters HD Model can be found in [1].

Table 2.3 Water level measurements used for validation of Danish Waters HD Model (Section 3.1). Locations are shown in Figure 2.1.

Station	Latitude (°N)	Longitude (°E)	Water Depth (mMSL)	HD model Water Depth (mMSL)	Period	Provider
FINO1	54.014	6.588	30.0	30.8	2004-02-16 to 2006-12-27	BSH
Hanstholm	57.130	8.600	9.2	6.9	2004-12-15 to 2006-03-01	DMI[7]
Hvide Sande	55.999	8.114	6.3	2.3	1995-01-01 to 2008-07-09	KDI

[5] Bundesamt für Seeschifffahrt und Hydrographie https://www.fino1.de/en/news-data/live-data.html

[6] https://www.vindenergi.dtu.dk/test-centers/hoevsoere_dk

[7] Danish Meteorological Institute

2.4 Wave measurements

Wave measurement data used for validation of Danish Waters Model (Section 3.2) are listed in Table 2.4. The RUNE measurement campaign is documented in [3]. A comprehensive list of all data used in setup, calibration and validation of the DHI Danish Waters Spectral Wave Model can be found in [1].

Table 2.4 Wave measurements used for validation of the Danish Waters SW Model (Section 3). Locations are shown in Figure 2.1.

Station	Latitude (°N)	Longitude (°E)	Water depth (mMSL)	SW model Water Depth (mMSL)	Period	Provider
FINO1	54.014	6.588	30.0	30.8	2011-01-01 to 2012-01-01	BSH
Fjaltring	56.474	8.057	17.5	17.1	1995-01-01 to 2013-05-08	KDI[8]
Nymindegab	55.809	7.939	20.0	20.7	1997-12-26 to 2013-05-08	KDI
RUNE	56.500	7.997	16.5	19.4	2015-11-04 to 2016-01-11	DHI

2.5 COSMO-REA6 reanalysis data

The DHI Danish Waters Model is forced with wind from the atmospheric model data set COSMO-REA6[9] (herein referred to as CREA6). It is a high-resolution reanalysis developed by the Hans-Ertel-Centre of the Deutscher Wetterdienst (German meteorological Office) and the University of Bonn in Germany. The atmospheric parameters of this reanalysis are provided over a high resolution of 0.055° (6km) grid and include the assimilation of observational data. The dataset is continuously extended since 1995 and is freely available. Data are hourly sampled.

Other reanalysis data sets were considered from forcing the Danish Waters model. One of these was the Climate Forecast System Reanalysis dataset (CFSR) by the National Centers for Environmental Prediction (NCEP) / National Center of Atmospheric Research (NCAR)[10]. In Figure 2.3 an example is given of the performance of CFSR vs CREA6: time series at 10mMSL in Hanstholm is compared to observations. In general, CFSR underestimates the wind speed while CREA6, in general, matches the observations much better. One of the main reasons for this is the wind model resolution, which is much coarser in CFSR, namely 0.3° (approx. 30km - compared to COSMO which is 6km). Other comparisons also indicate (for example [4]) that the CREA6 dataset is superior to CFSR in the Danish Waters. CFSR was renamed to CFSv2 from 2011 and onwards. Also, the spatial resolution was increased to 0.2° and a general update in data assimilation techniques was applied. For simplicity the name CFSR is, however, used in this report for data from both before and after 2011.

[8] Kystdirektoratet, Denmark

[9] https://reanalysis.meteo.uni-bonn.de/?COSMO-REA6

[10] https://climatedataguide.ucar.edu/climate-data/climate-forecast-system-reanalysis-cfsr

Based on the above it was decided to base the Danish Waters Model on CREA6. The time series comparison plot of wind speed between CREA6 and measurements from Hanstholm provided in Figure 2.3 highlights this trend.

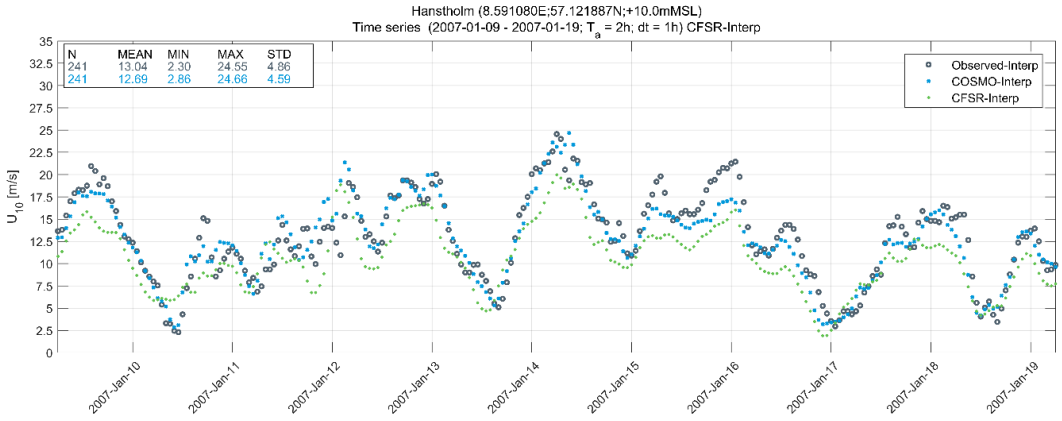

Figure 2.3 Time series of wind speed at 10m at Hanstholm between Observations (black), CREA6 (blue) and CFSR (green). Approximately 10 days of data is used in the plot.

2.5.1 Comparison at FINO1

CREA6 modelled wind speed at 100mMSL at the FINO1 location is compared to measurements at 102mMSL as shown in Figure 2.4. The height difference of 2m is assumed to be negligible and is therefore not corrected. Measurements are corrected for mast flow distortion. Scatter is relatively low with a Scatter index equal to 0.14 (see Appendix A for definitions of the statistical quantities used in the scatter plots). A low bias of 0.16m/s comes mainly from deviations at high wind speeds. Correlation is very high at 0.95. A slight overestimation of the highest wind speed (by CREA6 model) is observed with a Peak Ratio PR=1.09 (ratio of the annual two largest wind speeds in the ~7-year period).

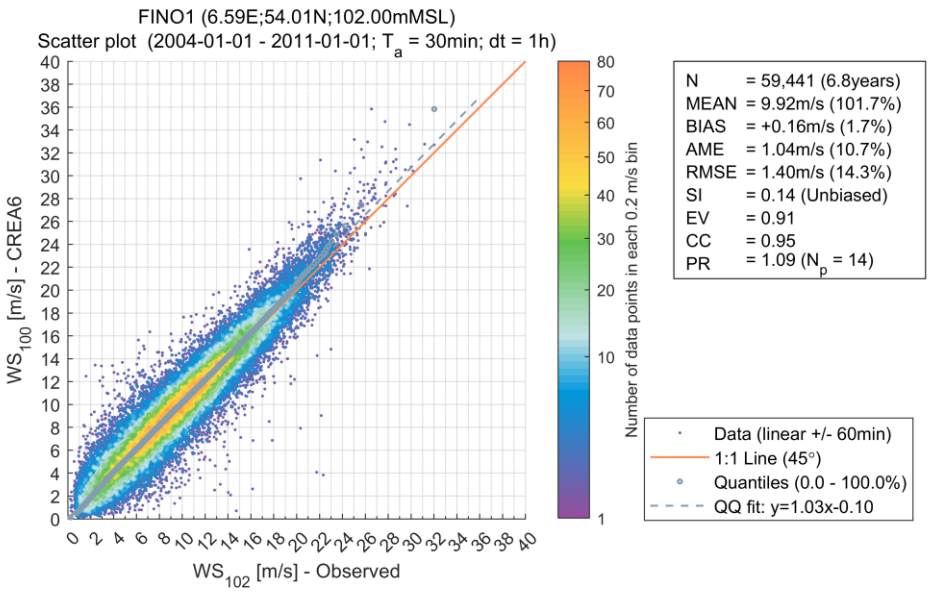

Figure 2.4 Wind speed at FINO1. CREA6 wind speed at 100mMSL against observations at 102mMSL. Approximately 7 years of data are used in the plot.

The measurements have been averaged with a central moving average filter over 30-minutes before comparison with the CREA6 data. This is much shorter than the two-hour averaging window that is normally considered when using CFSR data – see previously reported numbers in Section 3.3.1.2 in [5]. CREA6 data has a much higher spatial resolution compared to CFSR, and hence, the time scales which can be resolved will be somewhat shorter. As an example, it takes 10 minutes for an air parcel to pass through a grid cell of 6km assuming a mean wind speed of 10m/s. The time scales resolved in the numerical model behind the reanalysis data are therefore affected by the spatial resolution of the numerical model, and hence the delivered CREA6 data with a sampling time of one hour (See Section 4) represent wind speed implicitly averaged over some time T_a.

In Figure 2.5 the normalised spectrum of wind speed from CREA6 is compared with spectra of measured data at FINO1 at 102mMSL averaged over 10-minutes, 30-minutes, 1-hour and 2 hours, respectively. Although some aliasing is observed for the highest frequencies in the spectrum of CREA6 wind speed, the spectrum follows the 10-minutes and 30-minutes lines most closely, and 30-minutes is therefore chosen as the representative averaging time when comparing CREA6 wind data with measurements, i.e. T_a=30 minutes.

For normal wind conditions the specific averaging time (from 10-min to 2-hours) is not crucial [6] though for extreme conditions it matters, lowering the extremes for increased averaging time. There were no differences observed in the Peak Ratio between using 30-min and 1-h averaging filter.

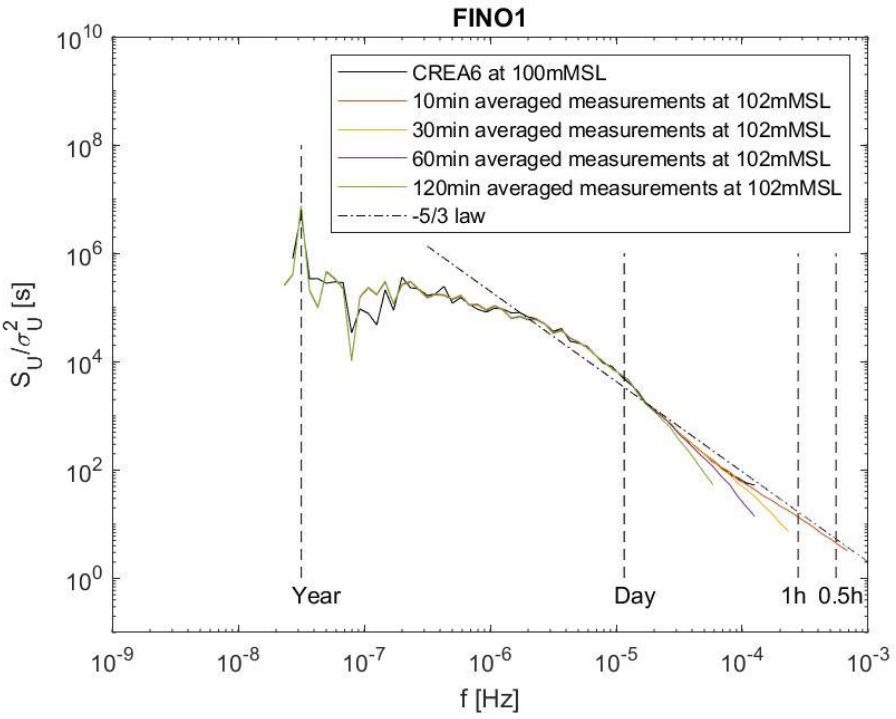

Figure 2.5 Normalised spectrum (S_U/σ_U^2) of wind speed at FINO1 as function of frequency. CREA6 at 100mMSL data are a solid black line and coloured lines represent measurements at 102mMSL averaged over 10-min, 30-min, 60-min and 120-min, respectively. A dimensional Kolmogorov spectrum '-5/3', is illustrated by the non-vertical dashed-dotted line.

2.5.2 Comparison at Horns Rev 1

In Figure 2.6, CREA6 wind speed at 60mMSL is compared to measurements at 62mMSL at the meteorological mast M2 at Horns Rev 1 OWF. A very small bias of -0.06m/s is observed. A small positive value is expected due to the slightly different heights being compared and hence on average higher measured wind speeds. The scatter index is very low (0.17), and the correlation is high (0.94). For wind speeds above 16m/s, positive bias (CREA6 wind speeds larger than measurements) is observed. This is also reflected in the peak ratio value which equals 1.10. The same features were also observed at FINO1 in Figure 2.4. This indicates that slightly conservative extreme wind speeds might be expected when performing extreme values analysis using CREA6 reanalysis data at sites in the western parts of the Danish coasts in the North Sea. Similar to the comparison with FINO1, wind speed measurements have been filtered with a central 30-min running mean.

Scatter comparison of wind directions between CREA6 and measurements at M2 is shown in Figure 2.7. The wind direction is measured at 60mMSL and CREA6 wind direction is also from 60mMSL. Results show that CREA6 compares well with the measurements.

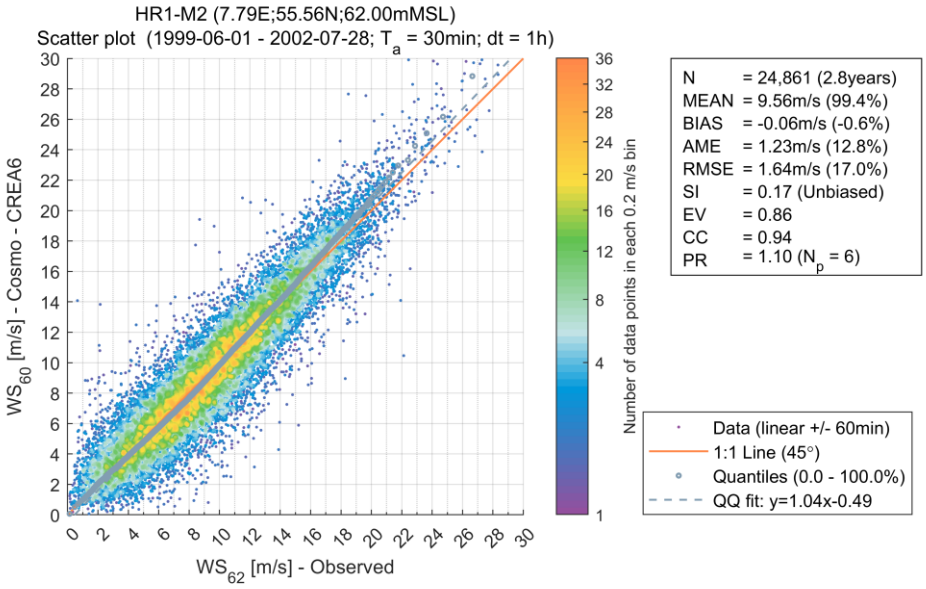

Figure 2.6 Scatter comparison of wind speeds between 60mMSL CREA6 model and 62mMSL measurements at Horns Rev 1 M2. The comparison covers almost 3 years of data.

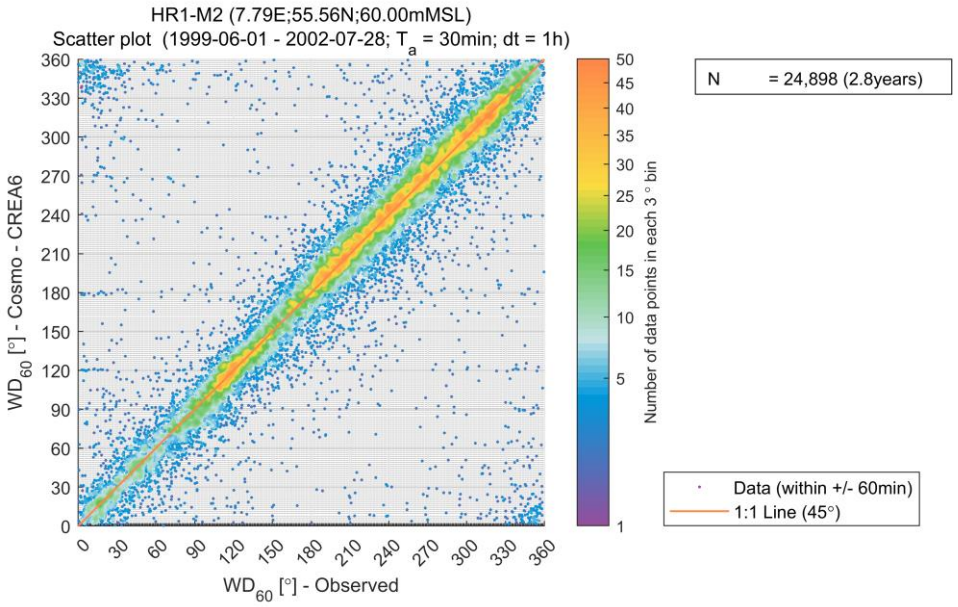

Figure 2.7 Scatter comparison of wind directions at 60mMSL between CREA6 model and measurements at Horns Rev 1 M2. The comparison covers almost 3 years of data.

2.5.3 Comparison at Høvsøre

The Høvsøre meteorological mast is the closest measurement station to Thor OWF (see Figure 2.1). It is, therefore, an important indicator of whether CREA6 can successfully represent the wind conditions at Thor OWF. The mast is located 2 km inland which means that internal boundary layers developing when the wind is westerly [7] are poorly resolved in CREA6 due to its 6km resolution and hence the poor representation of the local coastline. Scatter comparisons of wind speed are therefore divided into Easterlies (wind direction from 15-165°) and Westerlies (wind direction from 195-345°) sectors.

For Easterlies, the upstream conditions are close to homogeneous and hence ideal for successful representation of reanalysis data like CREA6, which cannot resolve local microscale effects. The scatter comparison of wind speed for Easterlies are shown in Figure 2.8. There is a very low bias throughout the full wind speed range, low scatter index, low root-mean-square-error (RMSE) and the high correlation indicate that CREA6 is fully capable of representing the local wind conditions at Høvsøre when the wind is from the east. However, PR=1.03 indicates that also at this site, CREA6 overestimates the highest wind speeds (in this case the nine largest annual maxima). A scatter comparison plot of wind direction is shown in Figure 2.9, and again, a good comparison is obtained (with slightly more scatter).

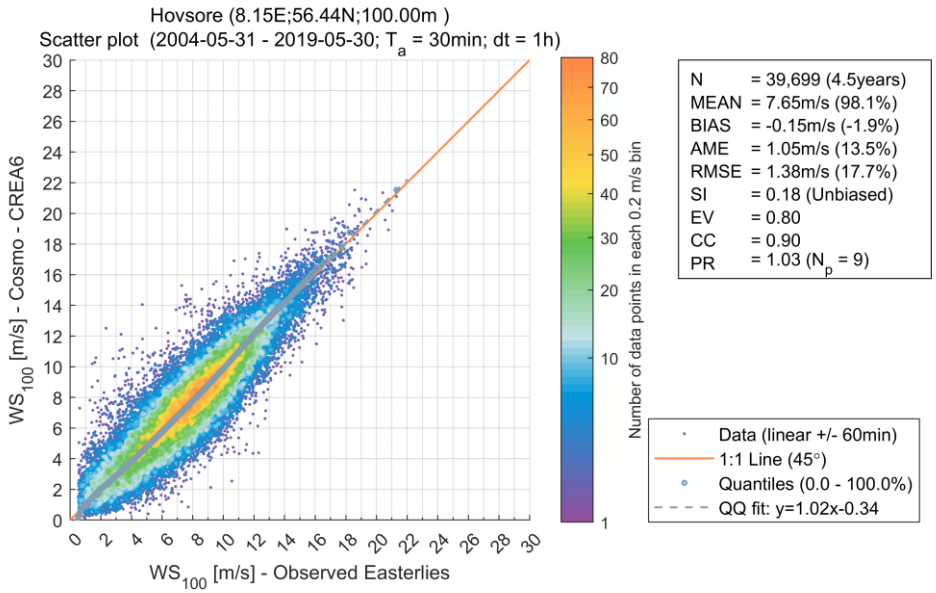

Figure 2.8 Scatter comparison of easterly wind speed between 100m CREA6 model and 100m measurements at Høvsøre. The comparison covers 15 years of data.

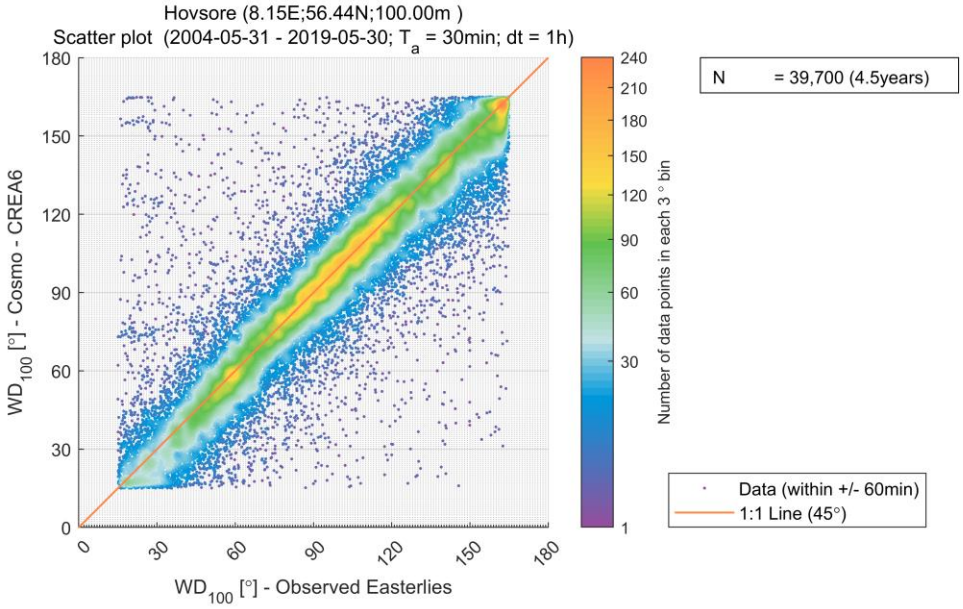

Figure 2.9 Scatter comparison of easterly of wind direction between 100m CREA6 model and 100m measurements at Høvsøre. The comparison covers 15 years of data.

Scatter comparison of westerly winds is shown in Figure 2.10. Scatter index and RMSE are low and the correlation is very high. However, a closer inspection (not shown) reveals that the bias is somewhat dependent on wind speed in contrast to Easterlies. This observation is in line with the existence of internal boundary layers which develop differently in different wind climates.

A scatter plot of wind direction is shown in Figure 2.11, and also here good comparisons are obtained.

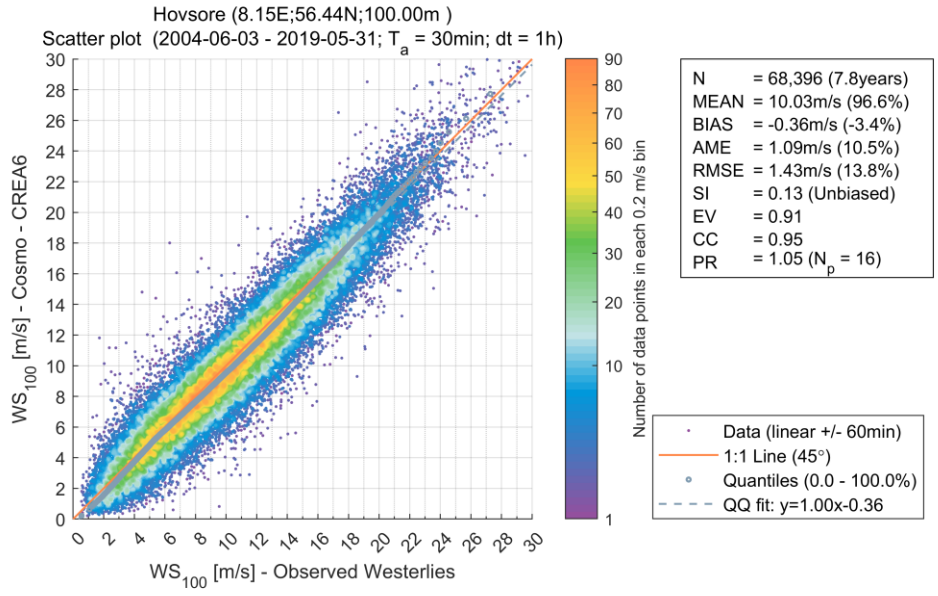

Figure 2.10 Scatter comparison of westerly wind speed between 100m CREA6 model and 100m measurements at Høvsøre. The comparison covers 15 years of data.

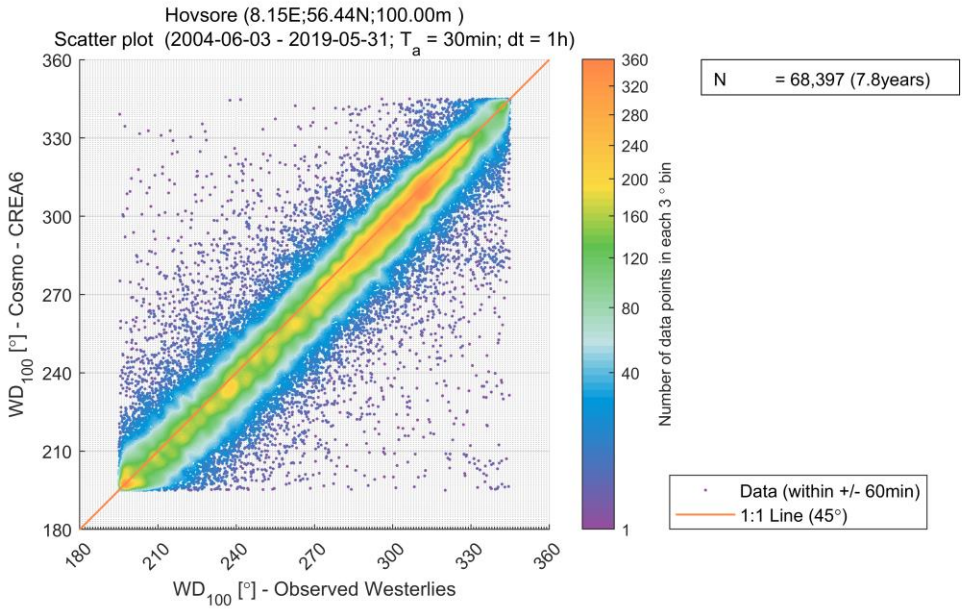

Figure 2.11 Scatter comparison of westerly wind direction between 100m CREA6 model and 100m measurements at Høvsøre. The comparison covers 15 years of data.

To conclude, wind speeds and directions from CREA6 at stations close to the Thor OWF area compare very well to observations. Since the DHI Danish model is forced with wind from CREA6, this adds confidence in the model results and quality. Only for the highest wind speed was discrepancy observed, namely a small overestimation of approximately 3-10% by CREA6. For extreme wind analysis based on CREA6 such an overestimation would need to be considered.

3 DHI Danish Waters Model

The basis of the metocean data used in this report is the DHI Danish Waters Model established using MIKE Powered by DHI modelling suite[11] including MIKE 21 hydrodynamic (HD) and spectral wave (SW) models for the period 1995-01-01 to 2018-12-31, i.e. 24 years.

Details about the setup, calibration and validation of the model can be found in [1].

3.1 Hydrodynamic Conditions

Water levels and 2D currents are supplied by the hydrodynamic (HD) model, MIKE 21 HD FM. The MIKE 21 Flow Model is a modelling system for 2D free-surface depth-averaged flows that is developed and maintained by DHI and offered as part of MIKE Powered by DHI. The model bathymetry at the Thor OWF area is shown in Figure 1.2. The HD model mesh resolution at the Thor OWF is approximately 1-2 kilometres.

Comparison of water level at FINO1 is presented in Figure 3.1. Quality results with close to zero bias and very high correlation are observed.

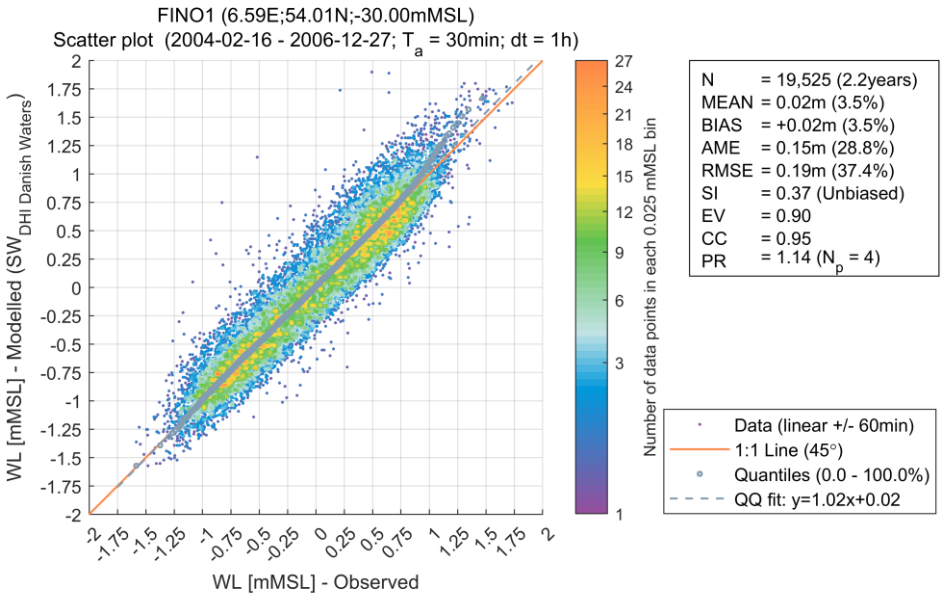

Figure 3.1 Scatter comparison of water level between DHI Danish Waters HD Model and measurements at FINO1. The comparison covers approximately 2 years of data.

Water level comparison at Hanstholm (instrument installed in the harbour) is presented in Figure 3.2. Similar to FINO1, high quality results are observed. There is, however, a small tendency that high water levels are slightly over-estimated in the Danish Waters HD Model which most likely is due to coarse resolution at the coast and inaccurate representation of the bathymetry in the model.

[11] https://manuals.mikepoweredbydhi.help/2020/MIKE_21.htm#MIKE_21_Documentation

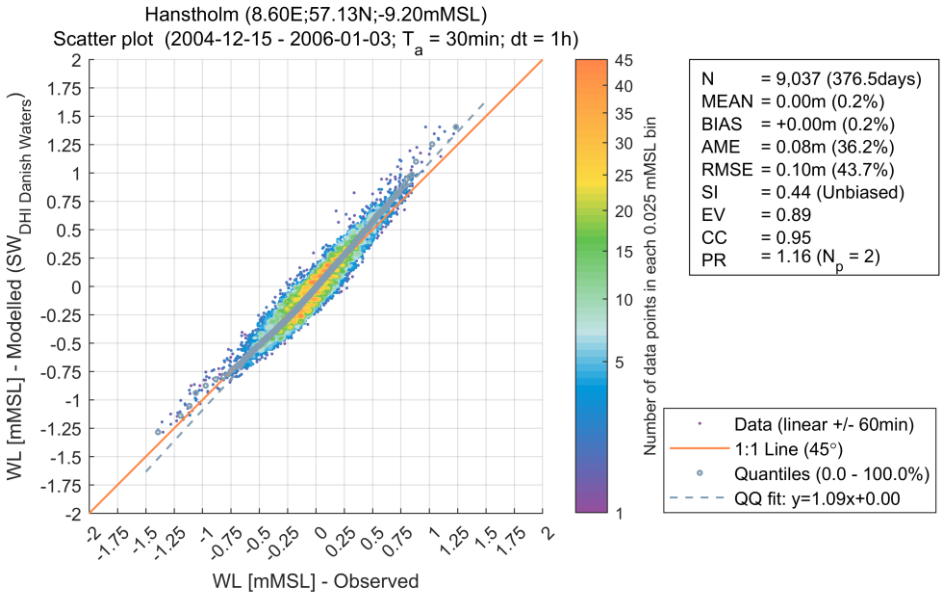

Figure 3.2 Scatter comparison of water level between DHI Danish Waters HD Model and measurements at Hanstholm. The comparison covers approximately 1 year of data after removing gaps.

Water level comparison at Hvide Sande is presented in Figure 3.3. The scatter index is lower compared to Hanstholm and the correlation is really high at 0.97.

More validations from other parts of the model area are presented in [1].

DHI have high confidence that the quality of water levels at the Thor OWF is high and hence the present DHI Danish Waters HD Model set-up is suitable for FEED purposes. However, for the detailed design stage, DHI recommends high resolution modelling to represent the currents in more detail.

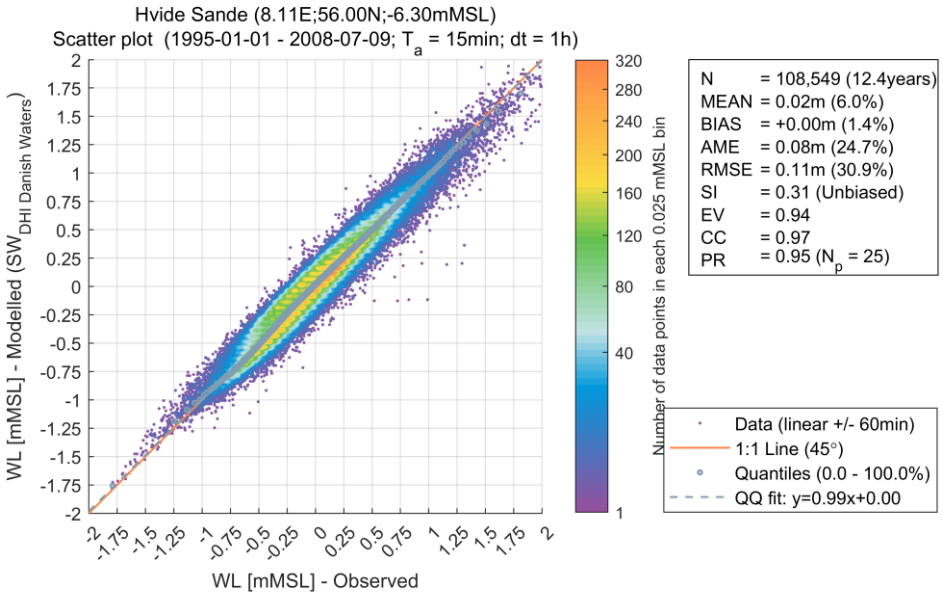

Figure 3.3 Scatter comparison of water level between DHI Danish Waters HD Model and measurements at Hvide Sande. The comparison covers approximately 12 years of data.

3.2 Spectral Waves

Spectral wave data were supplied from the MIKE 21 Spectral Wave (SW) Flexible Mesh (FM) model[12]. Like the other modules included in the FM series of MIKE Powered by DHI, the spectral wave model is based on an unstructured, cell-centred finite volume method and uses an unstructured mesh in geographical space. This approach, which has been available from DHI now for more than a decade and which is thus fully matured, gives the maximum degree of flexibility and allows the model resolution to be varied and optimised according to requirements in various parts in the model domain. MIKE 21 SW is a third-generation spectral wind-wave model based on unstructured meshes. The model simulates the growth, decay and transformation of wind-waves and swell waves in offshore and coastal areas.

The wave model was forced by boundary conditions from DHI's regional Northern Europe spectral wave model[13], wind forcing was taken from CREA6 and the water level and current forcing were from the DHI Danish HD model (described in the previous subsection). The computational domain and mesh are presented in Figure 3.4. A close-up of the mesh at the Thor OWF site was presented in Figure 1.2. The SW model mesh resolution at the Thor OWF is approximately 1-2 kilometres.

[12] https://manuals.mikepoweredbydhi.help/2020/MIKE_21.htm#MIKE_21_Documentation

[13] https://www.dhigroup.com/global/references/emea/overview/metocean-database-of-northern-european-seas

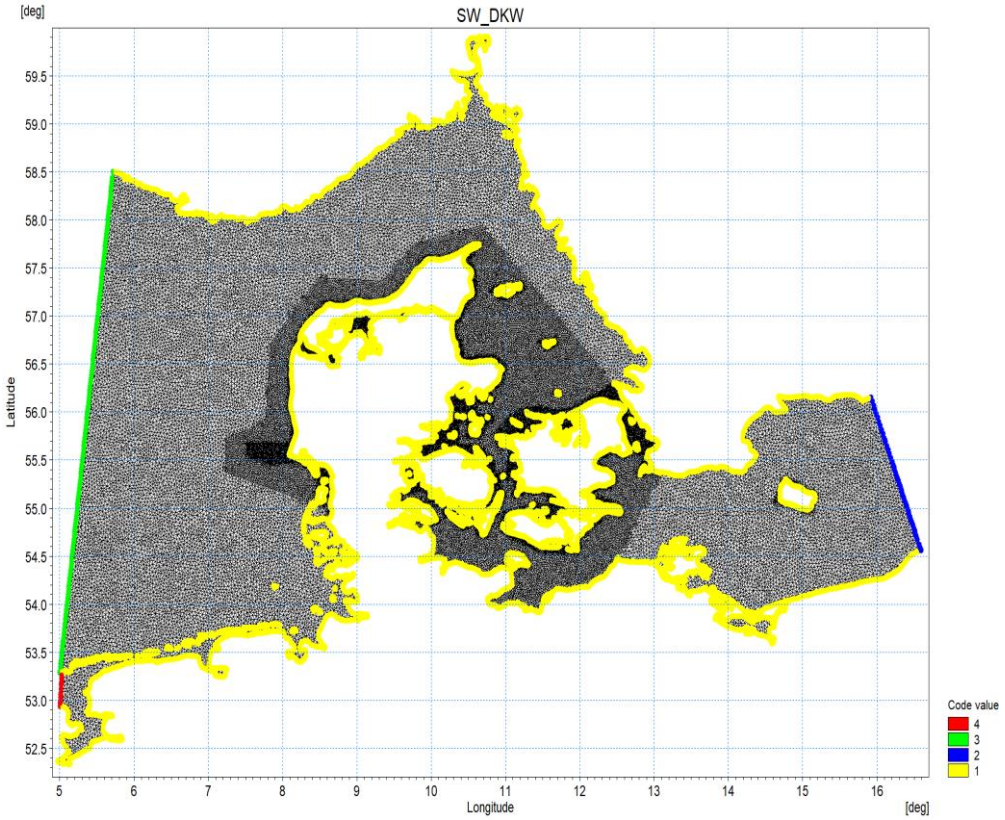

Figure 3.4 Computational mesh and domain of DHI Danish Waters SW Model for spectral waves. Colour codes (1-4) represents open boundaries.

Validation of modelled significant wave height against data from FINO1 has been carried out. In addition to the final DHI Danish Waters SW Model forced with CREA6 wind data, a comparison with its twin SW model forced with CFSR wind data (everything else being equal) is also shown. Significant wave height time series comparison of the two SW models and observations at FINO1 is shown in Figure 3.5. Scatter plot of FINO1 measurements vs CFSR forced SW model is shown in Figure 3.6 while scatter plot of FINO1 measurements vs CREA6 forced SW model (DHI Danish Waters SW Model used in this study) is shown in Figure 3.7. Both models perform well. The main advantage of using CREA6 compared to CFSR is at the coast and within inner Danish waters where land effects are not properly resolved by CFSR. The largest waves produced by the CREA6 forced spectral wave model are slightly lower compared to the largest waves produced by the CFSR forced spectral wave model.

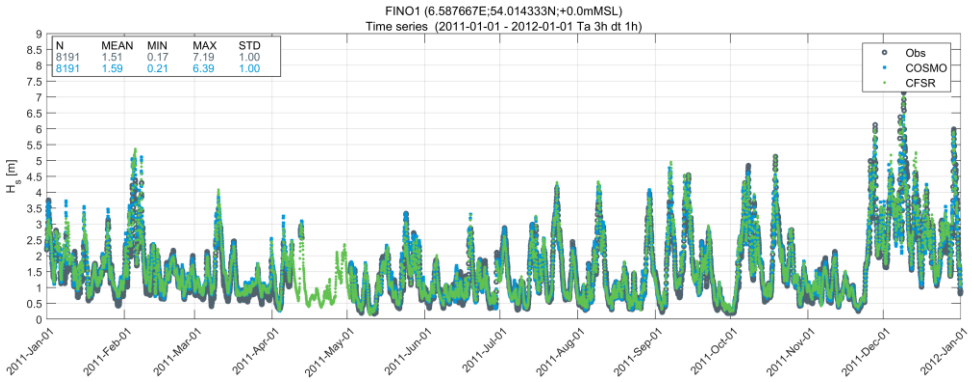

Figure 3.5 Time series of significant wave height (H_s is equivalent to H_{m0}) from observations (black) and DHI Danish Waters Model forced with CREA6 (Cosmo) wind (blue) and CFSR wind (green), respectively, at FINO1 for the year 2011. There is missing data around April 2011. Figure is taken from Section 4.2.2 in [1].

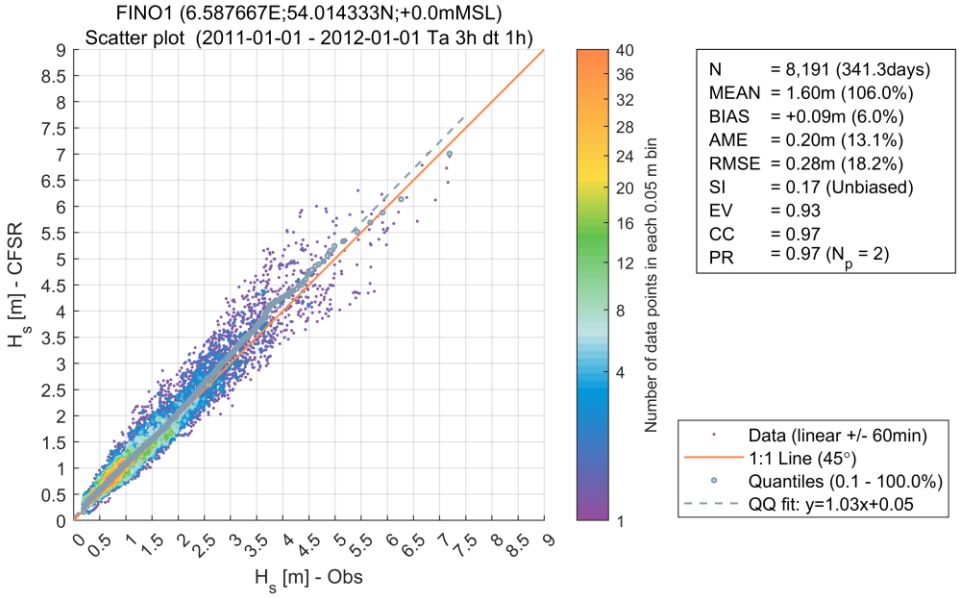

Figure 3.6 Scatter comparison of significant wave height (H_s is equivalent to H_{m0}) between DHI Danish Waters SW Model (forced with CFSR model wind data) and measurements at FINO1. The comparison covers approximately 1 year of data. Figure is taken from Section 4.2.2 in [1].

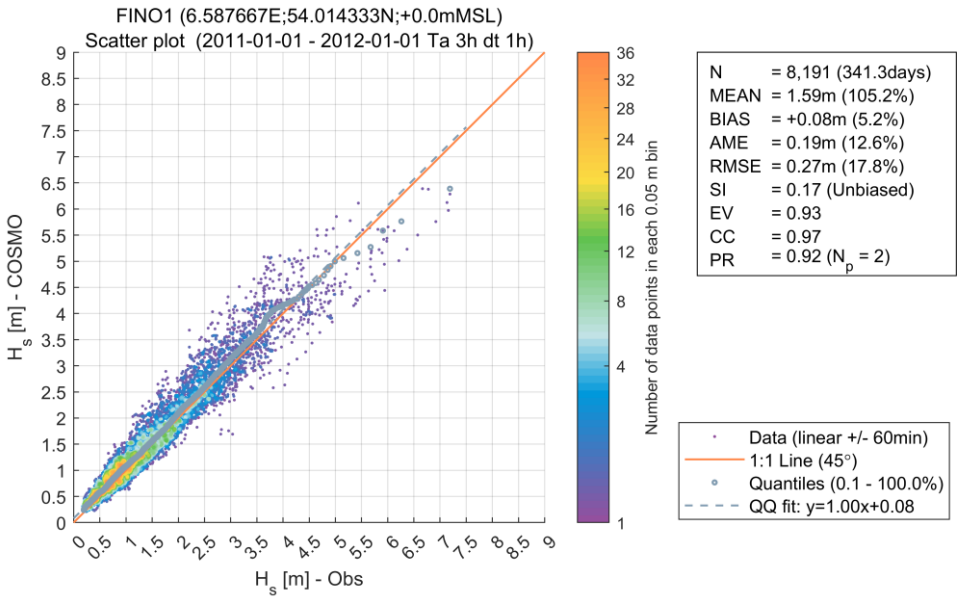

Figure 3.7 Scatter comparison of significant wave height (H_s is equivalent to H_{m0}) between DHI Danish Waters SW Model (forced with CREA6 model wind data) and measurements at FINO1. The comparison covers approximately 1 year of data. Figure is taken from Section 4.2.2 in [1].

Modelled significant wave height and mean wave direction are also compared with long measurement time series of more than 10 years at Fjaltring and Nymindegab on the west coast of Jutland (See Figure 2.1 for exact locations).

In Figure 3.8, scatter comparison of H_{m0} against measurements at Fjaltring is presented. Very good agreement between modelled and measured significant wave height is observed with very low bias, low scatter and very high correlation and only small overestimation (Peak ratio = 1.03 based on 33 events) of the most extreme waves.

Measured wave directions at Fjaltring (and Nymindegab) are delivered as 'Wave direction of spectrum peak' [14]. The data has, however, previously been presented as mean wave direction (MWD)[15]. In Figure 3.9 a scatter comparison between MWD and peak wave direction (PWD) from the Danish Waters Spectral model at Fjaltring is shown. Clearly visible is the discrete output format of the modelled PWD. Using circular statistics, the bias is found to be -0.4° while the circular correlation (calculated with formula in [8]) is 0.94. The difference between PWD and MWD is thus very very small in average, although - as can be expected from the two definitions of MWD and PWD - there are systematic differences between their values for some timestamps. In and in the following the measurements will be compared to modelled MWD for consistency with previous work.

[14] https://kystatlas.kyst.dk/public2/data/boelge/boelge_download_zip_en.html

[15] https://ens.dk/sites/ens.dk/files/Vindenergi/cowi_presentation_27_mar_2015_-_seminar_on_metocean_and_wind_resource-related_studies_at_energistyrelsen_-_rev_0_1.pdf and [1].

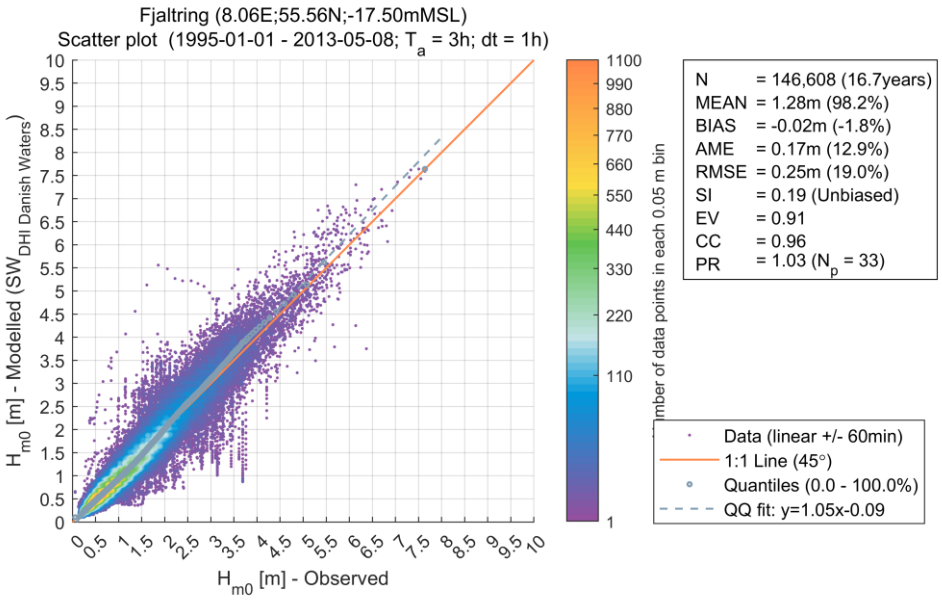

Figure 3.8 Scatter comparison of significant wave height (H_{m0}) between DHI Danish Waters SW Model and measurements at Fjaltring. The comparison covers approximately 17 years of data.

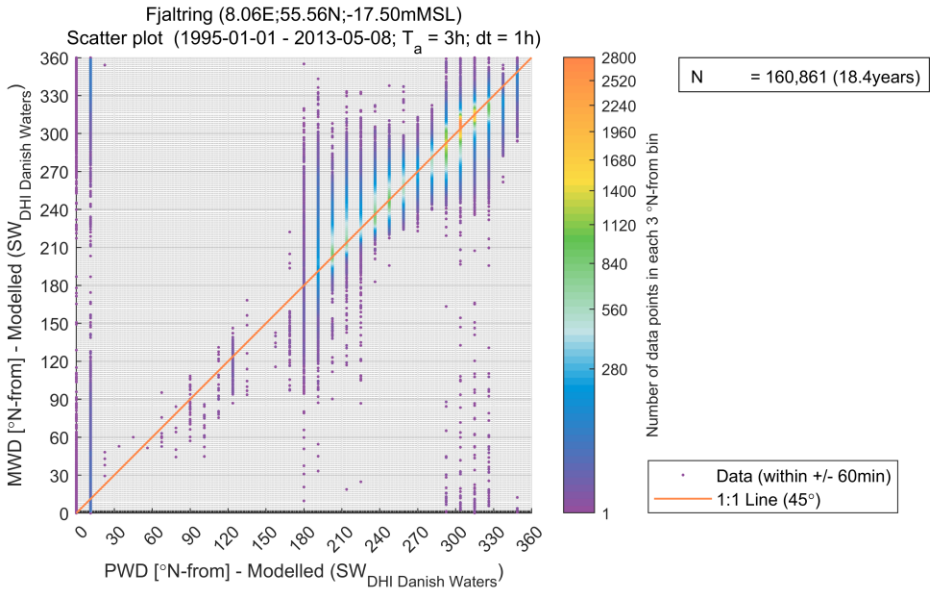

Figure 3.9 Scatter comparison of mean wave direction (MWD) against peak wave direction (PWD) of Danish Waters Spectral model at Fjaltring.

The wave rose comparison shown in Figure 3.10 shows good agreement but with some offset between bins in the dominant mean wave directions (210-330°). Scatter plot of MWD between model and measurements is shown in Figure 3.11. Large scatter is observed. Besides from a small sector in the measurements at around 310°, the agreement is very good. The discrepancy between model and measurements at around 310° is speculated to be due to a swell component that is hidden in the model data due to the definition of the used integral parameter. To verify this, a similar plot is shown in Figure 3.12, but this time only for H_{m0} larger than 1m. The scatter is significantly reduced

and the discrepancy at 310° band is also reduced. For a more fair comparison between the model and the measurements, the frequency range of the measurement instrument should be taken into account, and then by using the modelled spectrum, mean wave direction (or swell components etc.) should be calculated on the same frequency range. The frequency range of the measurement instruments were not known, and this matter was not further investigated by DHI.

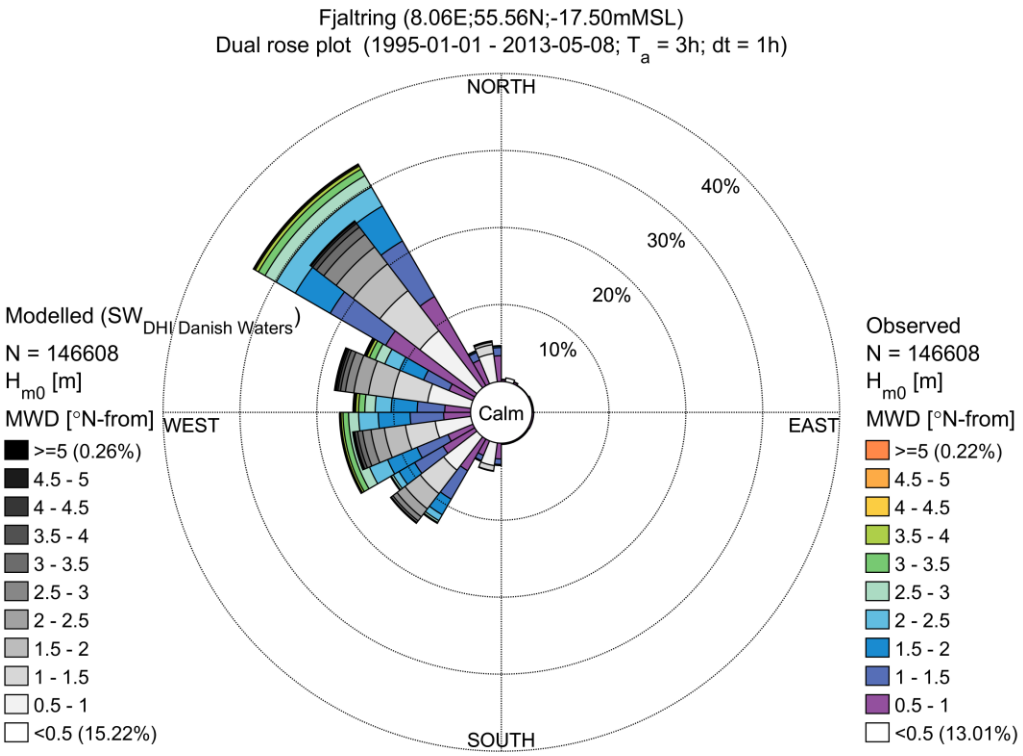

Figure 3.10 Comparison of wave roses of significant wave height (H_{m0}) and mean wave direction (MWD) between DHI Danish Waters SW Model and measurements at Fjaltring.

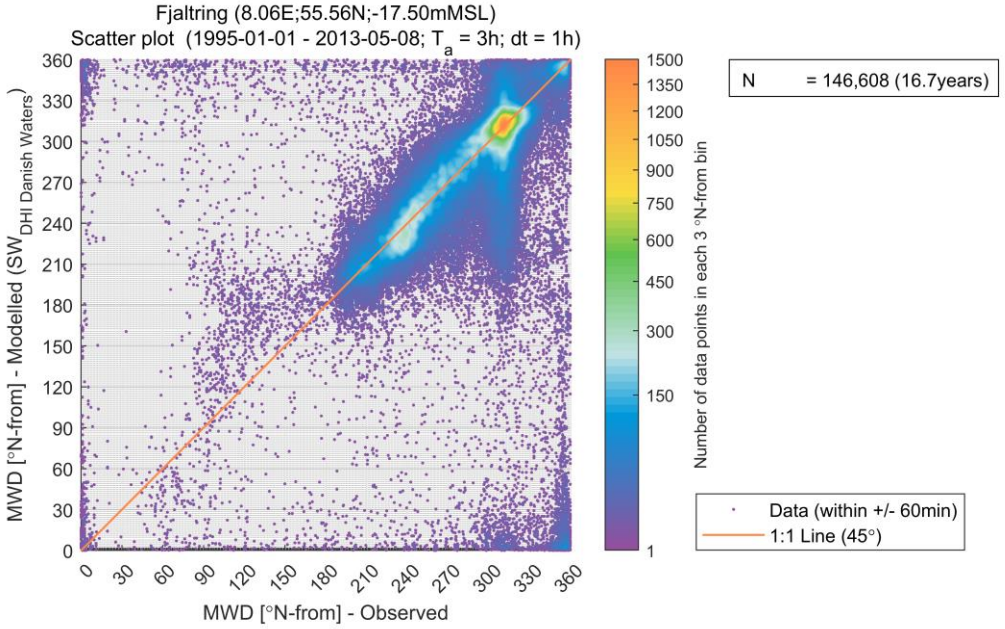

Figure 3.11 Scatter comparison of mean wave direction (MWD) between DHI Danish Waters SW Model and measurements at Fjaltring. The comparison covers approximately 17 years of data.

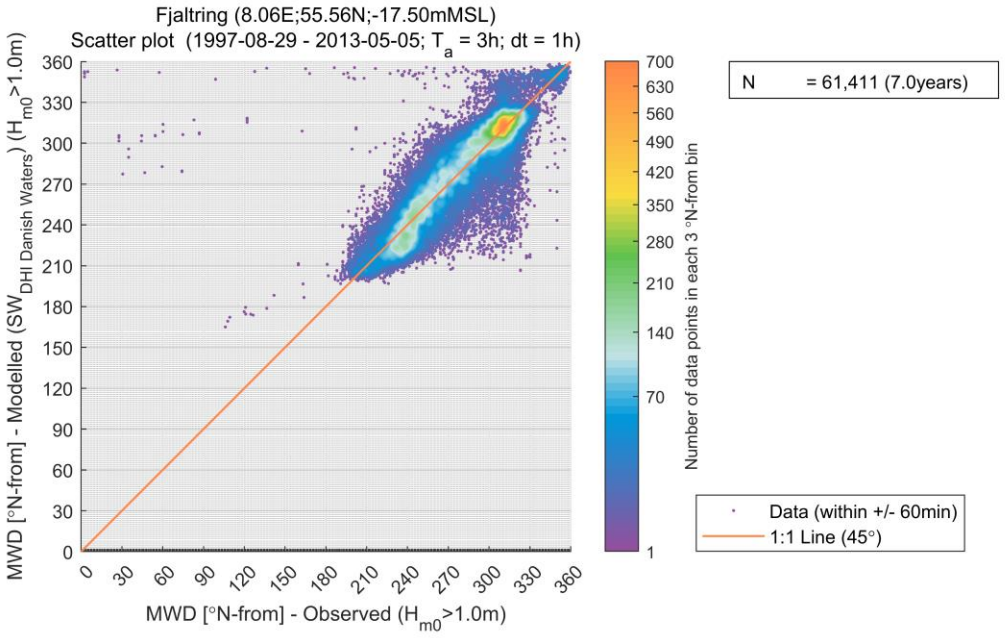

Figure 3.12 Scatter comparison of mean wave direction (MWD) conditioned on H_{m0}>1m between DHI Danish Waters SW Model and measurements at Fjaltring. The comparison covers approximately 7 years of data.

Mean-zero-crossing wave period (T_{02}) at Fjaltring is compared in Figure 3.13 for H_{m0}>1m. The linear relationship shows a trend towards overestimation of T_{02} by the model compared to measurements. At T_{02}=6s it amounts to approximately 1s. It is believed that this error is larger than the error of the actual model. Yet again, for fair comparison, T_{02}

should be calculated from the modelled spectrum using the same frequency range as the measurement instrument. This was demonstrated in Section 5.5.3 of [5].

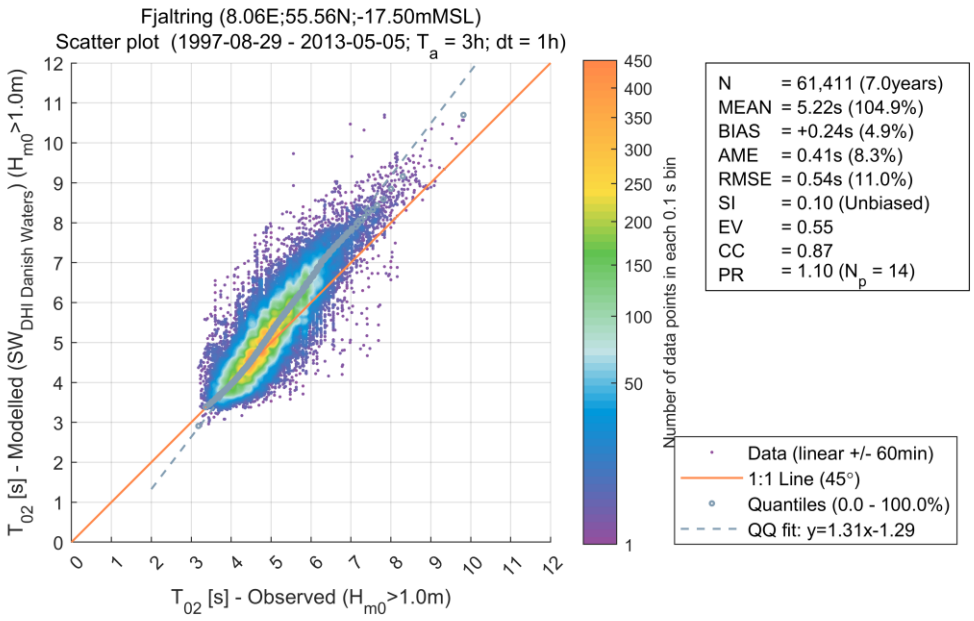

Figure 3.13 Scatter comparison of mean zero-crossing wave period (T_{02}) for H_{m0}>1m between DHI Danish Waters SW Model and measurements at Fjaltring. The comparison covers approximately 7 years of data.

Scatter comparison of modelled H_{m0} against measurements at Nymindegab is presented in Figure 3.14. The agreement between modelled and measured significant wave height is very good (low bias, low scatter index and high correlation etc.) for H_{m0}< 3.5m. For H_{m0}> 3.5m, the model underestimates the significant wave height leading to a peak ratio=0.92. This could be due to coarse model resolution around Nymindegab and local bathymetric features that are not well resolved. The corresponding wave rose comparison is shown in Figure 3.15. Small offsets in the dominant directional bins (240-330°) are observed but the general pattern agrees well.

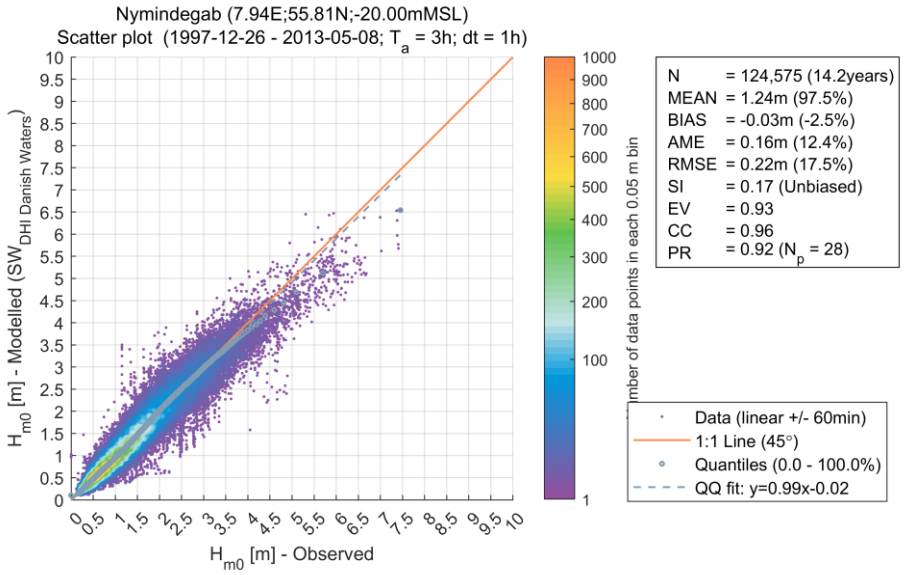

Figure 3.14 Scatter comparison of significant wave height (H_{m0}) between DHI Danish Waters SW Model and measurements at Nymindegab. The comparison covers approximately 14 years of data.

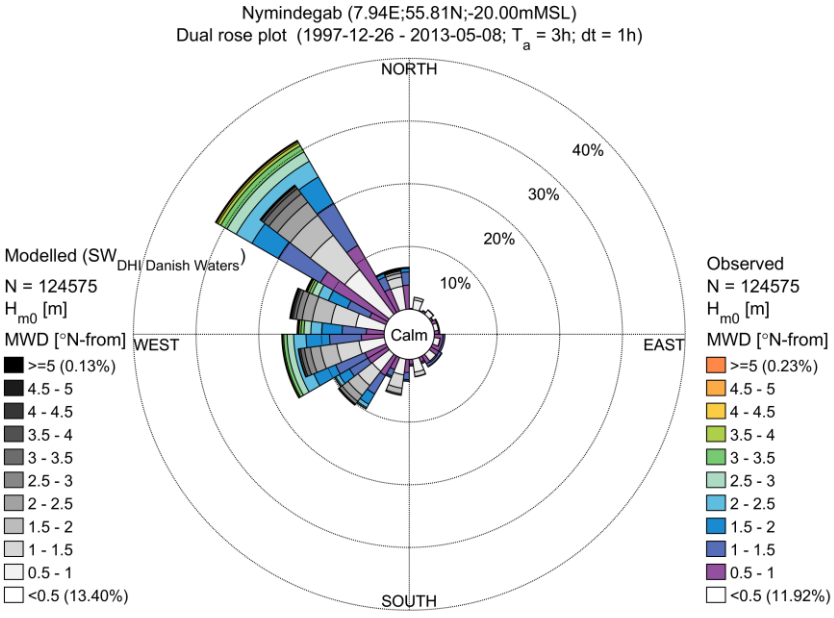

Figure 3.15 Comparison of wave roses of significant wave height (H_{m0}) and mean wave direction (MWD) between DHI Danish Waters SW Model and measurements at Nymindegab.

Scatter plot of MWD between model and measurements at Nymindegab is shown in Figure 3.16 for H_{m0}>1m. Similar to the results at Fjaltring, some discrepancy around 310° is observed. Again, the discrepancy between model and measurements at around 310° is speculated to be due to a swell component not seen in the model data due to definition of the used integral parameter. A bias of approximately 30° is observed between 90° and 150°, i.e. waves are coming from the coast.

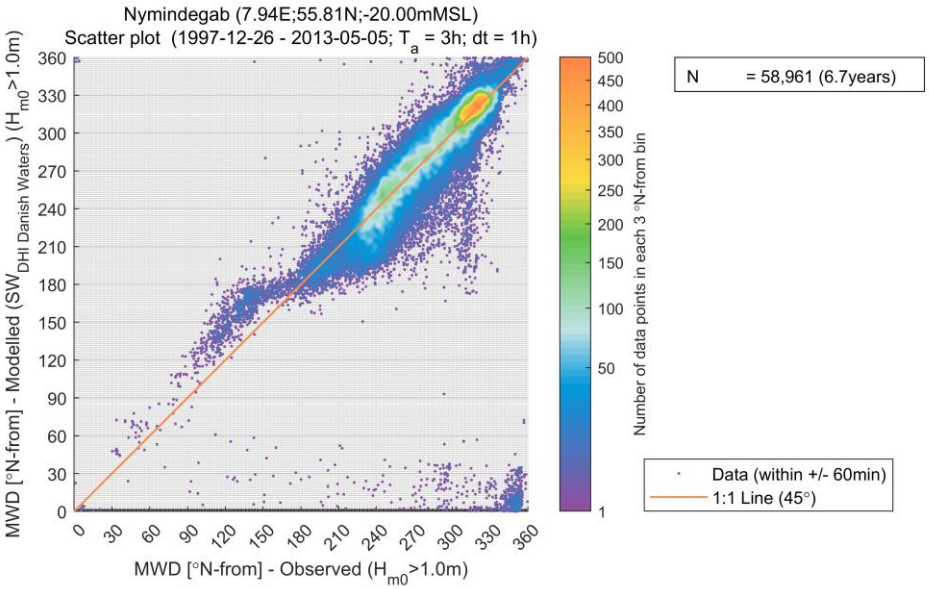

Figure 3.16 Scatter comparison of mean wave direction (MWD) conditioned on H_{m0}>1m between DHI Danish Waters SW Model and measurements at Nymindegab. The comparison covers approximately 7 years of data.

Mean-zero-crossing wave period (T_{02}) at Nymindegab is compared in Figure 3.17 for H_{m0}>1m. Good agreement is observed.

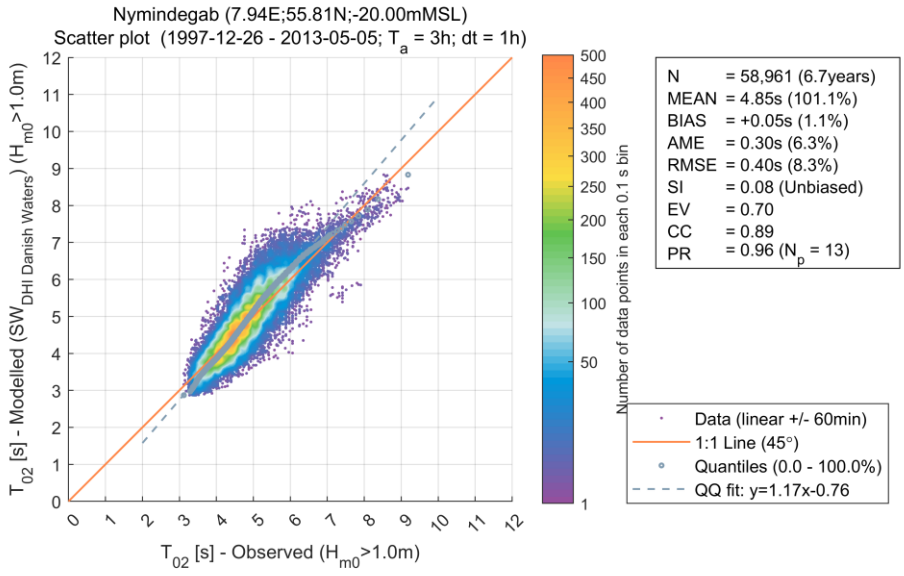

Figure 3.17 Scatter comparison of mean zero-crossing wave period (T_{02}) for H_{m0}>1m between DHI Danish Waters SW Model and measurements at Nymindegab. The comparison covers approximately 7 years of data.

The RUNE buoy deployed for a little longer than two months was located approximately 12 km west of the Thor OWF area and thus is the closest measurement station available. A comparison of H_{m0} between the measurements and DHI Danish SW Model showed in Figure 3.18 demonstrate a very good agreement with low bias, high correlation and low scatter. In Figure 3.19 the wave rose comparison (significant wave height and mean wave direction (MWD)) is provided. The agreement is good, though some small offset between the individual bins between 210° and 300° are observed. Peak wave period (T_p) and mean zero-crossing wave period (T_{02}) scatter comparison plots are shown in Figure 3.20 and Figure 3.21, respectively, for H_{m0} larger than 1m. Both T_p and T_{02} are slightly overestimated by the model for the largest periods. As mentioned before, such comparisons would most likely result in better results if the same frequency range between the model and measurements were considered.

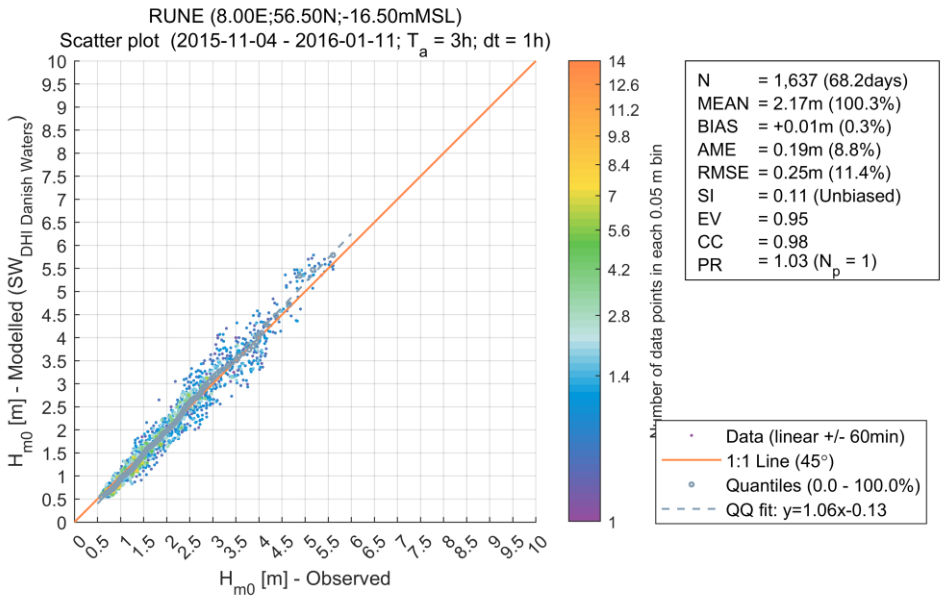

Figure 3.18 Scatter comparison of significant wave height (H_{m0}) between DHI Danish Waters SW Model and measurements at RUNE. The comparison covers approximately 2 months of data.

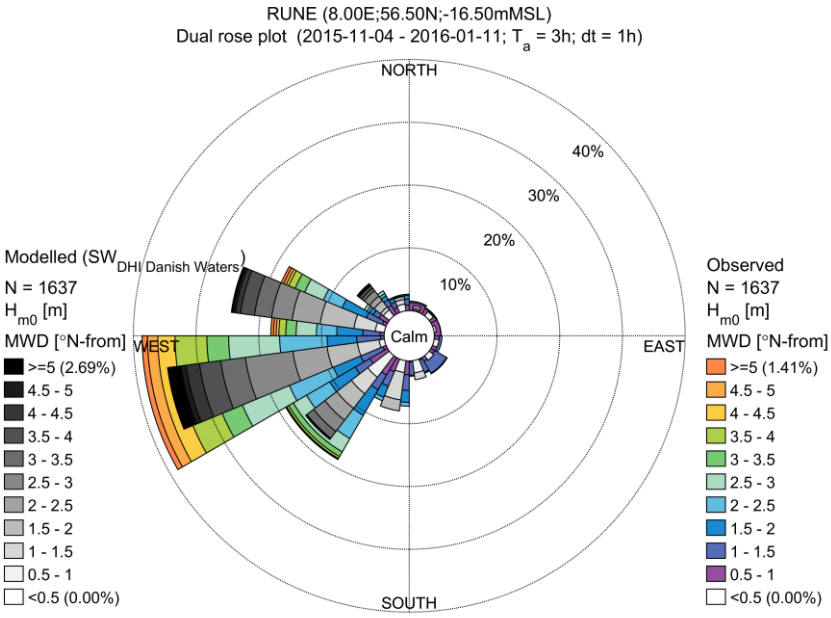

Figure 3.19 Comparison of wave roses of significant wave height (H_{m0}) and mean wave direction (MWD) between DHI Danish Waters SW Model and measurements at RUNE.

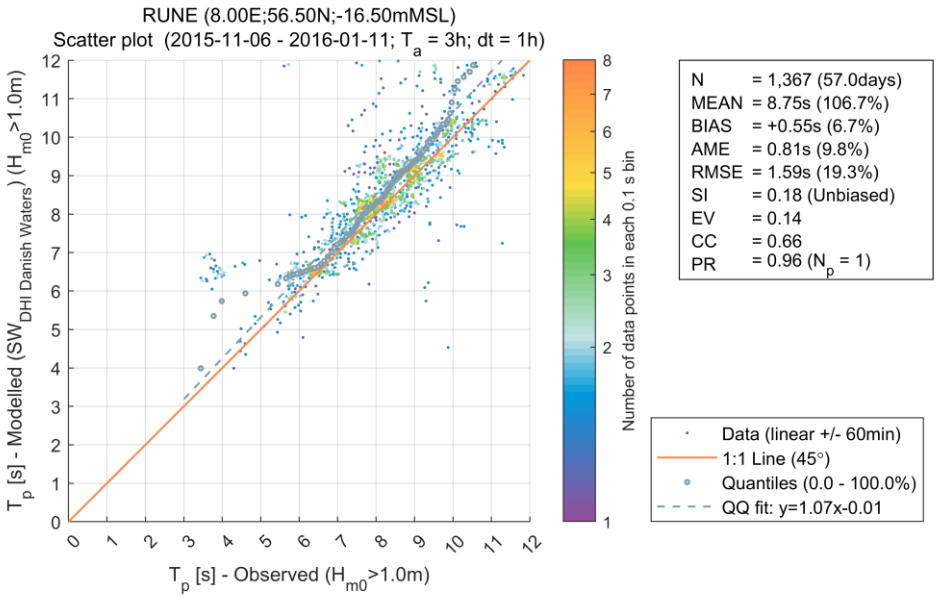

Figure 3.20 Scatter comparison of peak wave period (T_p) for H_{m0}>1m between DHI Danish Waters SW Model and measurements at RUNE. The comparison covers approximately 2 months of data.

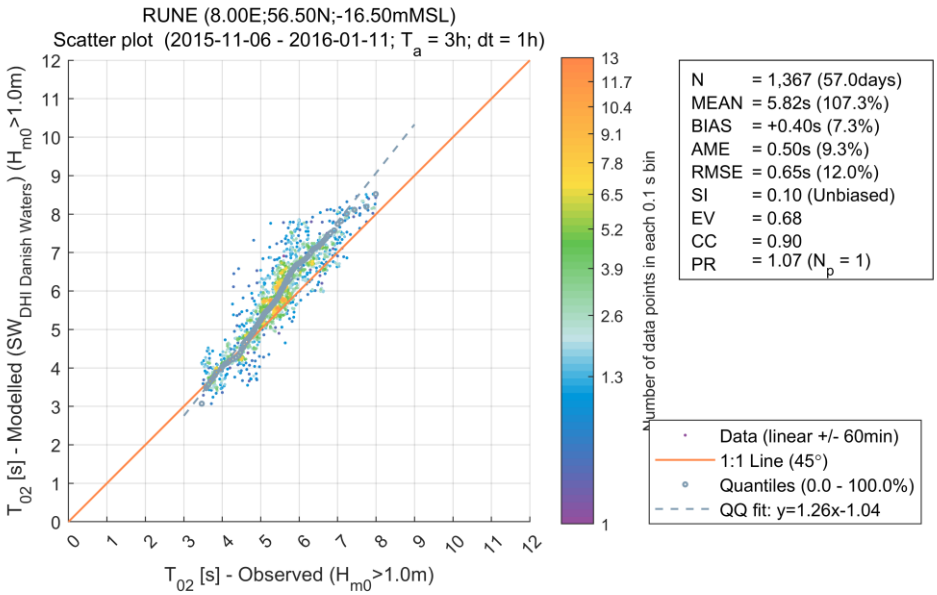

Figure 3.21 Scatter comparison of mean zero-crossing wave period (T_{02}) for H_{m0}>1m between DHI Danish Waters SW Model and measurements at RUNE. The comparison covers approximately 2 months of data.

Overall, the Danish Waters Spectral wave model compares very well with measurements. In general, the comparisons are sensitive to the measurement instrument set-ups and, as observed here, also the wave heights. Better results are usually achieved if the frequency range of the buoys are known, and then the same frequency range is applied to the modelled spectrum.

Overall, it is concluded that the DHI Danish Waters Spectral Wave Model is adequate and fully capable of successfully modelling the waves at the Thor OWF area for FEED design purposes. For detailed design modelling, high-resolution modelling is recommended.

4 Data Delivery

Time series data from the Danish Waters Model has been delivered at analysis points P1, P2 and P3 with coordinates listed in Table 1.1. The period is from 1995-01-01 to 2018-12-31. The output time step is 1 hour for all data. Implicit averaging time varies (see below).

From CREA6 the following wind data were delivered:

- Wind speed at 10mMSL (WS10)
- Wind direction at 10mMSL (WD10)
- Wind speed at 100mMSL (WS100)
- Wind direction at 100mMSL (WD100)

It should be noted that the CREA6 time series contain gaps. NaN thus indicates missing data. Information on how these gaps were filled for the purpose of forcing the DHI MIKE 21 HD and SW models is provided in Section 2.3.2 of [1]. From the arguments put forward in Section 2.5, the delivered CREA6 wind data has an implicit averaging time of T_a=30 minutes.

From the Hydrodynamic model (HD) the following variables were delivered

- Water level (WL)
- Current speed (CS, depth-averaged)
- Current direction (CD, depth-averaged)

Water levels are delivered from MIKE 21 HD model output. To get water level values in mMSL the global mean value must be subtracted. In addition, de-tided (see Section 5.1) time series of the above variables were also delivered. Previous studies (internal DHI) suggest that the delivered HD data has an implicit averaging time of T_a=15 minutes.

From the spectral wave model (SW), the following variables were delivered

- Significant wave height (H_{m0})
- Peak wave period (T_p)
- Mean wave period (T_{01})
- Mean-zero-crossing wave period (T_{02})
- Mean wave direction (MWD)
- Peak wave direction (PWD)
- Directional standard deviation (DSD)

Previous studies (such as Section 5.4.5 of [5]) suggest that the delivered SW data has an implicit averaging time of T_a=3 hours. The above variables are all spectral equivalent parameters and are delivered for wind-sea, swell and total components following a wave-age criterion [9]:

$$\frac{U_{10}}{c} cos(\theta - \theta_w) < 0.83, \qquad (4.1)$$

where U_{10}, is wind speed at 10mMSL [m/s] from the CREA6, c is the linear celerity [m/s], θ is the wind-direction corresponding to the wind speed, [coming-from ˚N] from CREA6, and θ_w is the wave direction corresponding to the celerity of the wave, [coming-from ˚N]. Waves which fulfil the criterion are described as swells, otherwise wind-sea.

The directional wave spectrum is extracted and delivered at point DSW only (see Figure 1.2).

5 Normal Conditions

In this section, normal conditions at P1, P2 and P3 are presented (figures for P2 and P3 are shown in Appendix B). The reference is mMSL assuming 0 mMSL = 0 mDVR90. If not otherwise stated; units are in meters and mMSL (vertical reference).

The main statistical (mean, minimum, maximum and standard deviation) omnidirectional parameters are shown in Table 5.1 to Table 5.3 for P1, P2 and P3, respectively. For the significant wave height (H_{m0}) the root-mean-square value (m_2) has been used, where m_n is defined

$$m_n = [mean({H_{m0}}^n)]^{1/n},$$

i.e. n=2. In general, P1 has slightly more severe wave conditions compared to P2 which is again slightly more severe compared to P3. Also, wind speed is largest at P1. The maximum recorded wind speed at all three analysis points is associated with the winter low pressure storm system 'Bodil' (internationally known as 'Xaver')[16] occurring around 2013-12-05. The difference between the maximum wind speeds at P1, P2 and P3, is an indication of the high resolution of CREA6. The maximum water levels are also associated with this event and peaking a few days after the peaks in wind speed.

Regarding water levels, the long-term average at each point has been subtracted from the time series from the HD model so that the mean value equals 0.0mMSL at each site.

Table 5.1 Main statistical omnidirectional parameters: mean, minimum (min), maximum (max) and standard deviation (std) at site P1. Data from 1995-01-01 – 2018-12-31 with hourly time steps.

P1	Mean	Min	Max	Std
m_2 [m]	1.9	-	-	-
T_p [s]	7.7	1.7	24.1	2.8
T_{02} [s]	4.7	1.3	10.8	1.3
WL [mMSL]	0.0	-1.4	1.8	0.3
CS [m/s]	0.1	0.0	0.9	0.1
WS @ 10m [m/s]	8.1	0.0	35.7	4.0
WS @ 100 m [m/s]	10.0	0.1	45.5	4.8

[16] https://en.wikipedia.org/wiki/Cyclone_Xaver

Table 5.2 Main statistical omnidirectional parameters: mean, minimum (min), maximum (max) and standard deviation (std) at site P2. Data from 1995-01-01 – 2018-12-31 with hourly time steps.

P2	Mean	Min	Max	Std
m_2 [m]	1.8	-	-	-
T_p [s]	7.6	1.7	23.5	2.8
T_{02} [s]	4.6	1.5	10.7	1.3
WL [mMSL]	0.0	-1.5	2.0	0.4
CS [m/s]	0.1	0.0	0.9	0.1
WS @ 10m [m/s]	8.0	0.0	32.7	4.0
WS @ 100 m [m/s]	9.9	0.1	40.5	4.7

Table 5.3 Main statistical omnidirectional parameters: mean, minimum (min), maximum (max) and standard deviation (std) at site P3. Data from 1995-01-01 – 2018-12-31 with hourly time steps.

P3	Mean	Min	Max	Std
m_2 [m]	1.8	-	-	-
T_p [s]	7.6	1.4	24.2	2.3
T_{02} [s]	4.5	1.4	10.4	1.3
WL [m]	0.0	-1.6	2.2	0.4
CS [m/s]	0.1	0.0	0.9	0.1
WS @ 10m [m/s]	7.9	0.0	33.2	4.0
WS @ 100 m [m/s]	9.8	0.1	41.8	4.6

5.1 De-tiding water level and current speed

Water level (WL) and depth-averaged current speed (CS) has been split into its tidal and residual components using the UTide toolbox [10]. UTide is based on the IOS tidal analysis method defined by the Institute of Oceanographic Sciences as described by [11], and integrates the approaches defined in [12] and [13]. The time series of WL and CS and the size of constituents are presented in Figure 5.1 and Figure 5.2 for site P1. Tidal levels for all three sites are provided in Table 5.4.

The total CS at P1 is shown in Figure 5.3. The main current direction is along the west coast of Jutland.

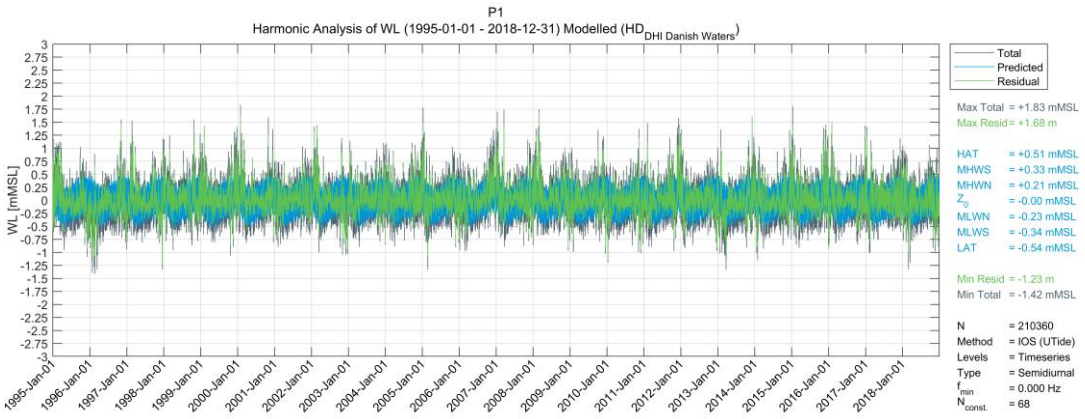

Figure 5.1 Time series of water level (WL) at P1. Total (black), Tidal component (Predicted, blue) and residual component (green).

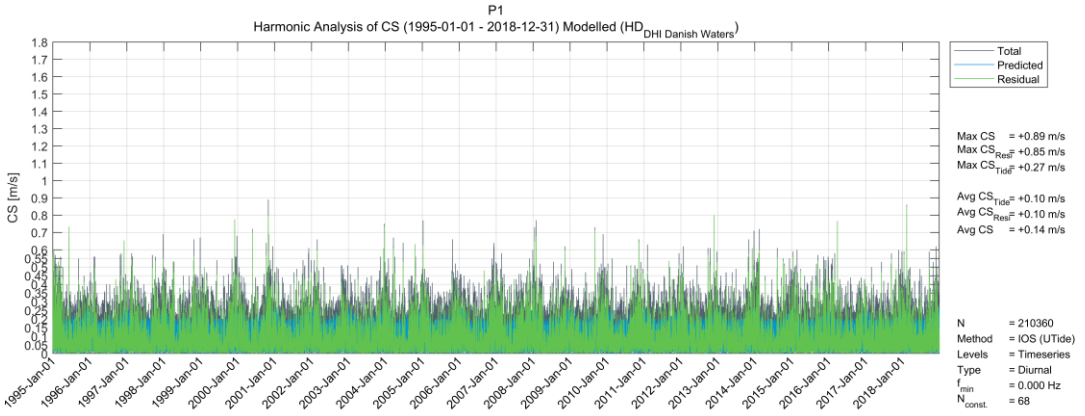

Figure 5.2 Time series of depth-averaged current speed (CS) at P1. Total (black), Tidal component (Predicted, blue) and residual component (green).

Table 5.4 Tidal levels from harmonic analysis from 1995-01-01 to 2018-12-31 using IOS UTide for P1, P2 and P3. All numbers in units of mMSL.

Tidal levels (mMSL)	P1	P2	P3
HSWL	1.8	2.0	2.2
HRL	1.7	1.7	1.9
HAT	0.5	0.5	0.6
MHWS	0.3	0.3	0.4
MHWN	0.2	0.2	0.2
MLWN	-0.2	-0.2	-0.3
MLWS	-0.3	-0.3	-0.4
LAT	-0.5	-0.6	-0.6
LRL	-1.2	-1.3	-1.4
LSWL	-1.4	-1.5	-1.6

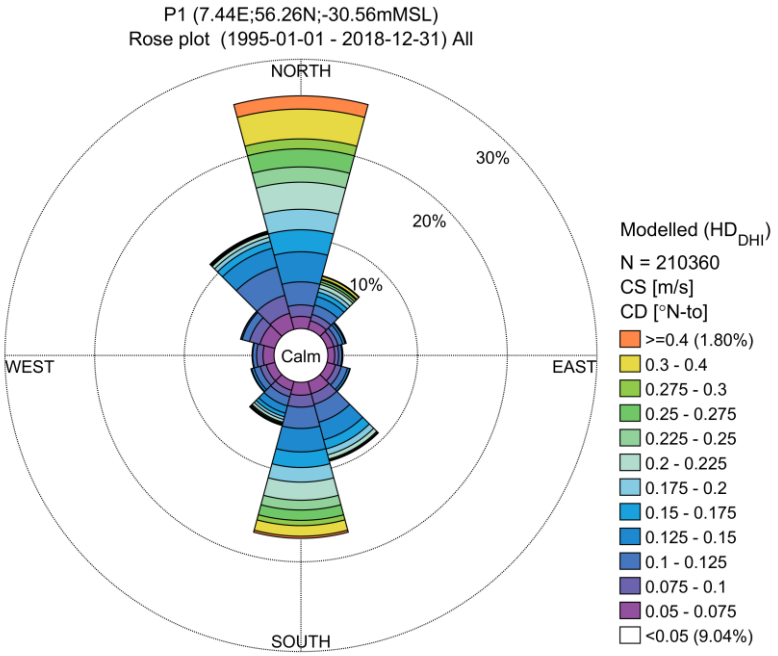

Figure 5.3 Rose plot of depth-averaged current speed (CS) at P1.

5.2 Wind speed and direction

Wind speed at 10mMSL and 100mMSL were extracted from the CREA6 data set. Distributions (probability density functions (pdf) and cumulative distribution functions (cdf)) of omnidirectional wind speed are shown in Figure 5.4 and Figure 5.5. The distribution of wind speed often follows a 2-p Weibull distribution with pdf given by (only defined for positive argument):

$$f(x) = \frac{k}{A}\left(\frac{x}{A}\right)^{k-1} exp\left(-\left(\frac{x}{A}\right)^{k}\right), \qquad (5.1)$$

with scale parameter (A) and shape parameter (k). Non-central moments of order *n* can then be estimated as

$$E(x^n) = A^n \Gamma\left(1 + \frac{n}{k}\right), \qquad (5.2)$$

where Γ is the mathematical Gamma function. Fit curves[17] (red curves) are shown on top of the pdfs in Figure 5.4 and Figure 5.5. Values (A and k) from Weibull fits are provided in Table 5.5 for P1, P2 and P3.

Wind roses are presented in Figure 5.6 and Figure 5.7 for 10mMSL and 100mMSL this shows the main wind directions from west - northwest.

[17] Fitting curves are obtained from fitting analytical Weibull functions to the first two moments of the distributions.

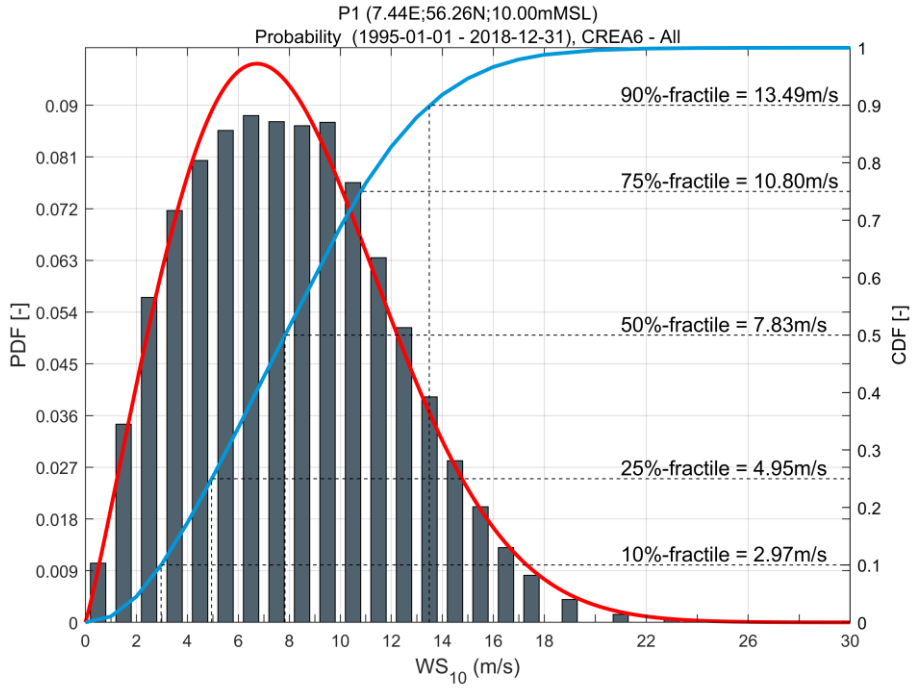

Figure 5.4 Probability density function (PDF) (bars) and cumulative distribution function (CDF) (light blue) of CREA6 wind speed at 10mMSL at P1. Weibull fit is added to the PDF.

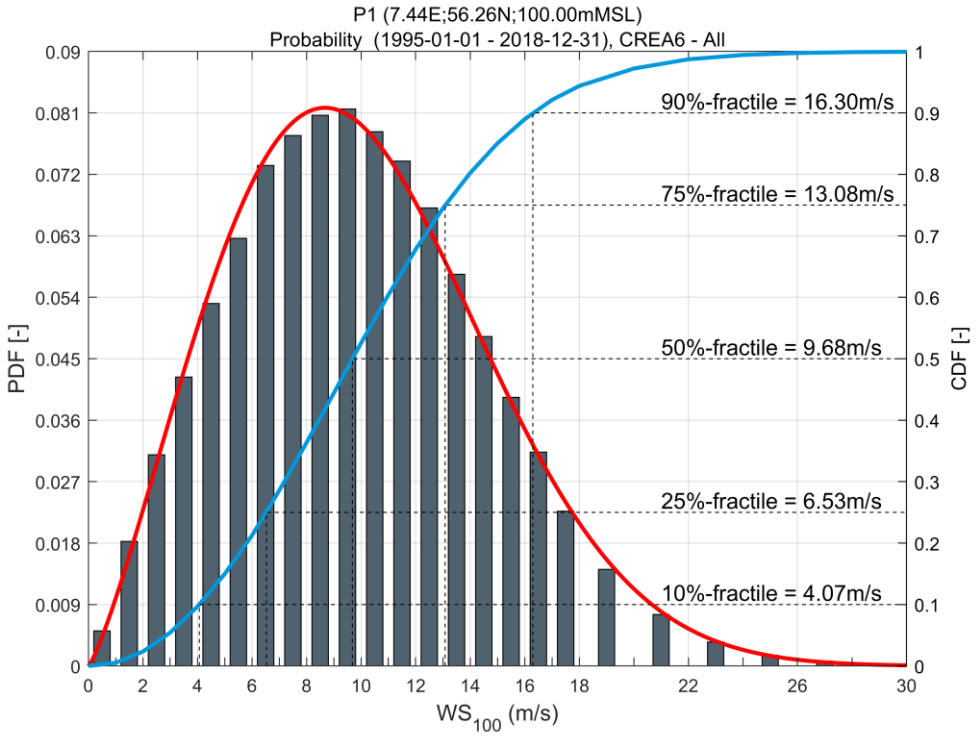

Figure 5.5 Probability density function (PDF) (bars) and cumulative distribution function (CDF) (light blue) of CREA6 wind speed at 100mMSL at P1. Weibull fit is added to the PDF.

Table 5.5 Weibull fit parameters (A and k for Weibull fit) to CREA6 wind speed at 10mMSL and 100mMSL at P1, P2 and P3.

Weibull fit	A_{10m} [m/s]	k_{10m} [-]	A_{100m} [m/s]	k_{100m} [-]
P1	9.13	2.11	11.32	2.23
P2	9.07	2.11	11.19	2.23
P3	8.91	2.10	11.02	2.22

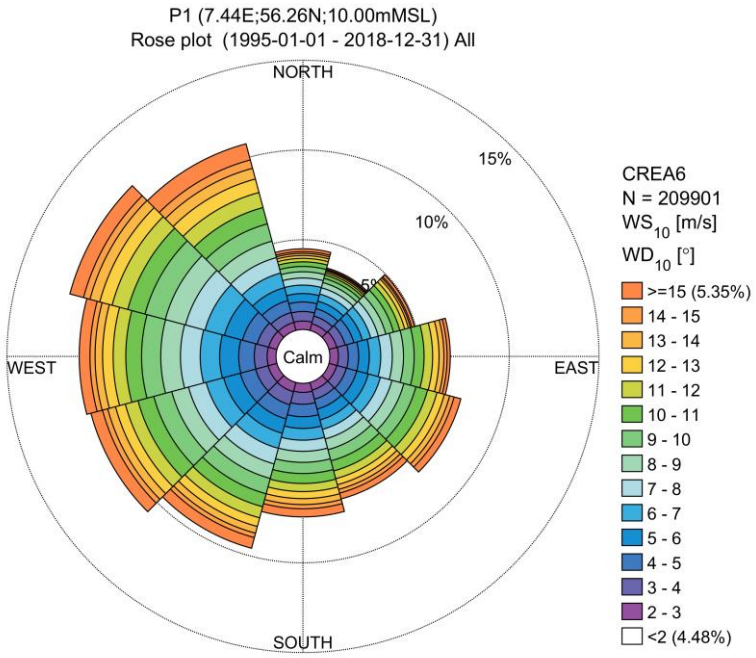

Figure 5.6 Wind rose of CREA6 wind speed at 10mMSL at P1.

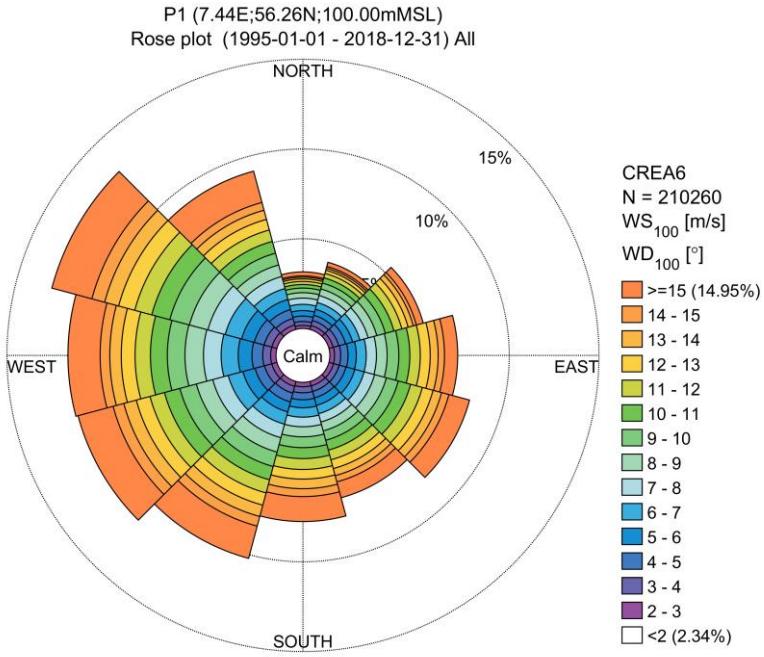

Figure 5.7 Wind rose of CREA6 wind speed at 100mMSL at P1.

5.3 Maps of non-extreme significant wave heights

To assess the severity of non-extreme waves across the wind farms, the power-mean significant wave heights were estimated according to moments (m_n) defined at the beginning of Section 5.

Figure 5.8 to Figure 5.10 shows the results for n=1, 2 & 5, respectively.

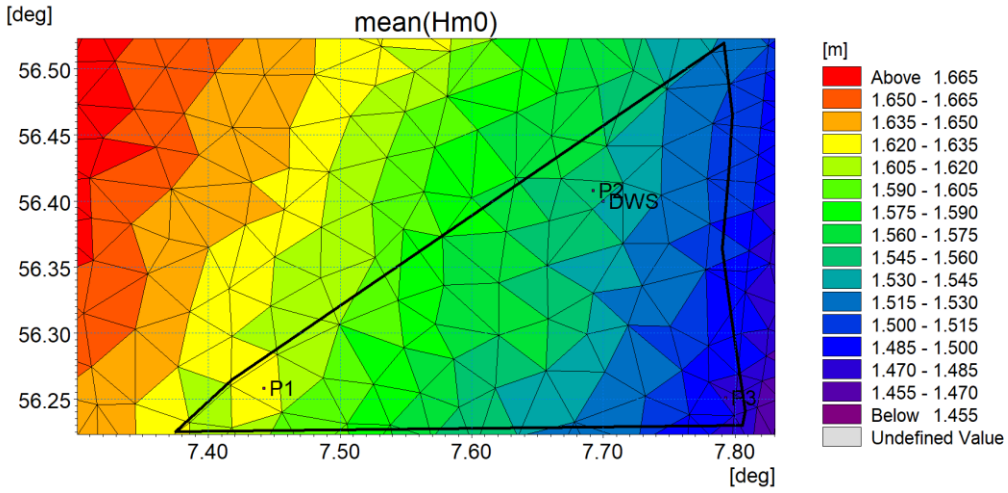

Figure 5.8 Moment m_1 of significant wave height (H_{m0}) from the DHI Danish Waters Model over the full Thor OWF project area (red curve). Analysis points, P1, P2 and P3 and directional wave spectrum point DWS is shown. Data from 1995-01-01 to 2018-12-31.

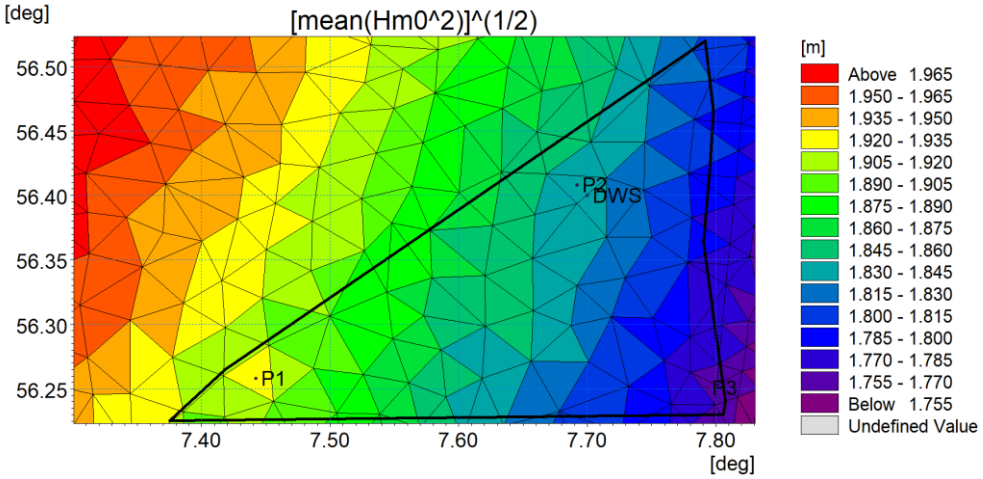

Figure 5.9 Moment m_2 (root-mean-square) of significant wave height (H_{m0}) from the DHI Danish Waters Model over the full Thor OWF project area (red curve). Analysis points, P1, P2 and P3 and directional wave spectrum point DWS is shown. Data from 1995-01-01 to 2018-12-31.

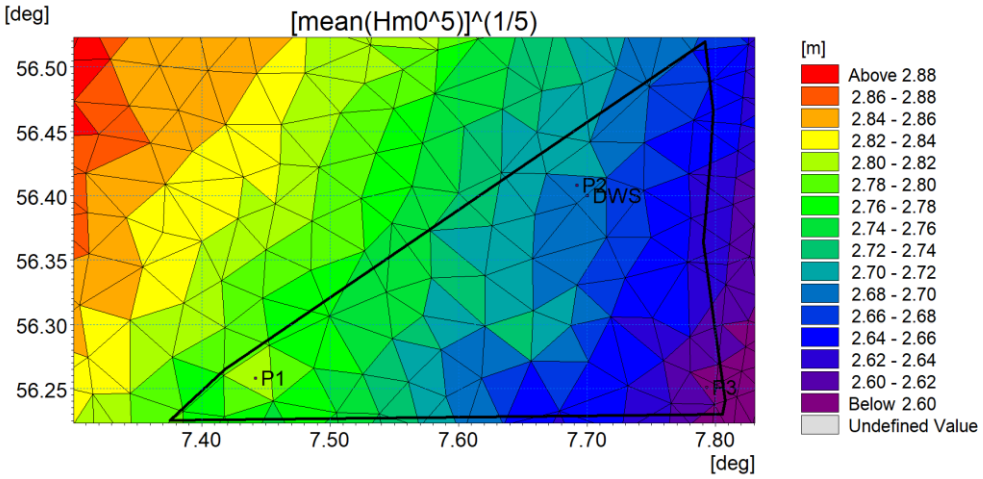

Figure 5.10 Moment m_5 of significant wave height (H_{m0}) from the DHI Danish Waters Model over the full Thor OWF project area (red curve). Analysis points, P1, P2 and P3 and directional wave spectrum point DWS is shown. Data from 1995-01-01 to 2018-12-31.

Probability of occurrence (histogram) and the cumulative distribution function (cdf) of significant wave height (H_{m0}) at P1 is shown in Figure 5.11, and a rose plot of H_{m0} and mean wave direction (MWD) is shown in Figure 5.12.

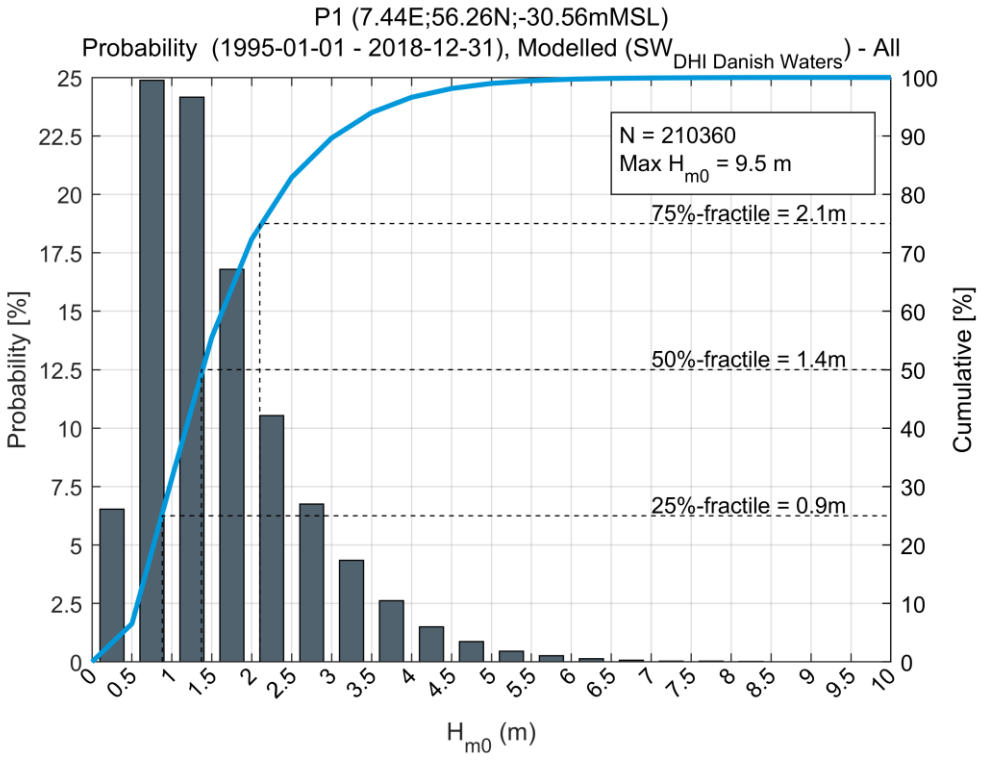

Figure 5.11 Probability of occurrence (bars) and cumulative probability (blue) of H_{m0} at P1.

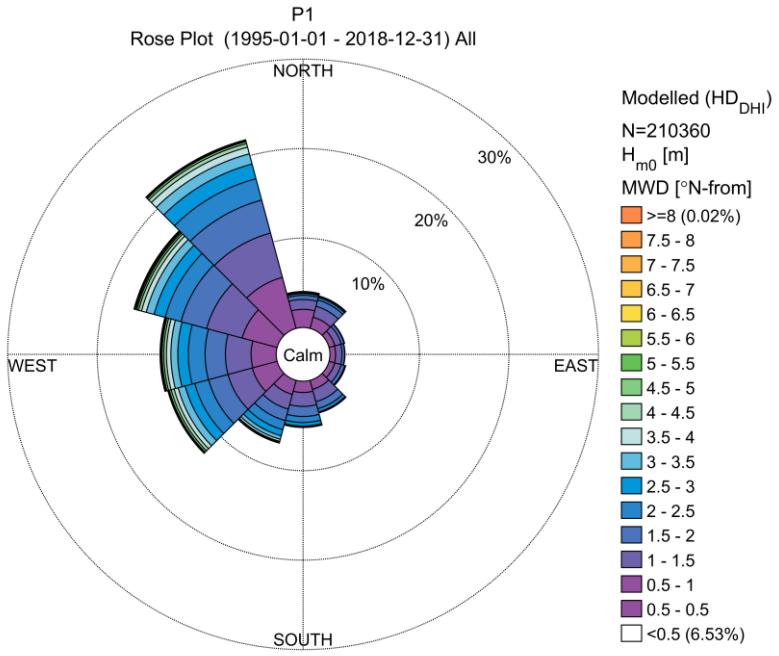

Figure 5.12 Significant wave height (H_{m0}) and mean wave direction (MWD) rose plot at P1.

5.4 Significant wave height and associated periods and water level

The largest significant wave heights (H_{m0}) are dominated by wind-sea in contrast to swell (based on DHI's experience). Hence, the fitting (regression analysis) used to derive associated periods and water levels were performed on the wind-sea part of the spectrum. Figure 5.13 and Figure 5.14 show the scatter plots of H_{m0} against T_p and T_{02} (wind-sea part), respectively. The power law form is given as:

$$T_{p,Sea} = a\,(\frac{H_{m0}}{[\mathrm{m}]})^b \text{ and } T_{02,Sea} = a\,(\frac{H_{m0}}{[\mathrm{m}]})^b$$

5%, 50% and 95% quantiles with fit parameters, *a* and *b* for $T_{p,Sea}$ and $T_{02,Sea}$ are given in Table 5.6 to Table 5.8 for P1, P2 and P3, respectively.

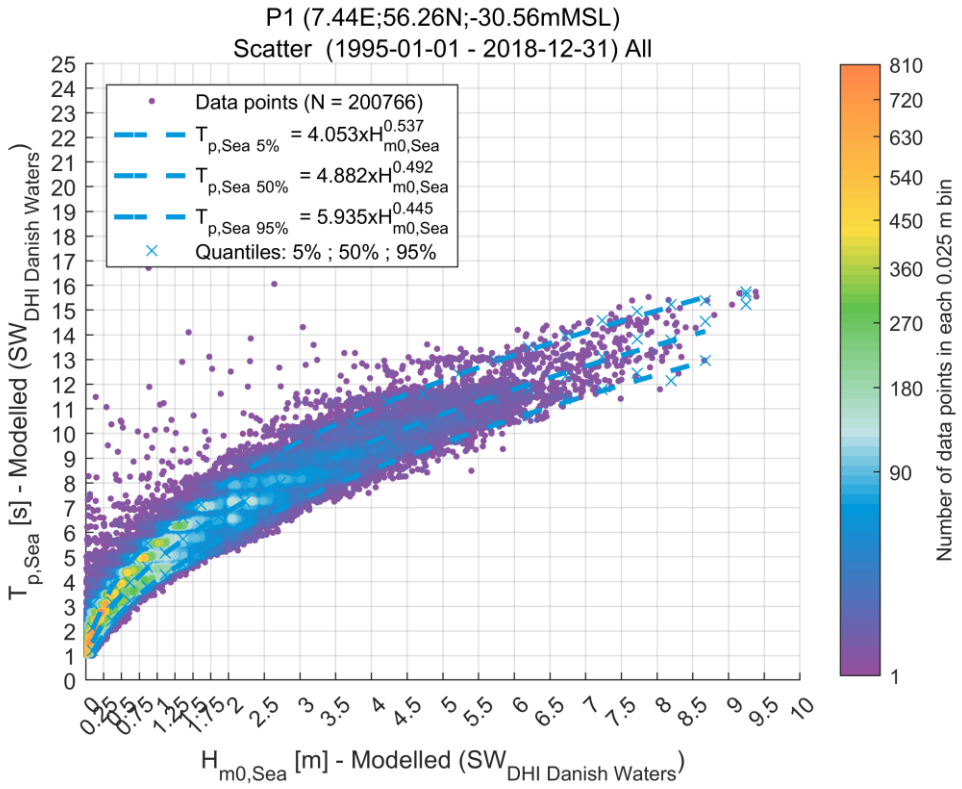

Figure 5.13 Scatter plot of wind-sea peak wave period ($T_{p,Sea}$) vs. wind-sea significant wave height ($H_{m0,Sea}$) at P1. Power law fits at quantiles 5%, 50% and 95% are shown in blue dashed lines.

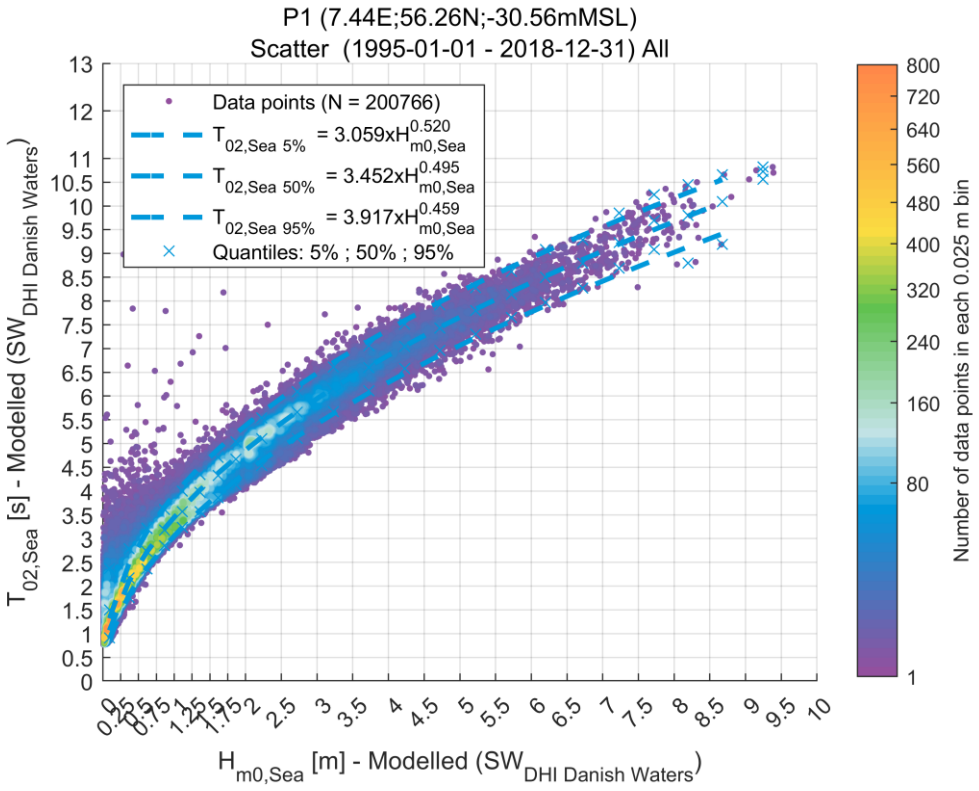

Figure 5.14 Scatter plot of wind-sea mean zero-crossing wave period ($T_{02,Sea}$) vs. wind-sea significant wave height ($H_{m0,Sea}$) at P1. Power law fits at quantiles 5%, 50% and 95% are shown in blue dashed lines.

Table 5.6 Power law fitting parameters of wind-sea peak wave period ($T_{p,Sea}$) and wind-sea mean zero-crossing wave period ($T_{02,Sea}$) vs wind-sea significant wave height ($H_{m0,Sea}$) at P1 for 5%, 50% and 95% quantiles.

P1	a [s]	b [-]
$T_{p,Sea}$ [s] - 5%	4.05	0.54
$T_{p,Sea}$ [s] - 50%	4.88	0.49
$T_{p,Sea}$ [s] - 95%	5.94	0.45
$T_{02,Sea}$ [s] - 5%	3.06	0.52
$T_{02,Sea}$ [s] - 50%	3.45	0.50
$T_{02,Sea}$ [s] - 95%	3.92	0.46

Table 5.7 Power law fitting parameters of wind-sea peak wave period ($T_{p,Sea}$) and wind-sea mean zero-crossing wave period ($T_{02,Sea}$) vs wind-sea significant wave height ($H_{m0,Sea}$) at P2 for 5%, 50% and 95 quantiles.

P2	a [s]	b [-]
$T_{p,Sea}$ [s] - 5%	3.92	0.58
$T_{p,Sea}$ [s] - 50%	4.88	0.50
$T_{p,Sea}$ [s] - 95%	5.92	0.46
$T_{02,Sea}$ [s] - 5%	2.98	0.55
$T_{02,Sea}$ [s] - 50%	3.43	0.50
$T_{02,Sea}$ [s] - 95%	3.90	0.46

Table 5.8 Power law fitting parameters of wind-sea peak wave period ($T_{p,Sea}$) and wind-sea mean zero-crossing wave period ($T_{02,Sea}$) vs wind-sea significant wave height ($H_{m0,Sea}$) at P3 for 5%, 50% and 95% quantiles.

P3	a [s]	b [-]
$T_{p,Sea}$ [s] - 5%	4.09	0.54
$T_{p,Sea}$ [s] - 50%	4.91	0.50
$T_{p,Sea}$ [s] - 95%	5.91	0.46
$T_{02,Sea}$ [s] - 5%	3.04	0.52
$T_{02,Sea}$ [s] - 50%	3.45	0.50
$T_{02,Sea}$ [s] - 95%	3.91	0.46

Scatter plot of water level vs significant wave height (H_{m0}) at P1 is shown in Figure 5.15. There is a clear positive correlation between H_{m0} and water level. Up to H_{m0}~3m there is still a relatively high occurrence of negative water levels while all waves with H_{m0}>6m occurs during positive water level (which is effectively the surge generated by strong winds).

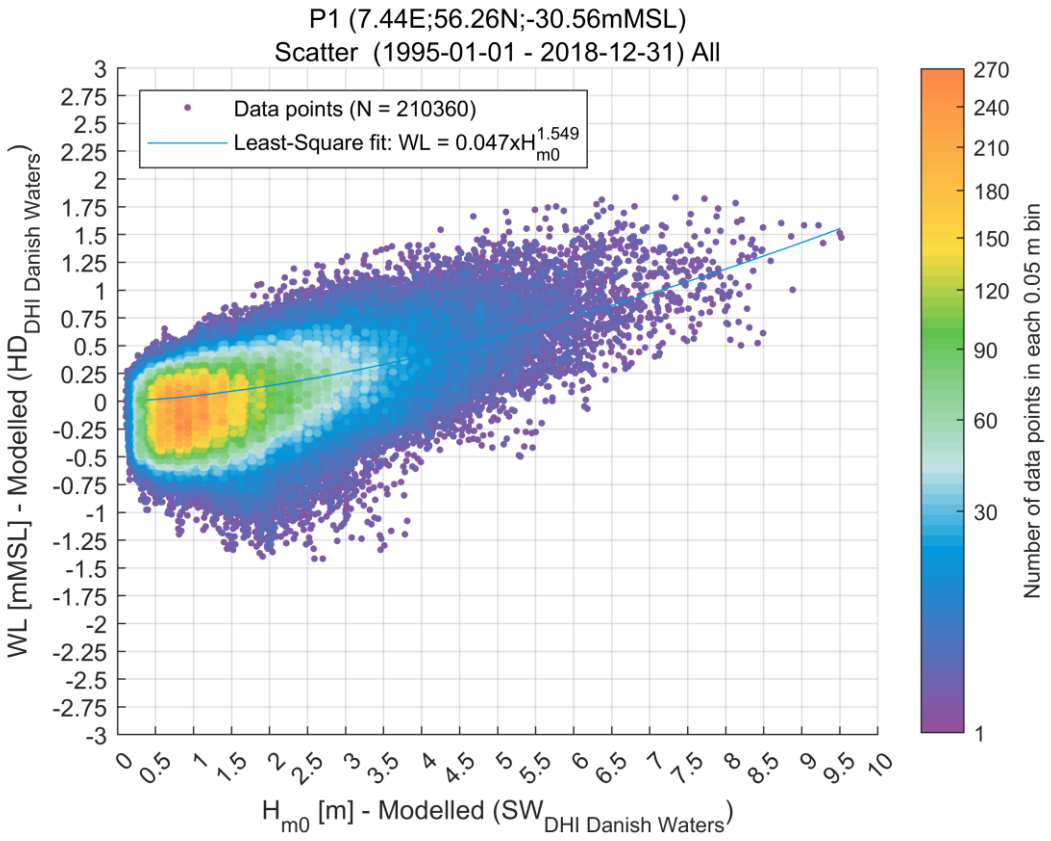

Figure 5.15 Scatter plot of water level vs significant wave height (H_{m0}) at P1.

6 Extreme Conditions

Extreme Value Analysis (EVA) is performed for the three analysis points P1, P2 and P3 for the return periods 1-year, 50-years and 100-years. All extreme values are omnidirectional. Figures are only provided in this section for P1. Figures for P2 and P3 can be found in Appendix B. Specific details about EVA methodology can be found in Appendix C.

A summary of the EVA results is also given in the Executive Summary at the start of the report.

6.1 Significant wave height, H_{m0}

A sensitivity analysis of the extreme significant wave height (H_{m0}) with a return period of 100-years has been carried out at the three points P1, P2 and P3. Various distribution types, fitting methods (least squares and maximum likelihood) were tested. An overview of these tests is shown in Figure 6.1. A spread of 2m in H_{m0} from 9.5m to 11.5m is observed. From individual inspection of how well the various distributions fitted data (24 years) the best fit at all three points were obtained with a 2-p Weibull distribution with two annual peaks and least squares fit. The distribution fit at P1 is presented in Figure 6.2. Given the shape parameter of the fits, DHI considers the fit to be slightly conservative for high return periods.

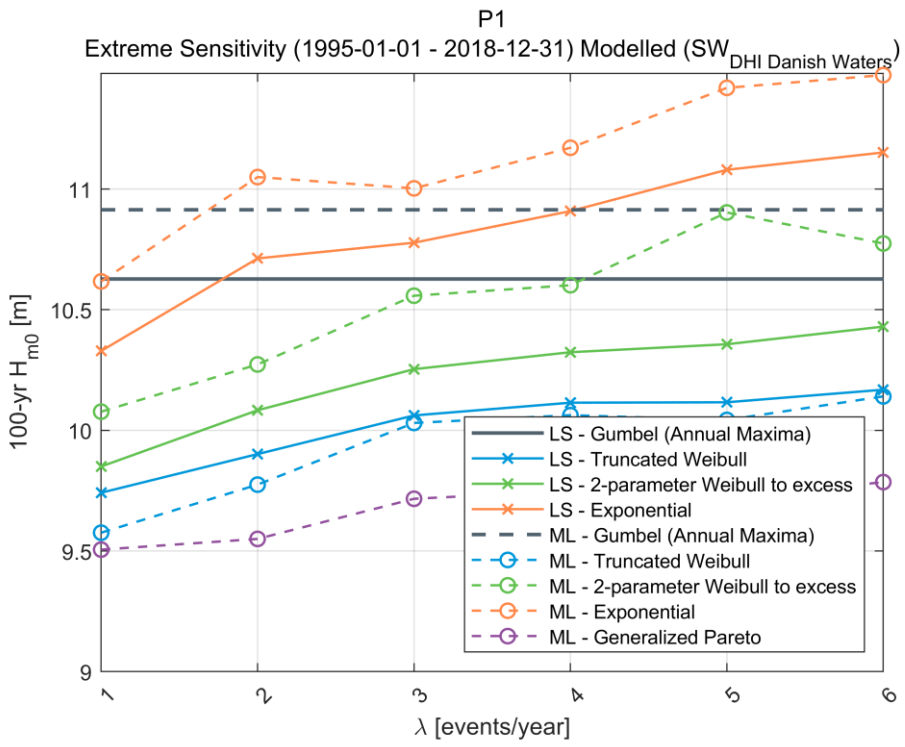

Figure 6.1 Sensitivity of extreme significant wave height (H_{m0}) with a return period of 100 years to an average number of annual peaks for various distributions and fitting methods (LS: Least Squares fit, ML: Maximum Likelihood).

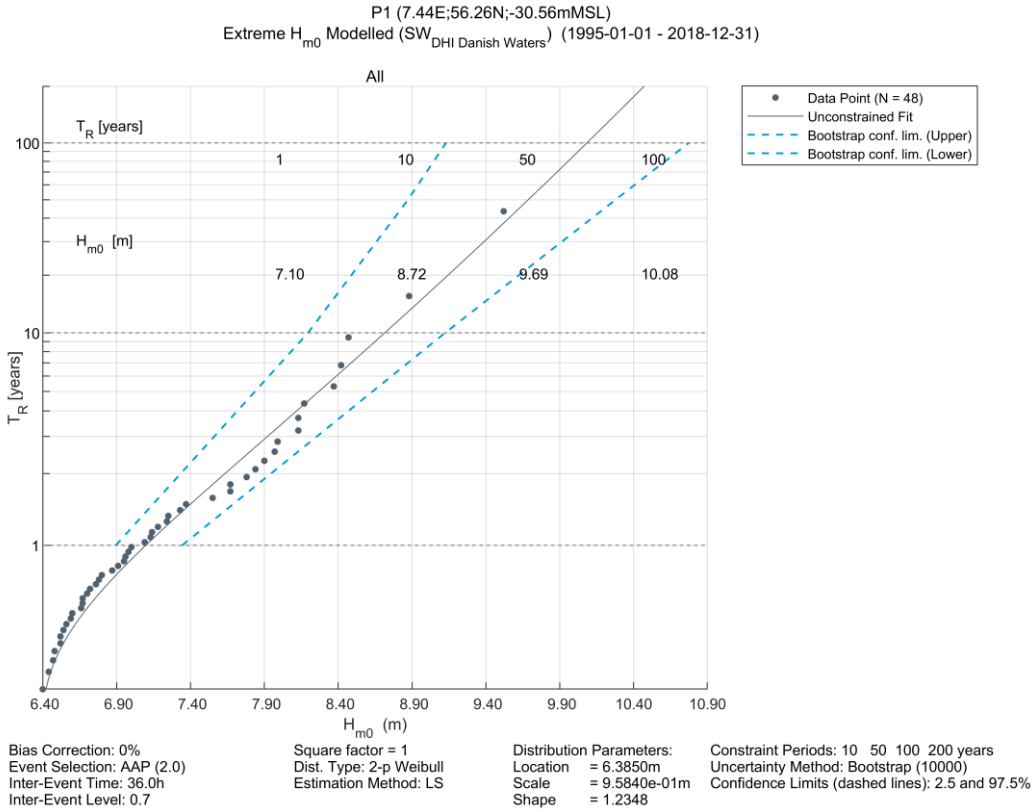

Figure 6.2 Extreme significant wave height (H_{m0}) at P1. Fit with 2-p Weibull distribution with two annual peaks and Least Squares fit. 24 years of data. Confidence bounds at 2.5% and 97.5% by bootstrapping (10000 samples).

Estimates of extreme significant wave height for 1, 50 and 100 years return period and associated lower and upper confidence intervals from bootstrapping are given in Table 6.1 to Table 6.3 for P1, P2 and P3, respectively. P1 has the largest significant wave heights while P3 has the smallest. This follows the water depth variations across the site.

Table 6.1 Extreme significant wave height (H_{m0}) with return periods of 1, 50 and 100 years at P1. Data from 1995-01-01 – 2018-12-31.

P1 – H_{m0}	1-YEAR [m]	50-YEAR [m]	100-YEAR [m]
Lower bound (2.5%)	6.9	8.9	9.1
Central Estimate	7.1	9.7	10.1
Upper bound (97.5%)	7.3	10.3	10.8

Table 6.2 Extreme significant wave height (H_{m0}) with return periods of 1, 50 and 100 years at P2. Data from 1995-01-01 – 2018-12-31.

P2 – Hm0	1-YEAR [m]	50-YEAR [m]	100-YEAR [m]
Lower bound (2.5%)	6.6	8.5	8.8
Central Estimate	6.8	9.2	9.6
Upper bound (97.5%)	7.0	9.7	10.2

Table 6.3 Extreme significant wave height (H_{m0}) with return periods of 1, 50 and 100 years at P3. Data from 1995-01-01 – 2018-12-31.

P3 – Hm0	1-YEAR [m]	50-YEAR [m]	100-YEAR [m]
Lower bound (2.5%)	6.3	8.1	8.3
Central Estimate	6.5	8.8	9.1
Upper bound (97.5%)	6.7	9.2	9.7

In Figure 6.3, the spatial map of 50-year extreme H_{m0} is shown. A 2p-Weibull distribution with an average of two annual peaks and Least Squares fit is used (based on the DHI Danish Waters wave model). The values inside the Thor OWF shape range from 8.7m to 9.7m with a trend towards lower values as the coast is approached following the bathymetry closely.

For more detailed spatial maps and lower uncertainty, DHI suggests high-resolution spectral wave modelling using detailed bathymetry at the site.

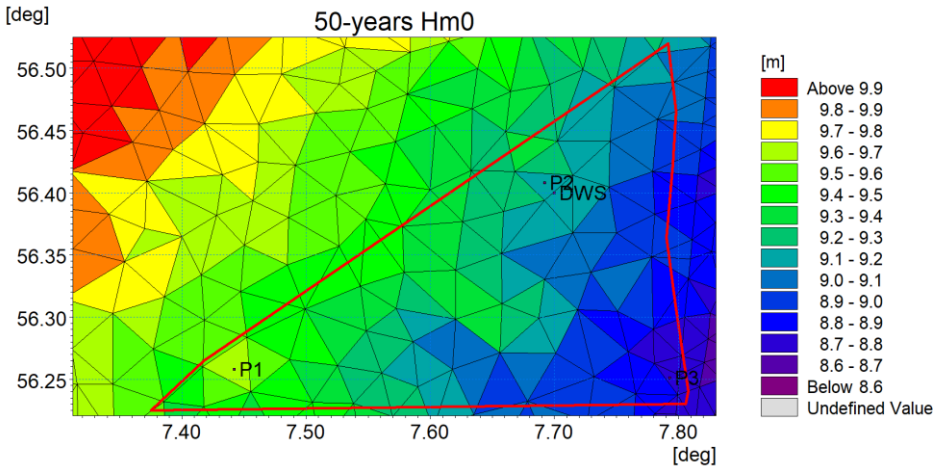

Figure 6.3 Spatial map of 50-years extreme H_{m0} from the DHI Danish Waters Model over the full Thor OWF project area (red curve). Analysis points P1, P2 and P3 and directional wave spectrum point DWS are shown. Data from 1995-01-01 – 2018-12-31.

6.2 Associated wave periods, T_p and T_{02} to extreme significant wave heights

The power law fits from Section 5.4 are used with extreme values of H_{m0} from Table 6.1 to Table 6.3 to obtain associated wave periods T_p and T_{02} to extreme H_{m0}. The fits are obtained for wind-sea only and total extreme H_{m0} are used here since no extreme analyses for wind-sea H_{m0} has been carried out, and since the wind-sea is the dominating part of the sea state for extreme H_{m0}. Values of 5%, 50% and 95% quantiles are given in Table 6.4 to Table 6.6 for P1, P2 and P3.

For later stages of the project, appropriate statistical analyses such as joint probability analyses are recommended to provide associated periods (and other parameters) to extreme significant wave heights.

Table 6.4 Associated wave period (T_p and T_{02}) to extreme H_{m0} at P1 with return periods of 1, 50 and 100 years. 5%, 50% and 95% quantiles are given.

P1	1-YEAR	50-YEAR	100-YEAR
T_p - 5% [s]	11.7	13.8	14.1
T_p - 50% [s]	12.8	14.9	15.1
T_p - 95% [s]	14.4	16.5	16.8
T_{02} - 5% [s]	8.5	10.0	10.2
T_{02} - 50% [s]	9.2	10.7	11.0
T_{02} - 95% [s]	9.7	11.1	11.4

Table 6.5 Associated wave period (T_p and T_{02}) to extreme H_{m0} at P2 with return periods of 1, 50 and 100 years. 5%, 50% and 95% quantiles are given.

P2	1-YEAR	50-YEAR	100-YEAR
T_p - 5% [s]	11.9	14.2	14.5
T_p - 50% [s]	12.7	14.8	15.1
T_p - 95% [s]	14.3	16.4	16.7
T_{02} - 5% [s]	8.5	10.1	10.3
T_{02} - 50% [s]	8.9	10.4	10.6
T_{02} - 95% [s]	9.4	10.8	11.0

Table 6.6 Associated wave period (T_p and T_{02}) to extreme H_{m0} at P3 with return periods of 1, 50 and 100 years. 5%, 50% and 95% quantiles are given.

P3	1-YEAR	50-YEAR	100-YEAR
T_p - 5% [s]	11.3	13.2	13.5
T_p - 50% [s]	12.5	14.5	14.8
T_p - 95% [s]	14.0	16.0	16.3
T_{02} - 5% [s]	8.1	9.4	9.6
T_{02} - 50% [s]	8.8	10.2	10.4
T_{02} - 95% [s]	9.3	10.6	10.8

6.3 Extreme maximum individual waves, H_{max}

The event-based method by 'Tromans and Vanderschuren' [14] has been used to determine the maximum individual wave height. It has been assumed that a Forristall distribution (see Appendix C for detail) would apply. The same extreme distribution (2p-Weibull) as for extreme H_{m0} has been used. The distribution fit for P1 is shown in Figure 6.4 with values for all points given in Table 6.7.

With H_{max} ~ 1.8-2.0 times H_{m0} and depths around 30mMSL, the wave height for the largest waves at 100 years return period are not directly limited by the water depth assuming that this will start occurring at H_{max}/d ~ 0.75 (shallow water ansatz) (Section 7.6 in [15]). The IEC 61400-3-1 gives a number H_{max}/d = 0.78 (Section B4 in [6]). Using the actual depths at P1, P2 and P3, the maximum wave heights that can exist are 23.8m, 22.8m and 21.7m, respectively (without considering the extra water depth due to high surge during extreme events). The values in Table 6.7 are all 3-4m below these margins at the 100-year return period.

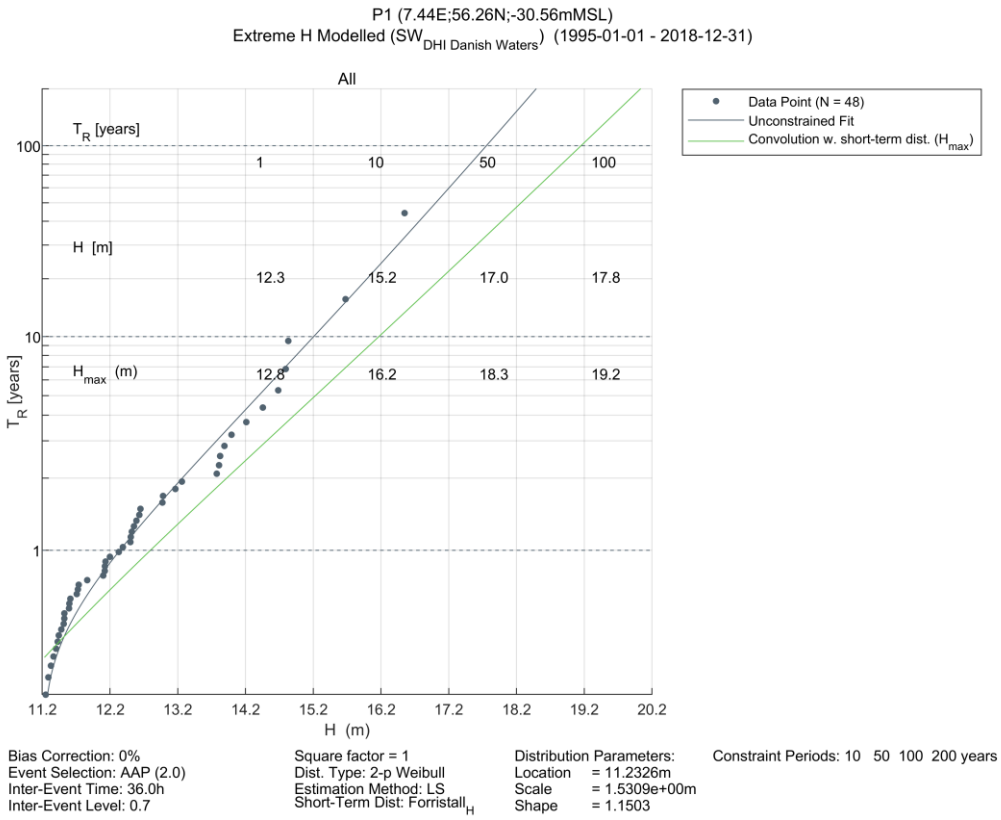

Figure 6.4 Extreme maximum individual wave height (H_{max}) at P1.

Table 6.7 Extreme maximum individual wave height (H_{max}) at P1, P2 & P3 with return periods of 1, 50 and 100 years at P1. Data from 1995-01-01 – 2018-12-31.

Location	H_{max} [m] central estimates		
	1-YEAR	50-YEAR	100-YEAR
P1	12.8	18.3	19.2
P2	12.2	17.4	18.2
P3	11.7	16.5	17.2

6.4 Maximum Crest Elevation, C_{max}

The 'convolution' methodology described in [14] has been used to calculate the maximum individual crest elevation. It has been assumed that wave crests follow a Forristall [16] distribution (see Appendix C for details). C_{max} is calculated relative to mean sea level (so the values contain the influence of water level variations including tide and surge). From here on the term 'Forristall' is used to distinguish it from the stream function method also being utilized

In addition to the above, Fenton's stream function theory for a single wave [17] [18] has been applied to quantify the limiting wave for the 50- and 100-year return periods. Using stream function theory, it is assumed that C_{max} and H_{max} occur for the same individual wave and that its associated period T_{max} is 0.8-1.1 times T_p (rough estimation based on

DHI's experience) at the 50% quantile as provided in Table 6.4, Table 6.5 and Table 6.6. A current speed of 0 m/s has been used, and the water level is obtained as the difference between C_{max} estimated from the convolution method with Forristall distribution for the two reference frames MSL and SWL, respectively. This way of defining an associated water level guarantees comparison between Forristall and stream function derived C_{max} values based on similar vertical reference level. Functional C_{max} is calculated as

$$C_{max,MSL} = \max\left(Z_{\psi}(D + WL, H, T)\right) + WL,$$

where Z_{ψ} is the crest elevation from stream function theory in SWL as a function of wave height (H), period (T) and water depth (D+WL). The stream function input values and solutions are provided in Table 6.8 and Table 6.9 for the 50-year and 100-year extremes, respectively.

Table 6.8 Stream function input parameters for 50-year return period extreme (depth , Water level (WL), wave height (H_{max}) and associated period (T_{max})) and solution (C_{max}).

50-YEAR					
Location	**Depth [mMSL]**	**WL [mMSL]**	**H_{max} [m]**	**T_{max} [s]**	**C_{max} [mMSL]**
P1	30.6	1.6	18.3	11.9-16.4	14.5-15.1
P2	29.2	1.7	17.4	11.8-16.3	13.9-14.5
P3	27.8	1.8	16.5	11.6-16.0	13.3-13.9

Table 6.9 Stream function input parameters for 100-year return period extreme (depth , Water level (WL), wave height (H_{max}) and associated period (T_{max})) and solution (C_{max}).

100-YEAR					
Location	**Depth [mMSL]**	**WL [mMSL]**	**H_{max} [m]**	**T_{max} [s]**	**C_{max} [mMSL]**
P1	30.6	1.7	19.2	12.1-16.6	15.5-16.1
P2	29.2	1.7	18.2	12.1-16.6	14.7-15.4
P3	27.8	1.9	17.2	11.8-16.3	14.1-14.7

The distribution fit (based on Forristall short-term distribution and convolution of the long-term distribution [14]) for P1 is shown in Figure 6.5 with values for all points given in Table 6.10. The maximum values from the stream function solution to C_{max} given in Table 6.8 and Table 6.9 are also provided. At all three analysis points are the stream function derived extreme C_{max} values for 50-year and 100-year return periods larger than the corresponding Forristall derived values. This means that according to the stream function theory waves with C_{max} values equal to those obtained from Forristall distribution can exist. In deep waters the two methods provide the same C_{max} values. In shallow water, however, the Forristall method might underestimate C_{max}, while there is a tendency that the stream function method overestimate C_{max}. This means that the true maximum crest elevation (C_{max}) obeys the inequality

$$C_{max,FORRISTALL} \leq C_{max} \leq C_{max,stream\ function}.$$

Values from both methods have therefore been added to the Executive Summary so that the user themselves can decide which approach to take.

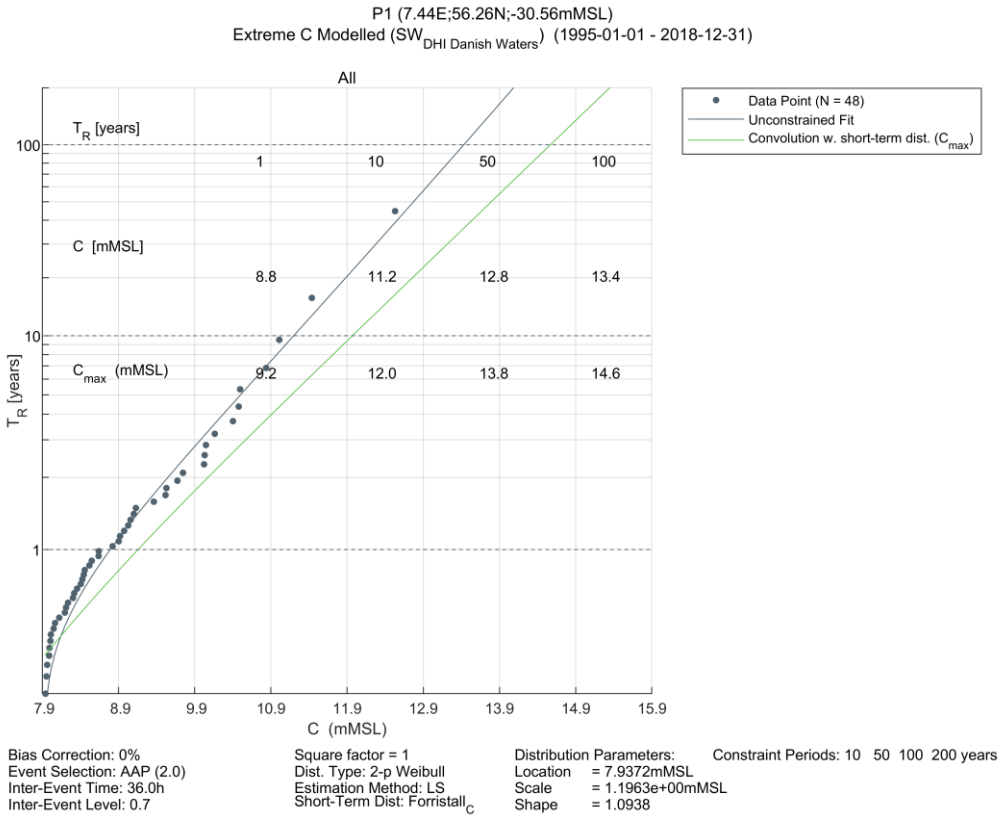

Figure 6.5 Extreme Crest elevation (C_{max}) at P1. Fit with 2-p Weibull distribution with two annual peaks and least-square-fit. 24 years of data. A short term Forristall distribution has been used for convolution (green curve).

Table 6.10 Maximum crest elevation (C_{max}) with return periods of 1, 50 and 100 years at P1. For 50-year and 100-year return periods both values from distributional fit (Forristall) and stream function theory are provided (the maximum value of the ranges provided in Table 6.8 and Table 6.9 have been used). Data from 1995-01-01 – 2018-12-31.

Location	C_{max} [mMSL] central estimates				
	1-YEAR	50-YEAR		100-YEAR	
	Forristall	Forristall	stream function	Forristall	stream function
P1	9.2	13.8	15.1	14.6	16.1
P2	8.9	13.3	14.5	14.0	15.4
P3	8.7	12.8	13.9	13.5	14.7

6.5 Depth-averaged current speed, CS

Only the total depth-averaged current speed is used for extreme value estimation, i.e. the tidal and residual components are not calculated explicitly. For example, for H_{m0}, a sensitivity study was carried out to find the optimal fitting distribution. The sensitivity of the 100-year current speed at P1 is shown in Figure 6.6. Additional visual inspections resulted in a 2-p Weibull distribution with three average annual peaks and Least Squares fit (green curve). This distribution along with bootstrap confidence bounds, are presented in Figure 6.7 for P1 and Table 6.11 to Table 6.13 contain extreme values for P1, P2 and P3, respectively.

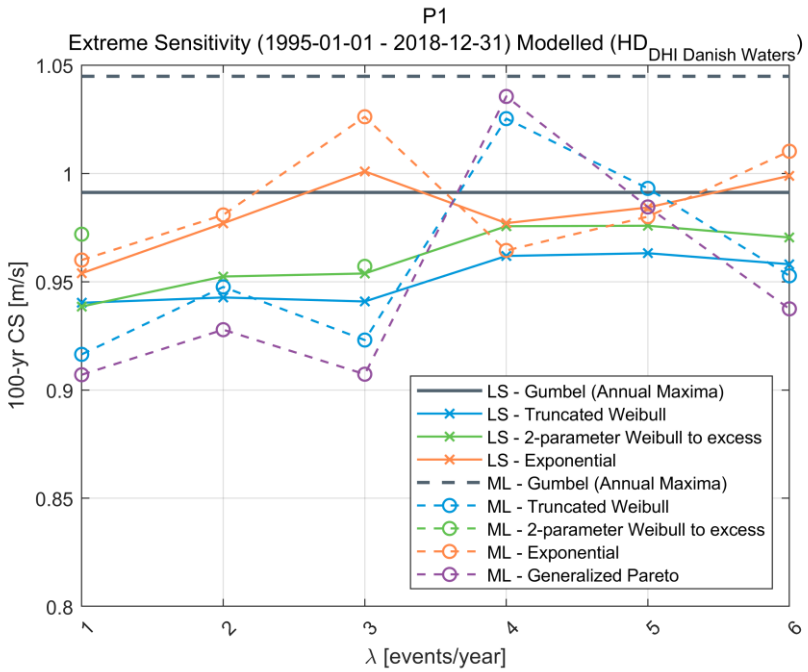

Figure 6.6 Sensitivity of extreme estimations of depth-averaged current speed (CS) at P1 with a return period of 100 years to an average number of annual peaks for various distributions and fitting methods (LS: Least Squares fit, ML: Maximum Likelihood).

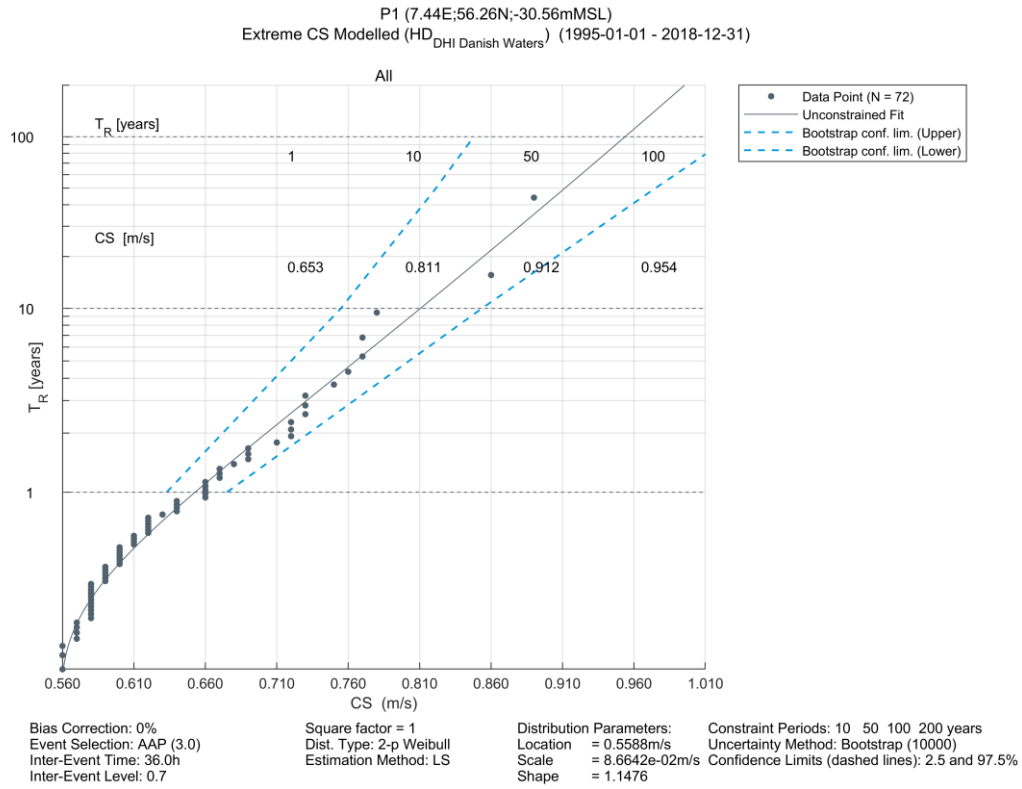

Figure 6.7 Extreme depth-averaged current speed (CS) at P1. Fit with 2-p Weibull distribution with three annual peaks and Least Squares fit. 24 years of data. Confidence bounds at 2.5% and 97.5% by bootstrapping (10000 samples).

Table 6.11 Extreme estimates of depth-averaged current speed (CS) with return periods of 1, 50 and 100 years at P1. Data from 1995-01-01 – 2018-12-31.

P1 – CS	1-YEAR [m/s]	50-YEAR [m/s]	100-YEAR [m/s]
Lower bound (2.5%)	0.6	0.8	0.9
Central Estimate	0.7	0.9	1.0
Upper bound (97.5%)	0.7	1.0	1.0

Table 6.12 Extreme estimates of depth-averaged current speed (CS) with return periods of 1, 50 and 100 years at P2. Data from 1995-01-01 – 2018-12-31.

P2 – CS	1-YEAR [m/s]	50-YEAR [m/s]	100-YEAR [m/s]
Lower bound (2.5%)	0.7	0.9	0.9
Central Estimate	0.7	0.9	1.0
Upper bound (97.5%)	0.7	1.0	1.1

Table 6.13 Extreme estimates of depth-averaged current speed (CS) with return periods of 1, 50 and 100 years at P3. Data from 1995-01-01 – 2018-12-31.

P3 – CS	1-YEAR [m/s]	50-YEAR [m/s]	100-YEAR [m/s]
Lower bound (2.5%)	0.6	0.8	0.9
Central Estimate	0.7	0.9	1.0
Upper bound (97.5%)	0.7	1.0	1.0

6.6 Water level, WL

Similar to the depth-averaged current speeds (Section 6.5), no explicit calculation based on the tidal and residual components of water level has been carried out. Only the total water level is considered for EVA.

Initially a sensitivity analysis has been carried out to find the optimal distribution for extreme water level estimation. This is shown in Figure 6.8. From this figure and from visual inspection of the individual distribution fits, the optimal distribution was found to be a 2-p Weibull distribution with four average annual peaks and Least Squares fit. This distribution is presented in Figure 6.9 for P1. The top data point (largest T_R on y-axis) is substantially lower than the fit, therefore, making the distribution somewhat conservative for high return periods. As can be observed in the sensitivity plot the difference in the 100-year water level to other types of distributions, like the truncated Weibull is very small (less than 5%).

Tables with extreme water levels for all three sites are given in Table 6.14 to Table 6.16. The extreme water level values are increased when going from P1 to P3, i.e. when the coast is approached (and shallower water depths).

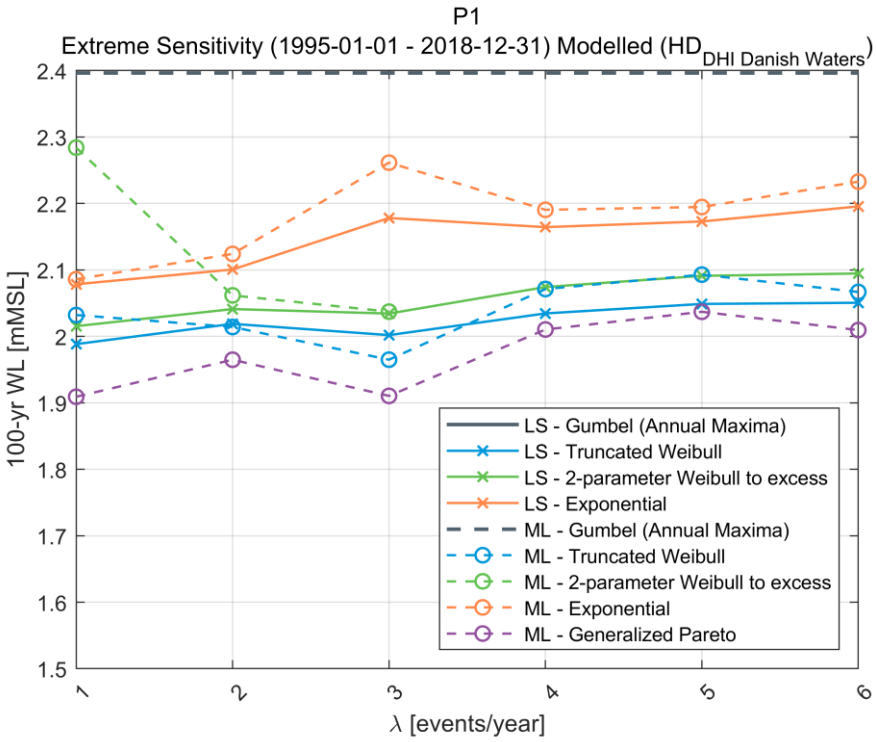

Figure 6.8 Sensitivity of extreme estimations of water level (WL) at P1 with a return period of 100 years to an average number of annual peaks for various distributions and fitting methods (LS: Least Squares fit, ML: Maximum Likelihood).

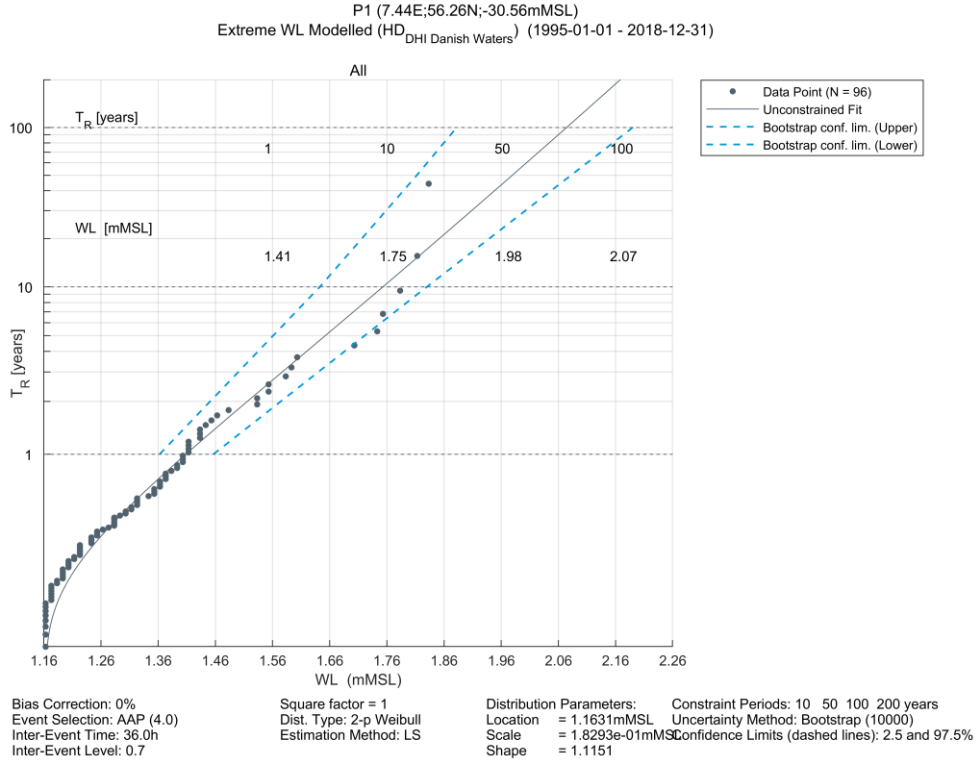

Figure 6.9 Extreme estimates of water level (WL) at P1. Fit with 2-p Weibull distribution with four annual peaks and least squares fit. 24 years of data. Confidence bounds at 2.5% and 97.5% by bootstrapping (10000 samples).

Table 6.14 Extreme estimates of water level (WL) with return periods of 1, 50 and 100 years at P1. Data from 1995-01-01 – 2018-12-31.

P1 – WL	1-YEAR [m]	50-YEAR [m]	100-YEAR [m]
Lower bound (2.5%)	1.4	1.8	1.9
Central Estimate	1.4	2.0	2.1
Upper bound (97.5%)	1.5	2.1	2.2

Table 6.15 Extreme estimates of water level (WL) with return periods of 1, 50 and 100 years at P2. Data from 1995-01-01 – 2018-12-31.

P2 – WL	1-YEAR [m]	50-YEAR [m]	100-YEAR [m]
Lower bound (2.5%)	1.5	1.9	2.0
Central Estimate	1.5	2.1	2.2
Upper bound (97.5%)	1.5	2.2	2.3

Table 6.16 Extreme estimates of water level (WL) with return periods of 1, 50 and 100 years at P3. Data from 1995-01-01 – 2018-12-31.

P3 – WL	1-YEAR [m]	50-YEAR [m]	100-YEAR [m]
Lower bound (2.5%)	1.5	2.0	2.1
Central Estimate	1.6	2.2	2.3
Upper bound (97.5%)	1.6	2.4	2.5

7 Conclusion

In this report, results of normal and extreme value analyses were provided at the Thor OWF project area. The data was based on DHI's existing regional Danish Waters Model covering the period 1995-2018 (24 years).

Validations provided at different measurement locations showed that the model performs well compared to measurements. These provided confidence in the quality of the data used for Thor OWF project area. DHI did not include any specific conservatism in the analyses as the data quality was judged to be good.

To lower the uncertainties, it is recommended to perform high resolution modelling using local bathymetry data. This will result in the more accurate spatial representation of wave heights and currents across the site. In addition, it is recommended to apply sophisticated extreme value analyses methodologies (and preferably non-stationary methods) to derive less conservative extreme values (for return periods above 100-years) and more accurate joint probabilities.

For the final design stage, DHI recommends that the below tasks are performed to meet certification criteria and provide more accurate metocean data to be used:

- DHI recommends using the high resolution CREA6 wind fields for forcing of the numerical models.
- High resolution modelling of the hydrodynamic conditions to represent the currents in more detail. Mesh convergence analysis would be recommended to obtain the best possible results in terms of accuracy and CPU time.
- High resolution modelling of wave conditions is recommended. This will help to resolve the bathymetric features and reduce uncertainties. The wave model should include the effects of water level and currents. The forcing of the high-resolution model should be with spectral data or a validated model of the North Sea (preferably using the CREA6 wind fields for better consistency).
- DHI recommends performing wave breaking assessment as there will be depth-induced breaking at Thor OWF for such return periods (see Section 9.9 of [19] as an example).
- DHI recommends that non-stationary extreme value analyses are performed to provide monthly and directional extreme values as well as accurate joint probabilities (see Section 9 of [19] as an example of such a method).

8 References

[1] DHI, “Wave and Water Level Hindcast of Danish Waters - Spectral wave and hydrodynamic modelling,” in *this link*, Hørsholm, 2019.

[2] E. B. Consortium, “EMODnet Digital Bathymetry (DTM 2018),” 10.12770/18ff0d48-b203-4a65-94a9-5fd8b0ec35f6, 2018.

[3] DHI, “RUNE D.3.3 Metocean Conditions and Wave Modelling,” DHI, 2016.

[4] N. Fery , B. Tinz and L. Gates, “Reproduction of storms over the North Sea and the Baltic with the regional reanalysis COSMO-REA6,” in *ISRR 2018, 17-19.07.2018, Bonn, https://www2.meteo.uni-bonn.de/isrr/slides/ISRR2018_Slides21_Fery.pdf*, 2018.

[5] DHI, “MetOcean Study - Wind farm zone Hollandse Kust (zuid) & Hollandse Kust (noord), v 2.3,” DHI, Copenhagen, 2017.

[6] IEC, “International Standard, Wind energy generation systems - Part 3-1: Design requirements for fixed offshore wind turbines. IEC 61400-3-1, ed.1.0,” International Electrotechnical Commission, Geneva, Switzerland, 2019.

[7] A. Peña, R. Floors , A. Sathe, S.-E. Grynning, R. Wagner, M. S. Courtney, X. G. Larsén, A. N. Hahmann and C. B. Hasager, “Ten Years of Boundary-Layer and Wind-Power,” *Boundary Layer Meteorology,* vol. 150, pp. 69-89, 2015.

[8] P. Berens, “CircStat: A MATLAB Toolbox for Circular Statistics,” *Journal of Statistical Software,* vol. 31, no. 10, pp. 1-21, 2009.

[9] M. A. Donelan, J. Hamilton and W. H. Hui, “Directional spectra of wind-generated ocean waves,” *Philosophical Transactions of the Royal Society A,* vol. 315, pp. 509-562, 1985.

[10] D. L. Codiga, “Unified Tidal Analysis and Prediction Using the UTide Matlab Functions, Technical Report 2011-01.,” Graduate School of Oceanography, University of Rhode Island, Narragansett, RI., 2011.

[11] R. Pawlowicz, B. Beardsley and S. Lentz, “Classical tidal harmonic analysis including error estimates in MATLAB using T-TIDE,” vol. 28, no. pp 929-937, 2002.

[12] K. E. Leffler and D. A. Jay, “Enhancing tidal harmonic analysis: Robust (hybrid L-1/L-2) solutions,” vol. 29, no. pp. 78-88, 2009.

[13] M. G. G. Foreman, J. Y. Cherniawsky and V. A. Ballantyne, “Versatile Harmonic Tidal Analysis: Improvements and Applications.,”,” vol. 26, no. pp. 806-817, 2009.

[14] P. S. Tromans and L. Vanderschuren, “Response Based Design Conditions in the North Sea: Application of a New Method,” in *Offshore Technology Conference Texas, USA May 1995*, Texas, USA, 1995.

[15] L. H. Holthuijsen, Waves in Oceanic and Coatal Waters, Cambridge, UK: Cambridge University Press, 2007.

[16] G. Z. Forristall, “On the Statistical Distribution of Wave Heights in a Storm,” *Journal of Geophysical Research ,* vol. 83, pp. 2353-2358, 1978.

[17] J. D. Fenton, “The numerical solution of steady water wave problems,” *Computers & Geosciences,* vol. 14, pp. 357-368, 1988.

[18] J. D. Fenton, “Nonlinear Wave Theories,,” in *The Sea, Vol.9: Ocean Engineering Science*, New York, Wiley , 1990.

[19] DHI, “Metocean Desk study and database for the Dutch Wind Farm Zones- Hollandse Kust (noord) v2.4,” RVO.nl, Utrecht, 2019.

APPENDICES

Appendix A – Model Quality Indices

A Model Quality Indices

To obtain an objective and quantitative measure of how well the model data compared to the observed data, several statistical parameters, so-called quality indices (QIs), are calculated.

Prior to the comparisons, the model data is synchronized to the time stamps of the observations so that both time series had equal length and overlapping time stamps. For each valid observation, measured at time t, the corresponding model value is found using linear interpolation between the model time steps before and after t. Only observed values that had model values within ± the representative sampling or averaging period of the observations are included (e.g. for 10-min observed wind speeds measured every 10 min compared to modelled values every hour, only the observed value every hour is included in the comparison).

The comparisons of the synchronized observed and modelled data are illustrated in (some of) the following figures:

- Time series plot including general statistics
- Scatter plot including quantiles, QQ-fit and QIs (dots are coloured according to the density)
- Histogram of occurrence vs. magnitude or direction
- Histogram of bias vs. magnitude
- Histogram of bias vs. direction
- Dual rose plot (overlapping roses)
- Peak event plot including joint (coinciding) individual peaks

The quality indices are described below, and their definitions are listed in Table A1. Most of the quality indices are based on the entire dataset, and hence the quality indices should be considered averaged measures and may not be representative of the accuracy during rare conditions.

The MEAN represents the mean of modelled data, while the bias is the mean difference between the modelled and observed data. AME is the mean of the absolute difference, and RMSE is the root-mean-square of the difference. The MEAN, BIAS, AME and RMSE are given as absolute values and relative to the average of the observed data in percent in the scatter plot.

The scatter index (SI) is a non-dimensional measure of the difference calculated as the unbiased root-mean-square difference relative to the mean absolute value of the observations. In open water, an SI below 0.2 is usually considered a small difference (excellent agreement) for significant wave heights. In confined areas or during calm conditions, where mean significant wave heights are generally lower, a slightly higher SI may be acceptable (the definition of SI implies that it is negatively biased (lower) for time series with high mean values compared to time series with lower mean values (and same scatter/spreading), although it is normalised).

EV is the explained variation and measures the proportion [0 - 1] to which the model accounts for the variation (dispersion) of the observations.

The correlation coefficient (CC) is a non-dimensional measure reflecting the degree to which the variation of the first variable is reflected linearly in the variation of the second variable. A value close to 0 indicates very limited or no (linear) correlation between the two data sets, while a value close to 1 indicates a very high or perfect correlation. Typically, a CC above 0.9 is considered a high correlation (good agreement) for wave heights. It is noted that CC is 1 (or -1) for any two fully linearly correlated variables, even

if they are not 1:1. However, the slope and intercept of the linear relation may be different from 1 and 0, respectively, despite CC of 1 (or -1).

The Q-Q line slope and intercept are found from a linear fit to the data quantiles in a least-square sense. The lower and uppermost quantiles are not included on the fit. A regression line slope different from 1 may indicate a trend in the difference.

The peak ratio (PR) is the average of the N_{peak} highest model values divided by the average of the N_{peak} highest observations. The peaks are found individually for each dataset through the Peak-Over-Threshold (POT) method applying an average annual number of exceedances of 4 and an inter-event time of 36 hours. A general underestimation of the modelled peak events results in a PR below 1, while an overestimation results in a PR above 1.

An example of a peak plot is shown in Figure A1. 'X' represents the observed peaks (x-axis), while 'Y' represents the modelled peaks (y-axis), based on the POT methodology, both represented by circles ('o') in the plot. The joint (coinciding) peaks, defined as any X and Y peaks within ±36 hours[18] of each other (i.e. less than or equal to the number of individual peaks), are represented by crosses ('x'). Hence, the joint peaks ('x') overlap with the individual peaks ('o') only if they occur at the same time exactly. Otherwise, the joint peaks ('x') represent an additional point in the plot, which may be associated with the observed and modelled individual peaks ('o') by searching in the respective X and Y-axis directions, see example with red lines in Figure A1. It is seen that the 'X' peaks are often underneath the 1:1 line, while the 'Y' peaks are often above the 1:1 line.

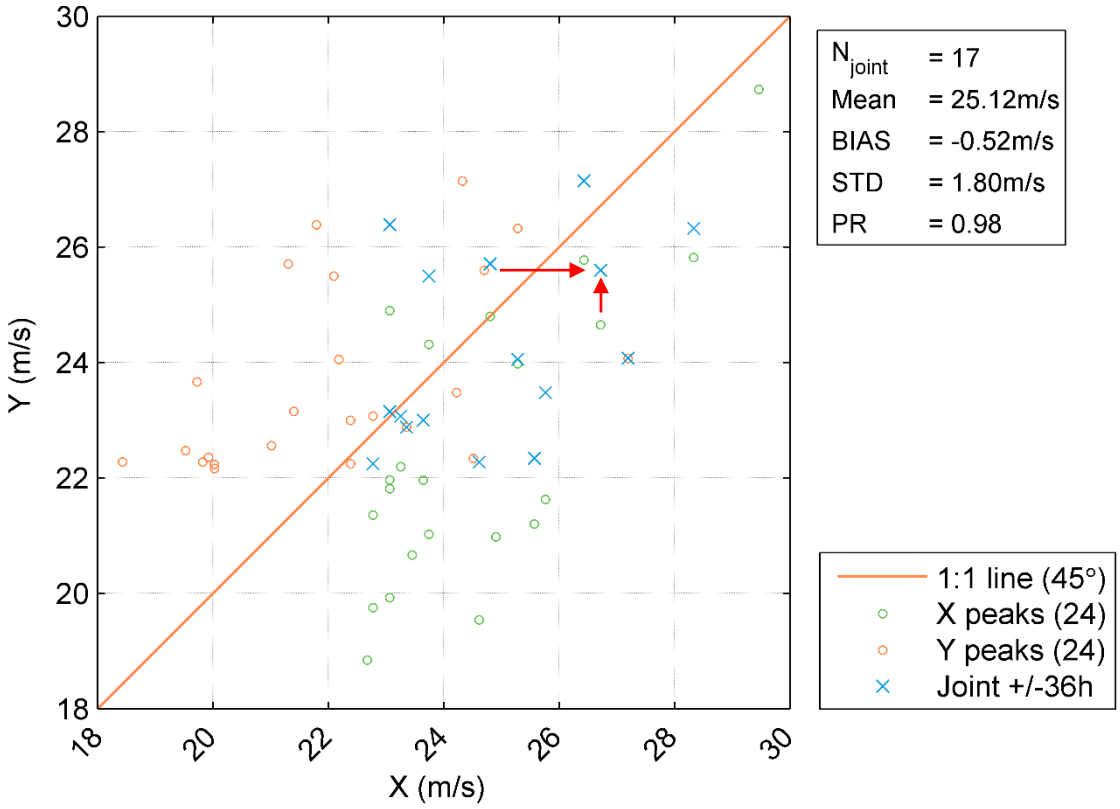

Figure A1 Example of peak event plot (wind speed)

[18] 36 hours is chosen arbitrarily as representative of an average storm duration. Often the observed and modelled storm peaks are within 1-2 hours of each other.

Table A1 Definition of model quality indices (X = Observation, Y = Model)

Abbreviation	Description	Definition
N	Number of data (synchronized)	–
MEAN	Mean of Y data Mean of X data	$\frac{1}{N}\sum_{i=1}^{N} Y_i \equiv \overline{Y}$, $\frac{1}{N}\sum_{i=1}^{N} X_i \equiv \overline{X}$
STD	Standard deviation of Y data Standard deviation of X data	$\sqrt{\frac{1}{N-1}\sum_{i=1}^{N}(Y-\overline{Y})^2}$, $\sqrt{\frac{1}{N-1}\sum_{i=1}^{N}(X-\overline{X})^2}$
BIAS	Mean difference	$\frac{1}{N}\sum_{i=1}^{N}(Y-X)_i = \overline{Y}-\overline{X}$
AME	Absolute mean difference	$\frac{1}{N}\sum_{i=1}^{N}(\lvert Y-X\rvert)_i$
RMSE	Root-mean-square difference	$\sqrt{\frac{1}{N}\sum_{i=1}^{N}(Y-X)_i^{\,2}}$
SI	Scatter index (unbiased)	$\frac{\sqrt{\frac{1}{N}\sum_{i=1}^{N}(Y-X-\mathrm{BIAS})_i^{\,2}}}{\frac{1}{N}\sum_{i=1}^{N}\lvert X_i\rvert}$
EV	Explained variance	$\frac{\sum_{i=1}^{N}(X_i-\overline{X})^2-\sum_{i=1}^{N}[(X_i-\overline{X})-(Y_i-\overline{Y})]^2}{\sum_{i=1}^{N}(X_i-\overline{X})^2}$
CC	Correlation coefficient	$\frac{\sum_{i=1}^{N}(X_i-\overline{X})(Y_i-\overline{Y})}{\sqrt{\sum_{i=1}^{N}(X_i-\overline{X})^2\sum_{i=1}^{N}(Y_i-\overline{Y})^2}}$
QQ	Quantile-Quantile (line slope and intercept)	Linear least square fit to quantiles
PR	Peak ratio (of N_{peak} highest events)	$PR = \frac{\sum_{i=1}^{N_{peak}} Y_i}{\sum_{i=1}^{N_{peak}} X_i}$

Appendix B – Figures of Data Analytics at P2 and P3

B Figures of Data Analytics at P2 and P3

B.1 Normal conditions at P2

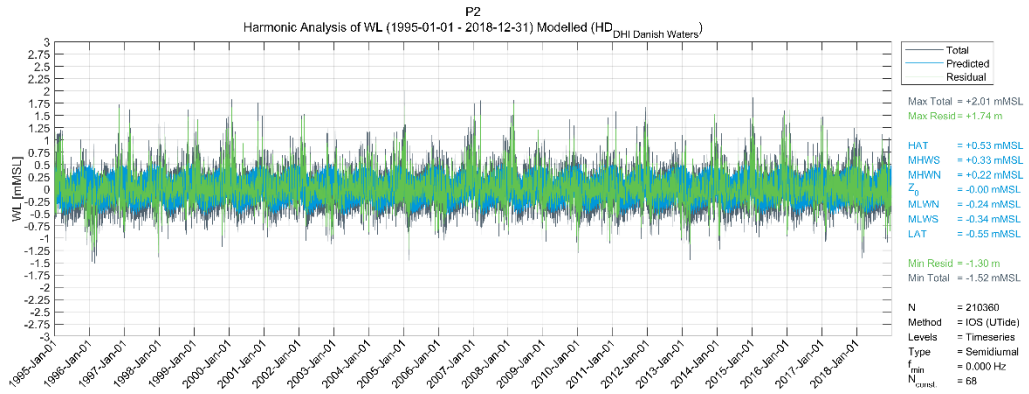

Figure B. 1

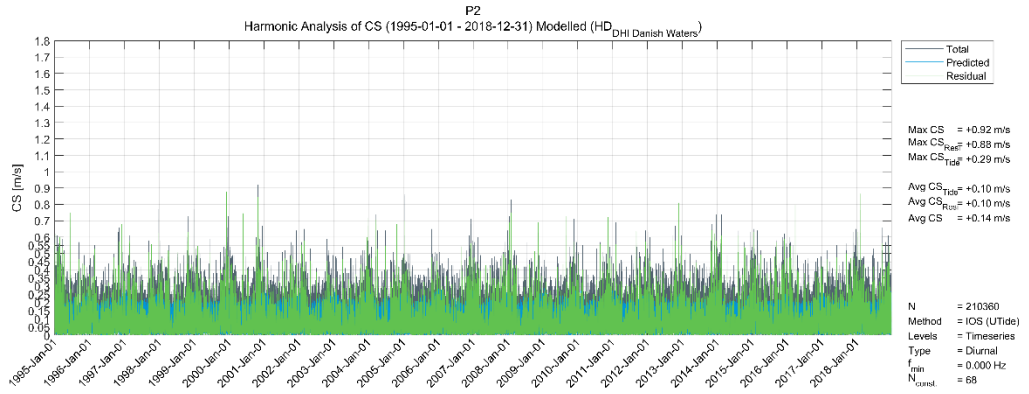

Figure B. 2

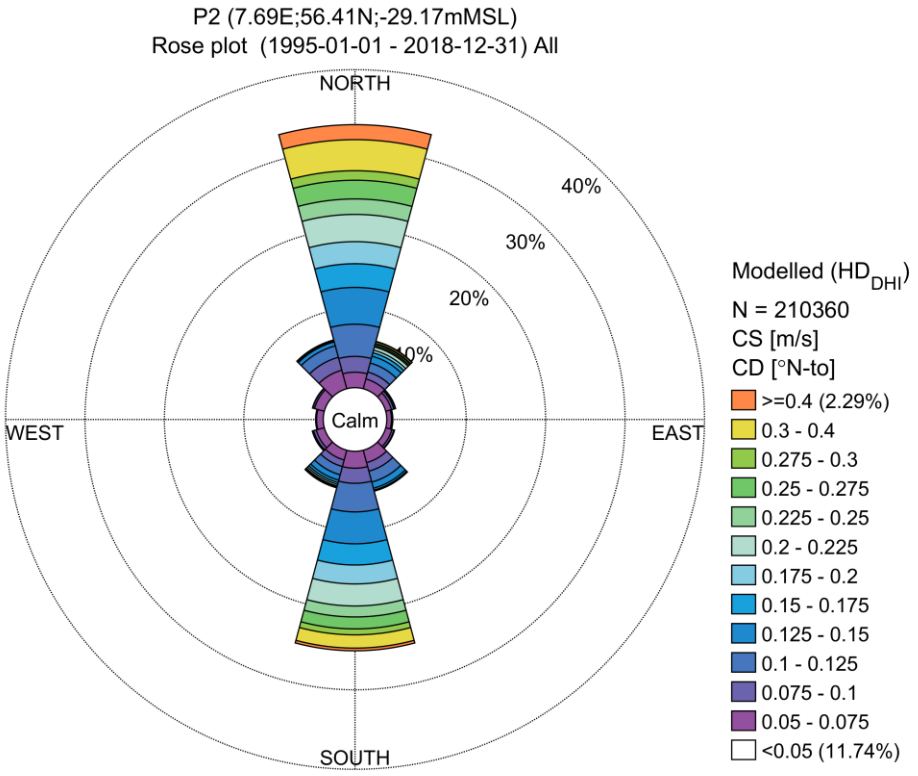

Figure B. 3

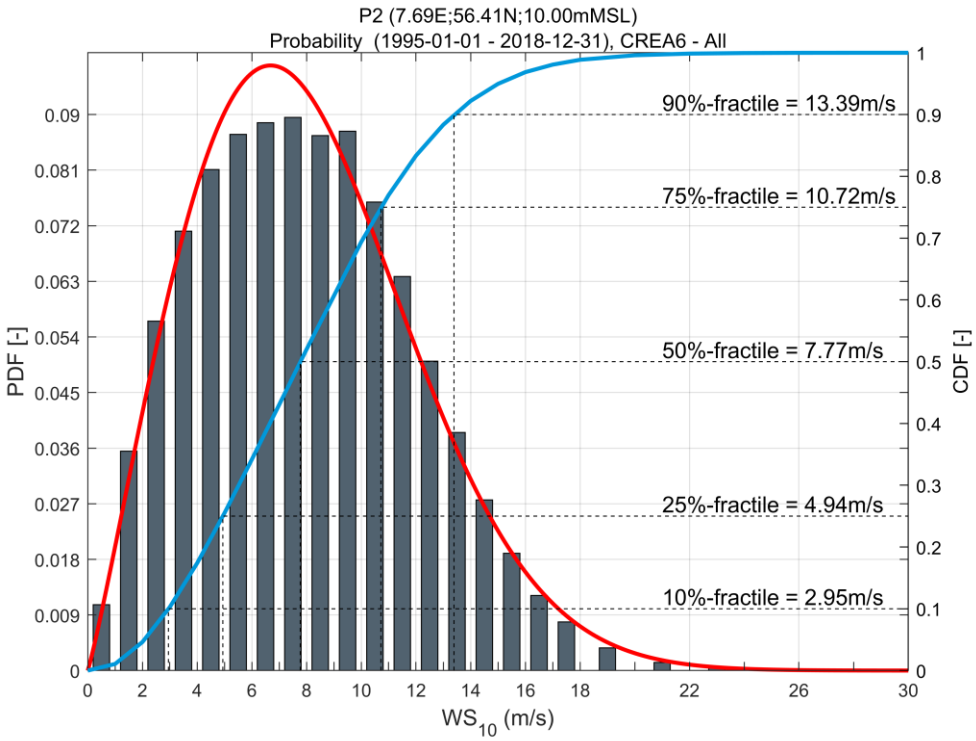

Figure B. 4

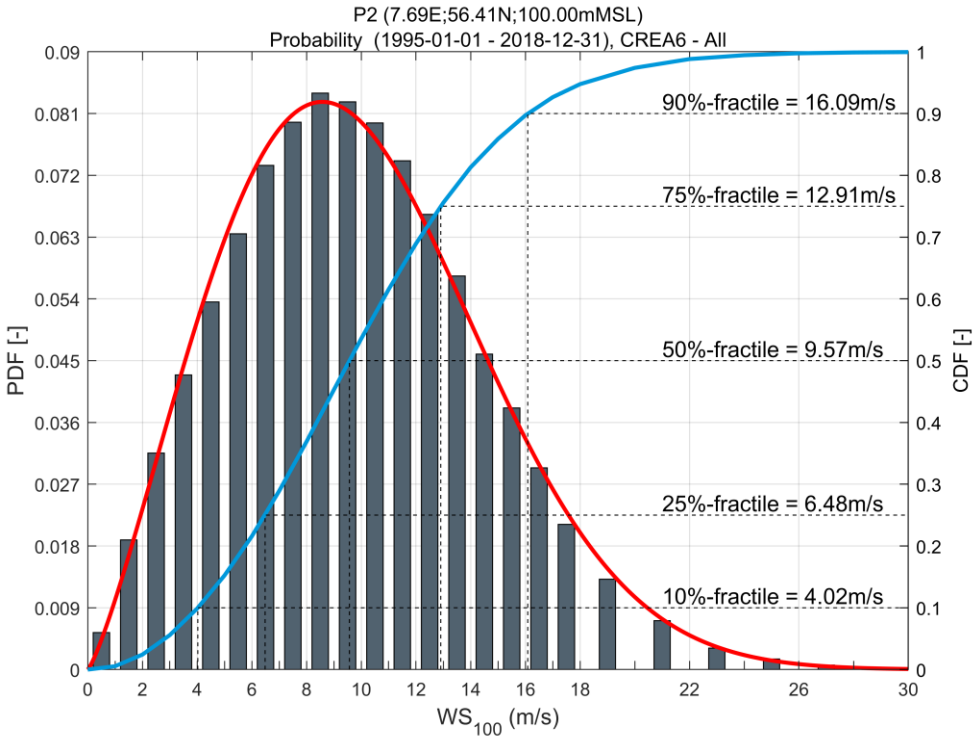

Figure B. 5

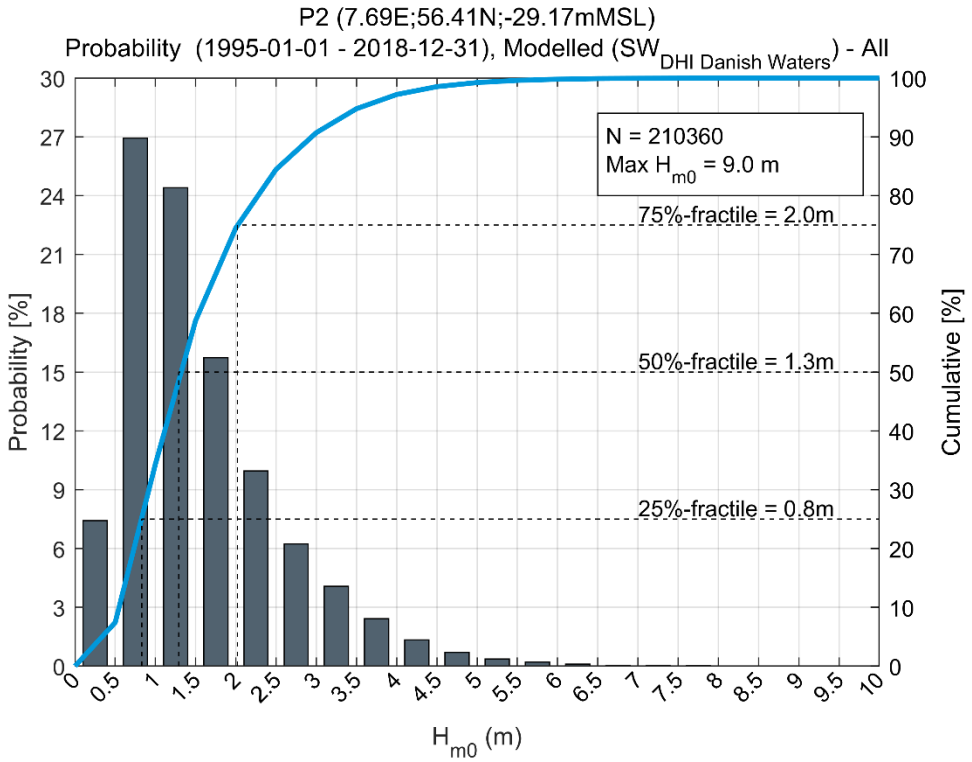

Figure B. 6

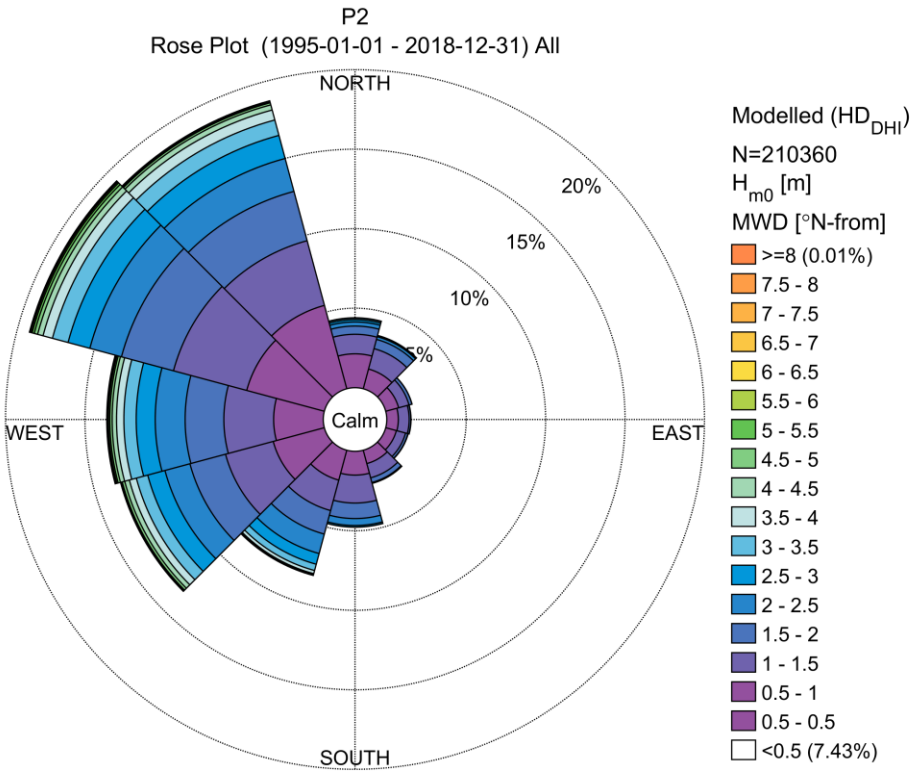

Figure B. 7

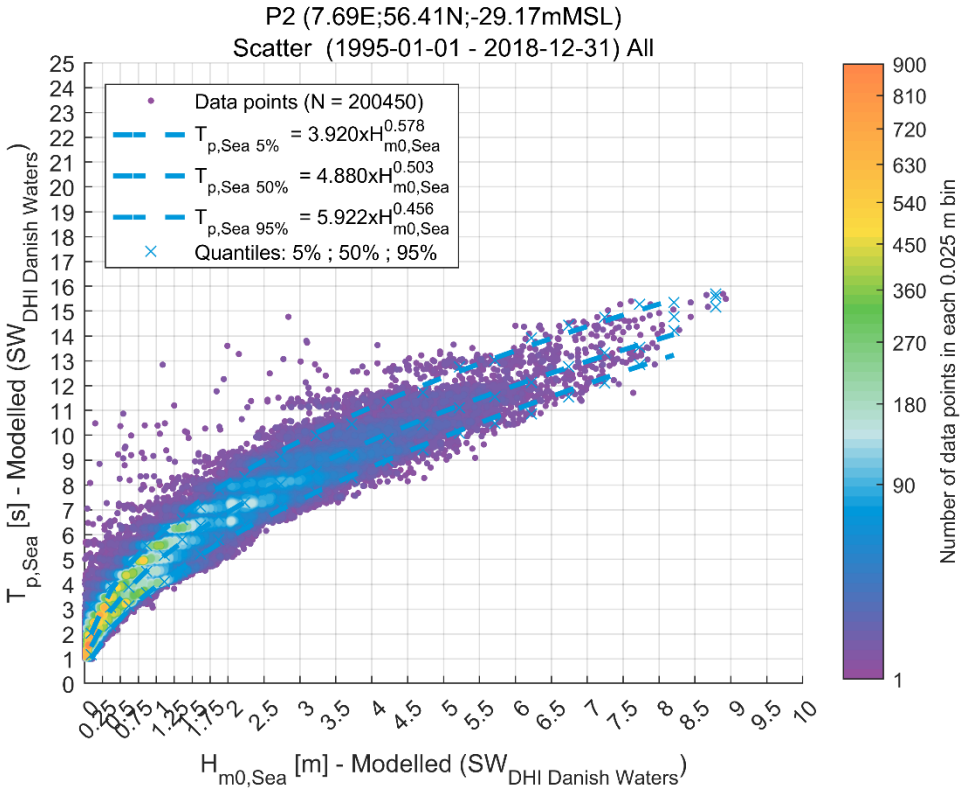

Figure B. 8

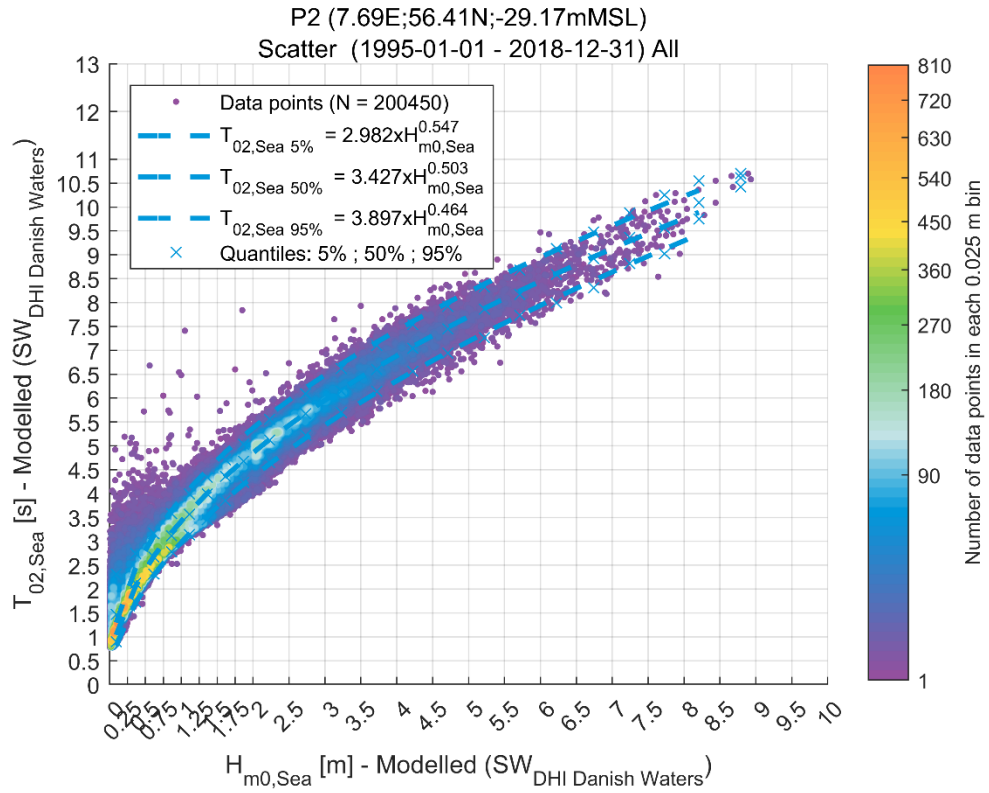

Figure B. 9

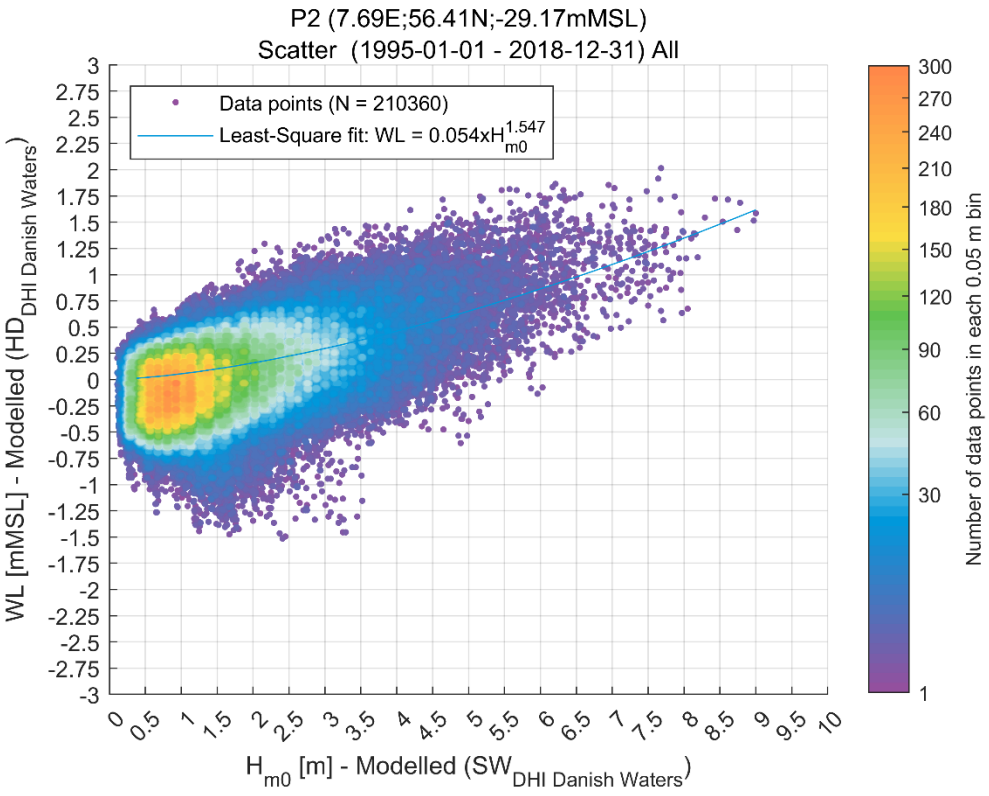

Figure B. 10

B.2 Extreme conditions at P2

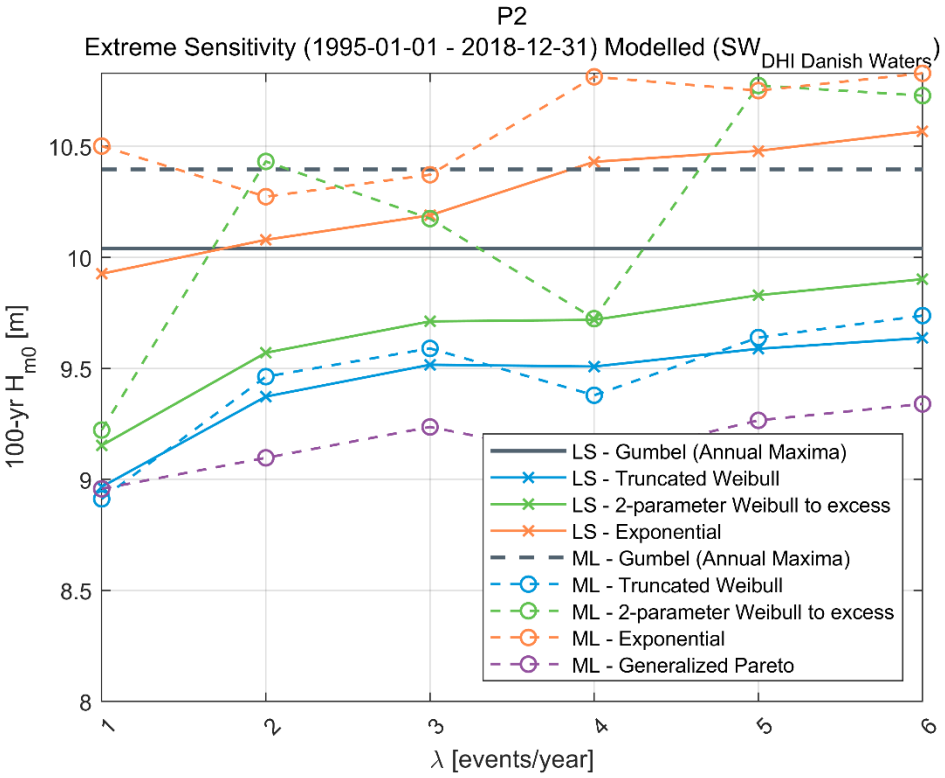

Figure B. 11

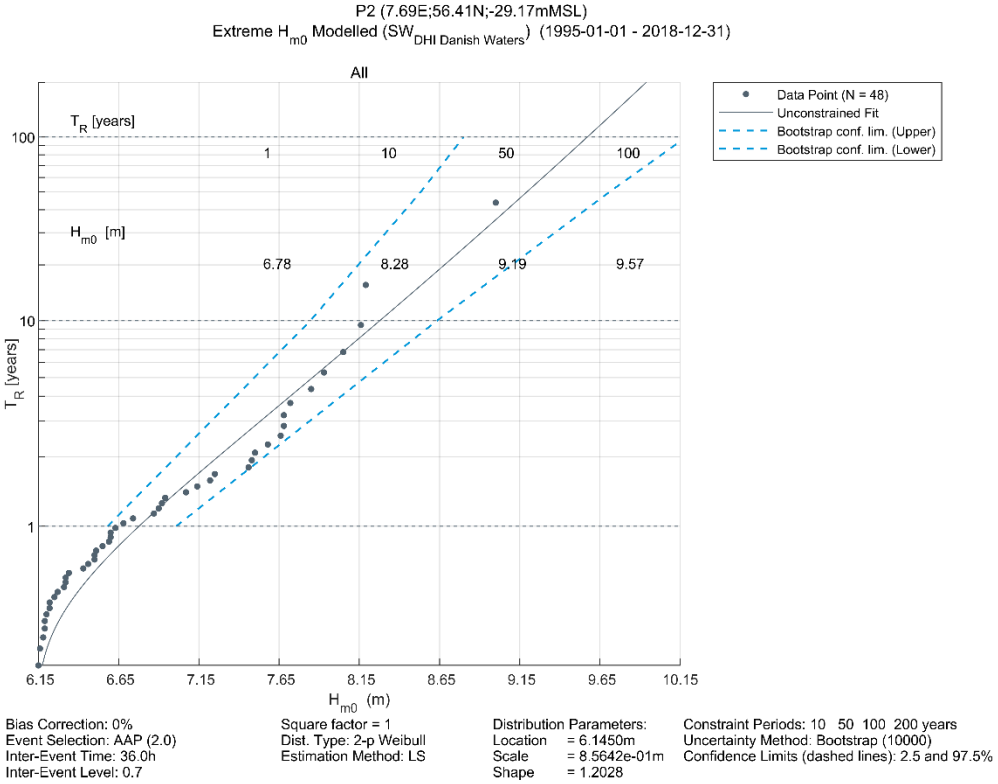

Figure B. 12

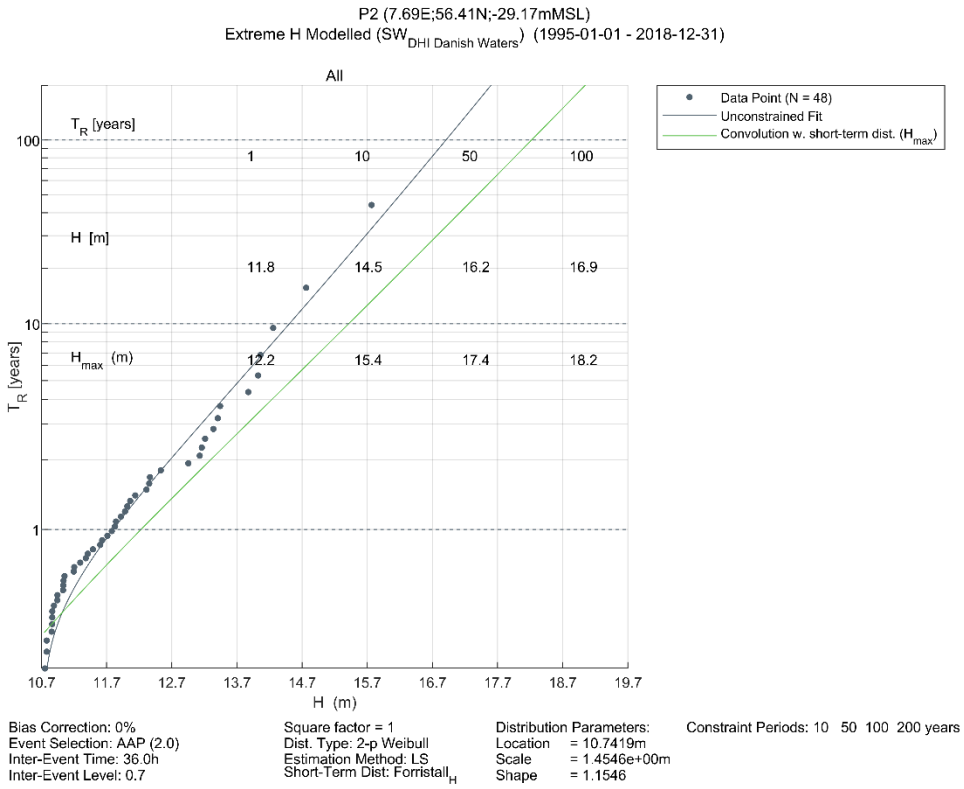

Figure B. 13

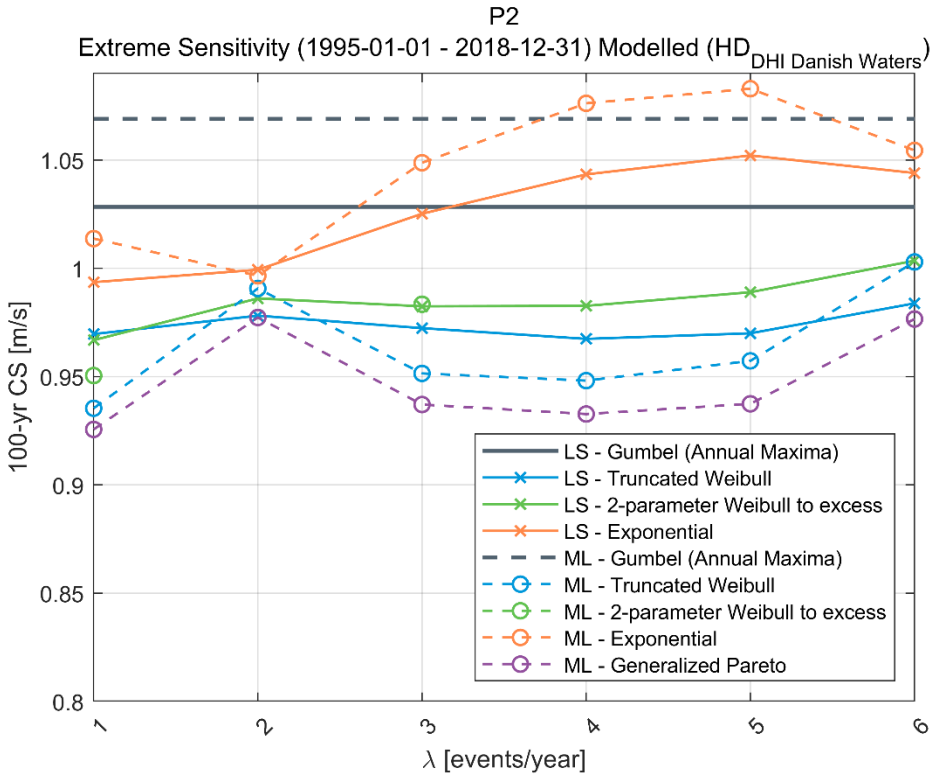

Figure B. 14

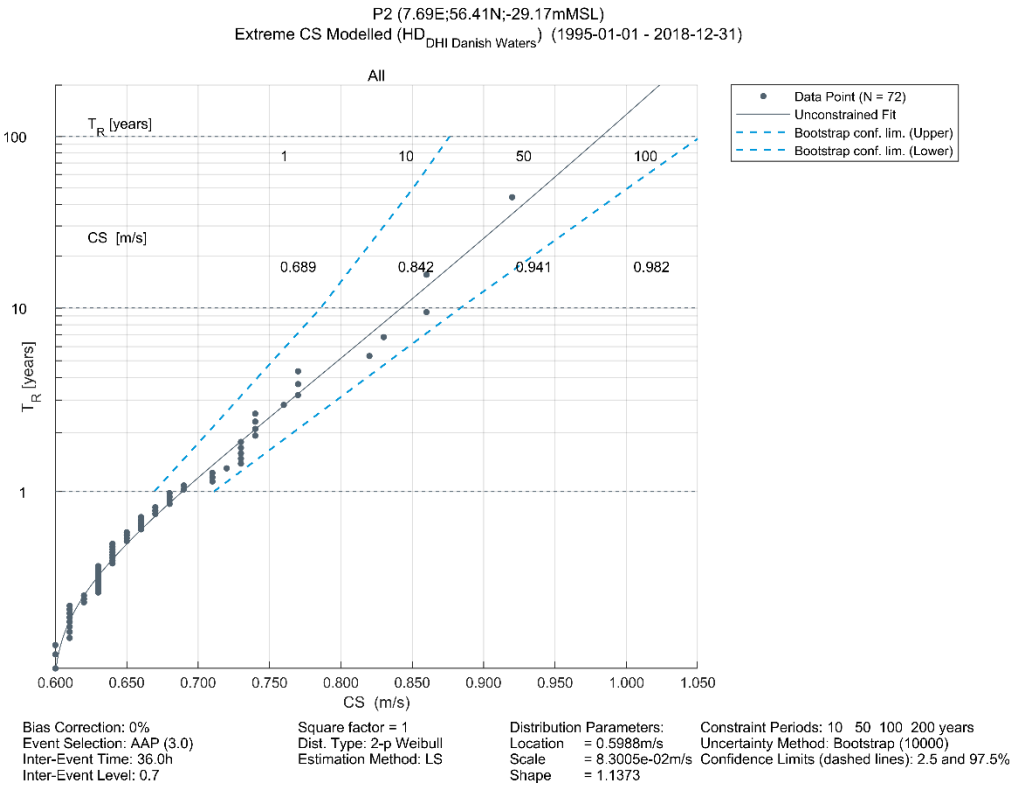

Figure B. 15

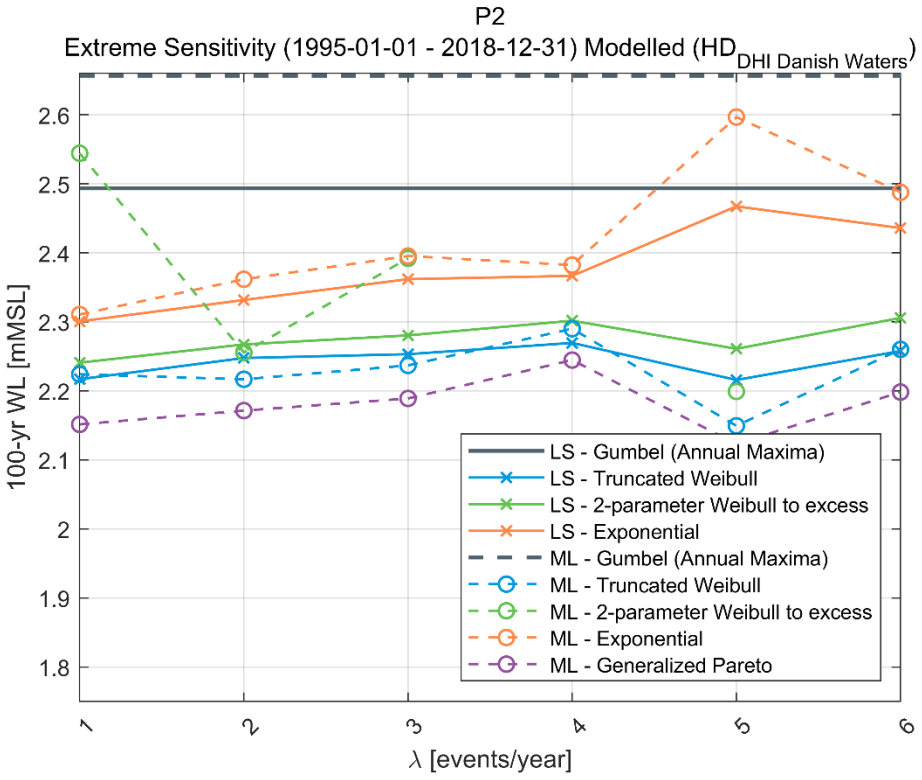

Figure B. 16

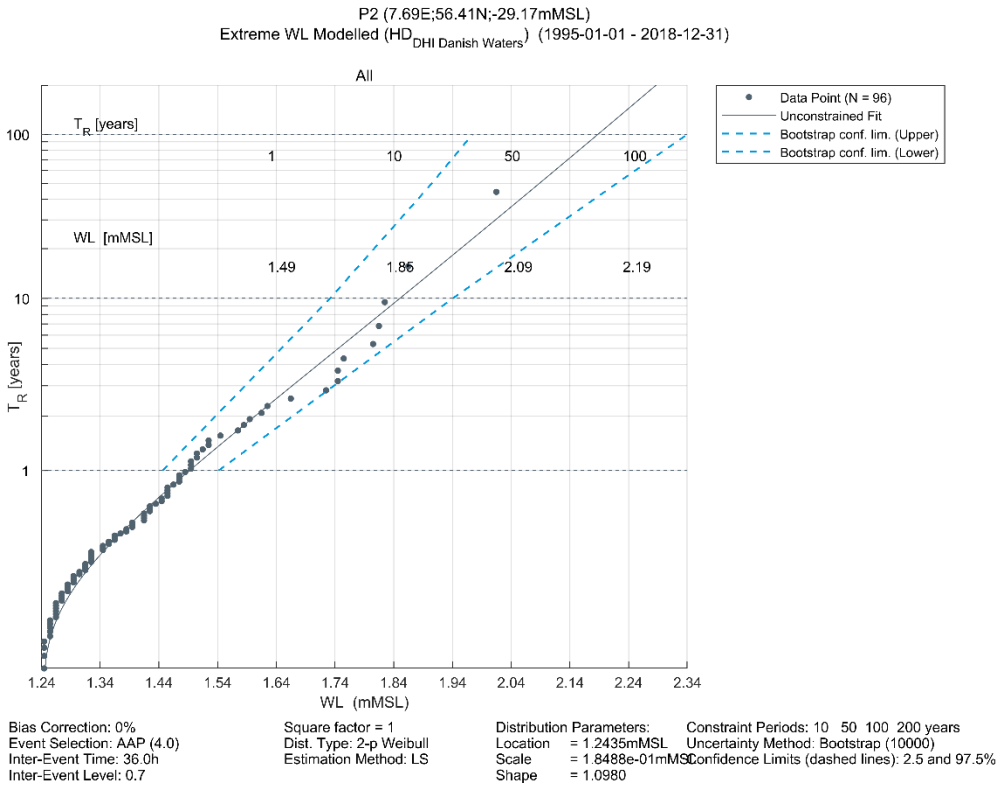
P2 (7.69E;56.41N;-29.17mMSL)
Extreme WL Modelled (HD DHI Danish Waters) (1995-01-01 - 2018-12-31)
All
Data Point (N = 96)
Unconstrained Fit
Bootstrap conf. lim. (Upper)
Bootstrap conf. lim. (Lower)
T_R [years]
WL [mMSL]
1
10
50
100
1.49
1.86
2.09
2.19
100
10
1
T_R [years]
1.24
1.34
1.44
1.54
1.64
1.74
1.84
1.94
2.04
2.14
2.24
2.34
WL (mMSL)
Bias Correction: 0%
Event Selection: AAP (4.0)
Inter-Event Time: 36.0h
Inter-Event Level: 0.7
Square factor = 1
Dist. Type: 2-p Weibull
Estimation Method: LS
Distribution Parameters:
Location = 1.2435mMSL
Scale = 1.8488e-01mMSL
Shape = 1.0980
Constraint Periods: 10 50 100 200 years
Uncertainty Method: Bootstrap (10000)
Confidence Limits (dashed lines): 2.5 and 97.5%

Figure B. 17

B.3 Normal conditions at P3

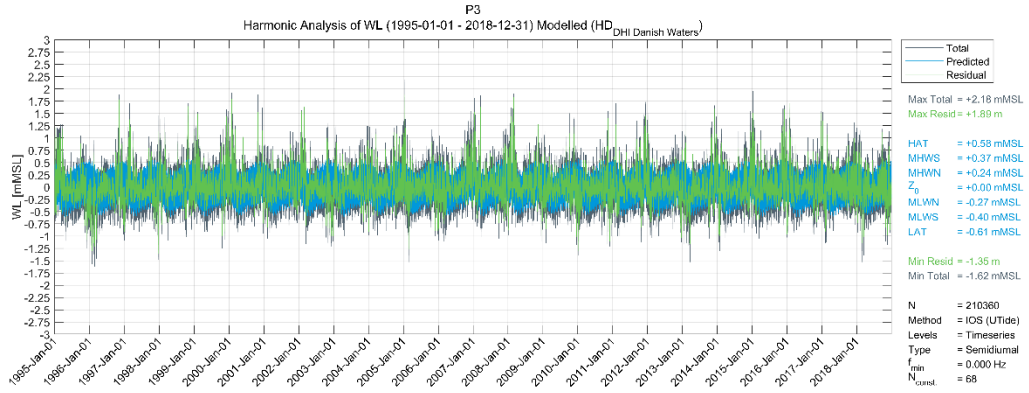

Figure B. 18

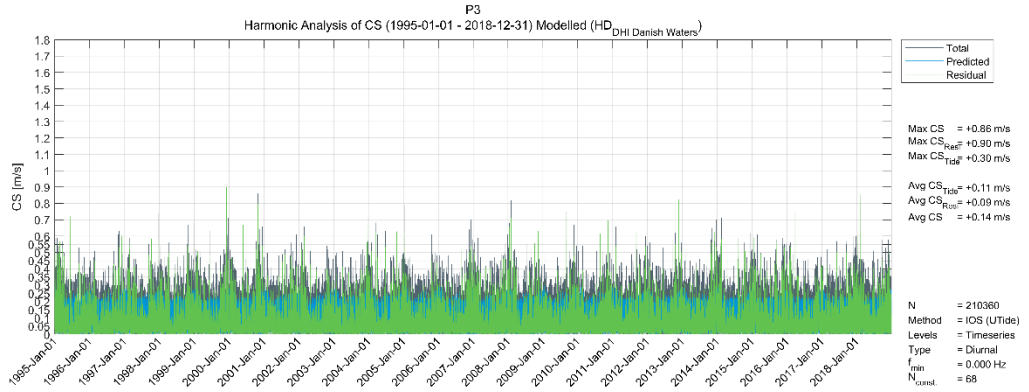

Figure B. 19

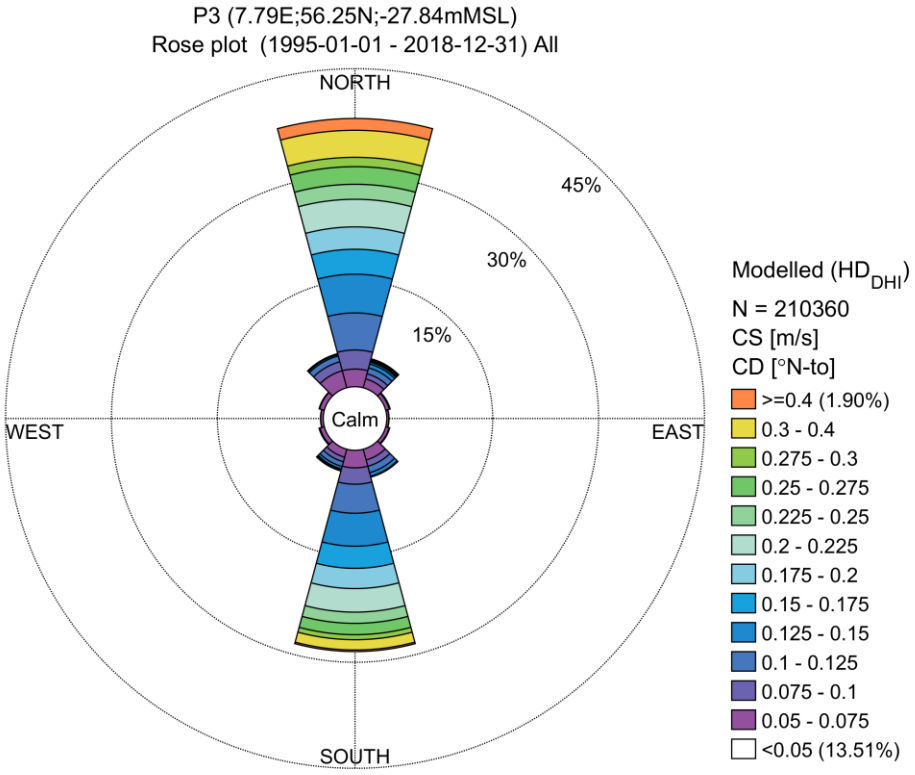

Figure B. 20

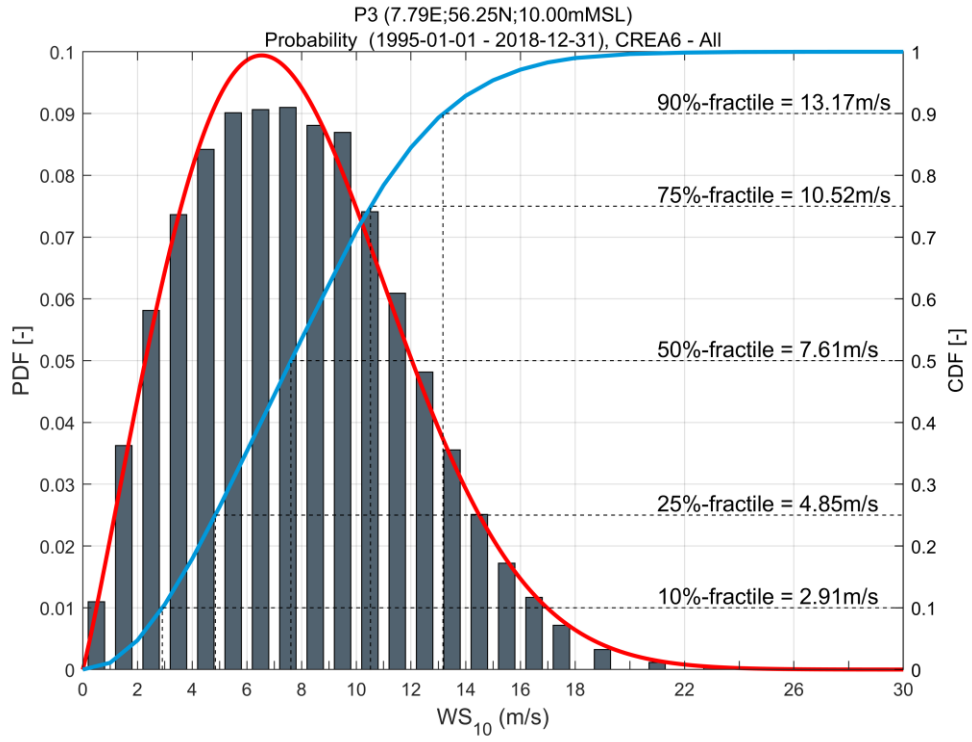

Figure B. 21

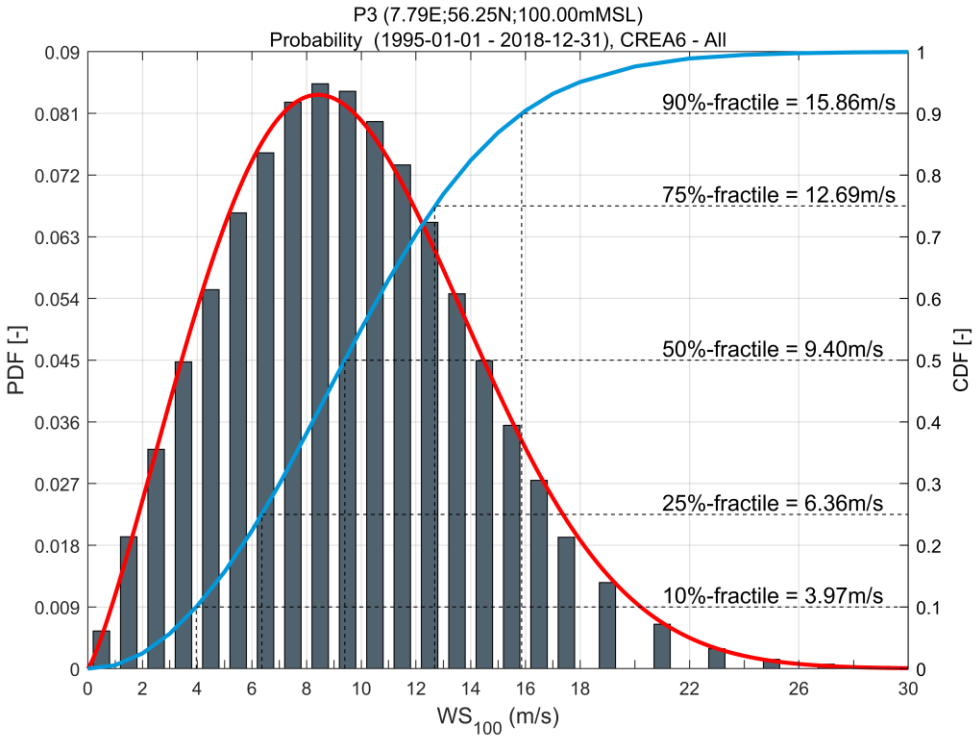

Figure B. 22

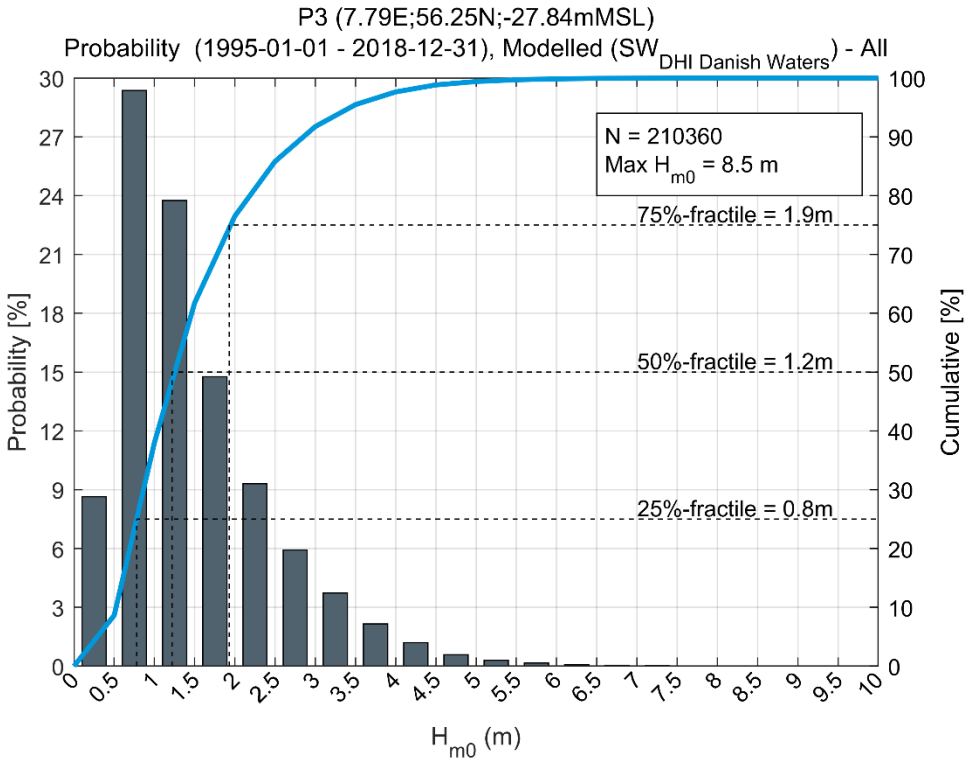

Figure B. 23

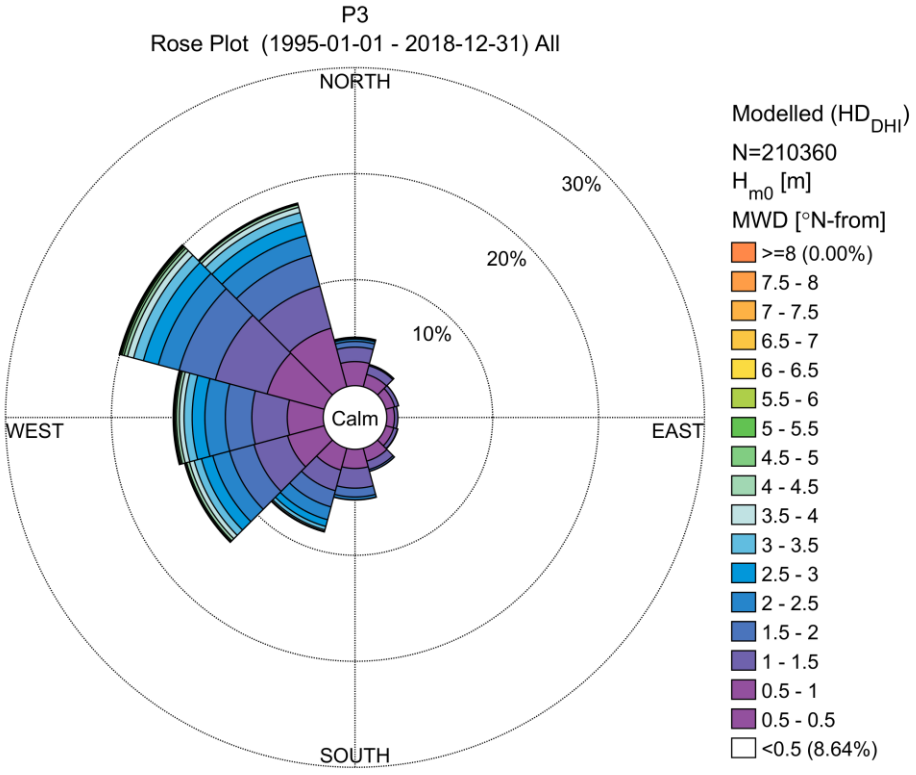

Figure B. 24

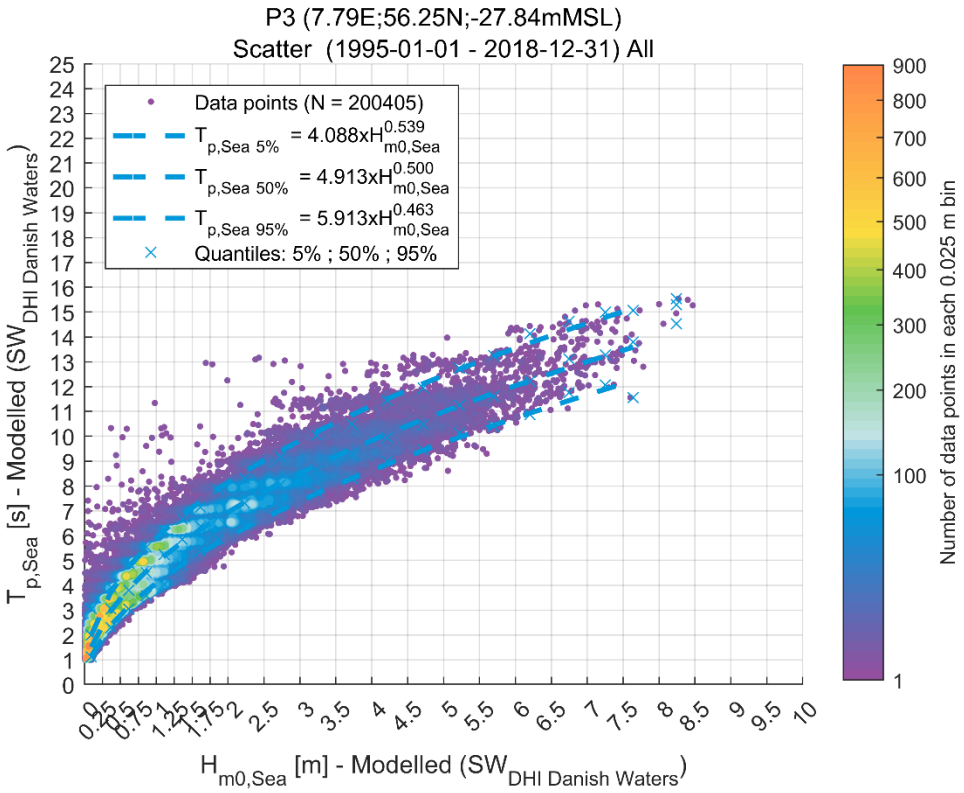

Figure B. 25

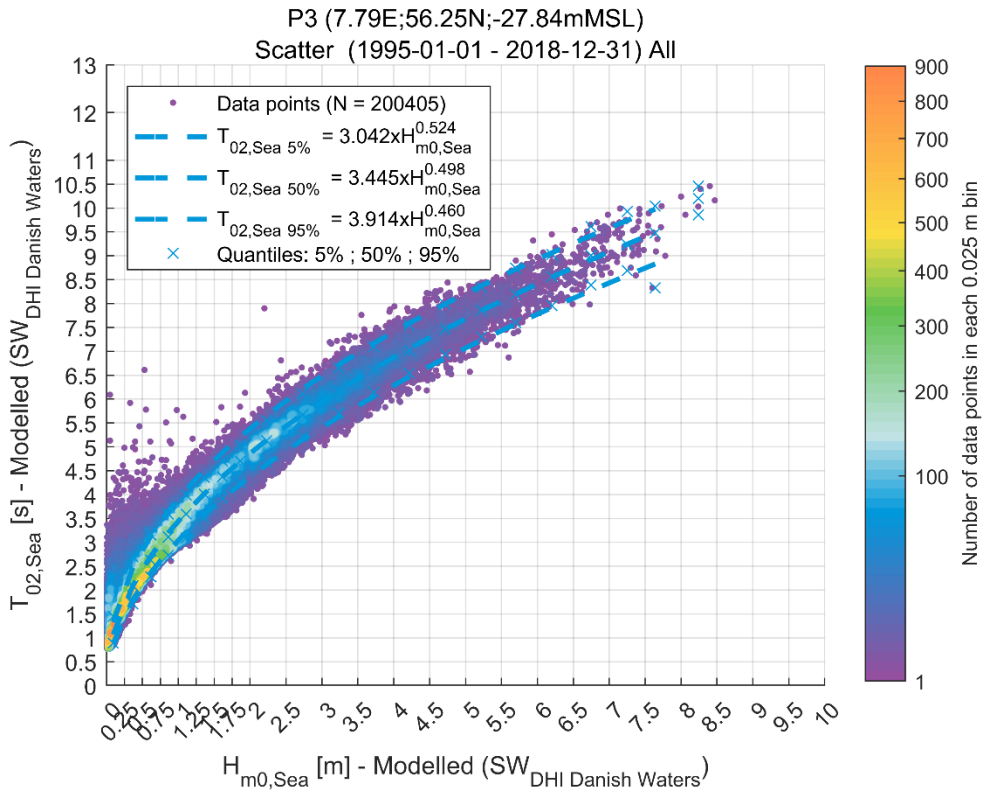

Figure B. 26

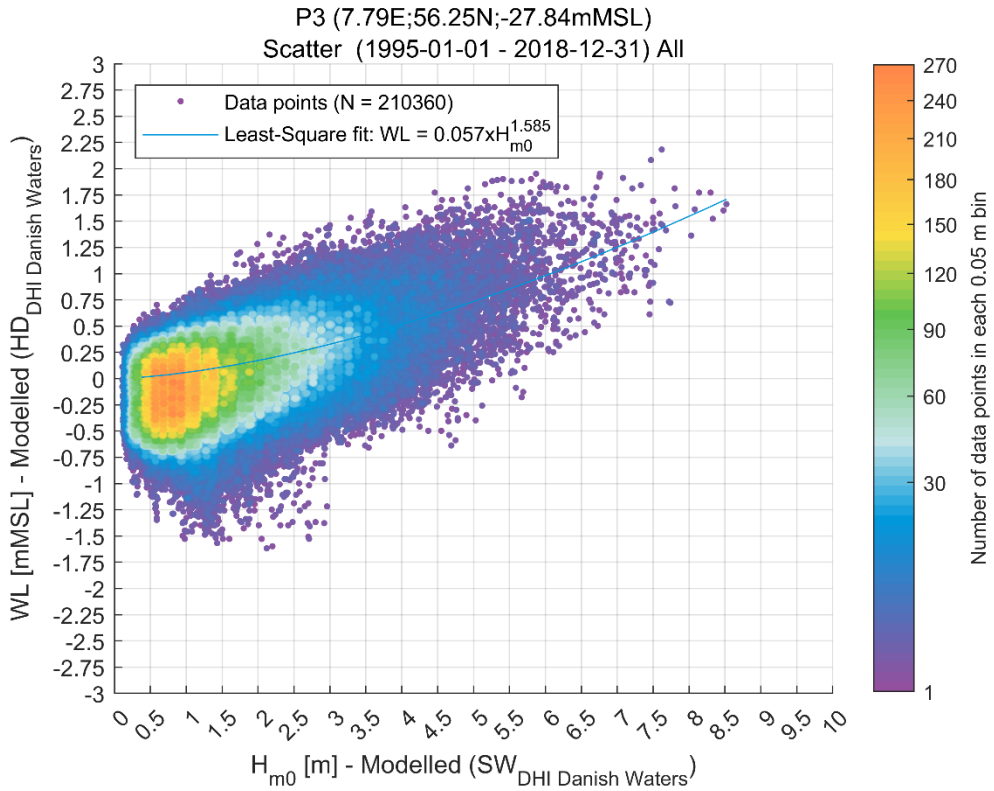

Figure B. 27

B.4 Extreme conditions at P3

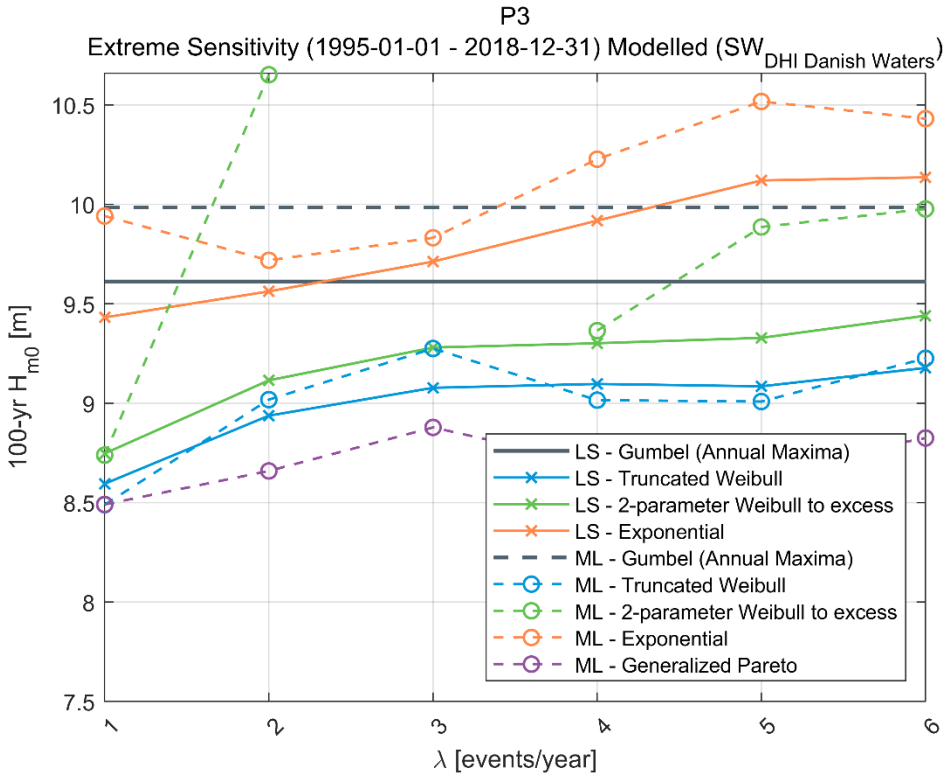

Figure B. 28

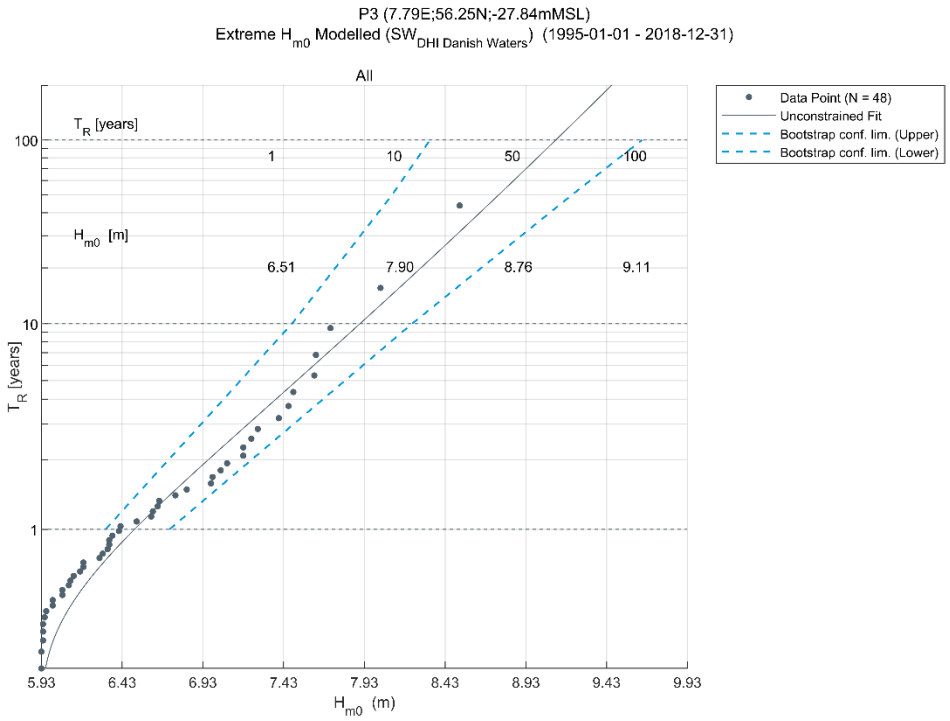

Figure B. 29

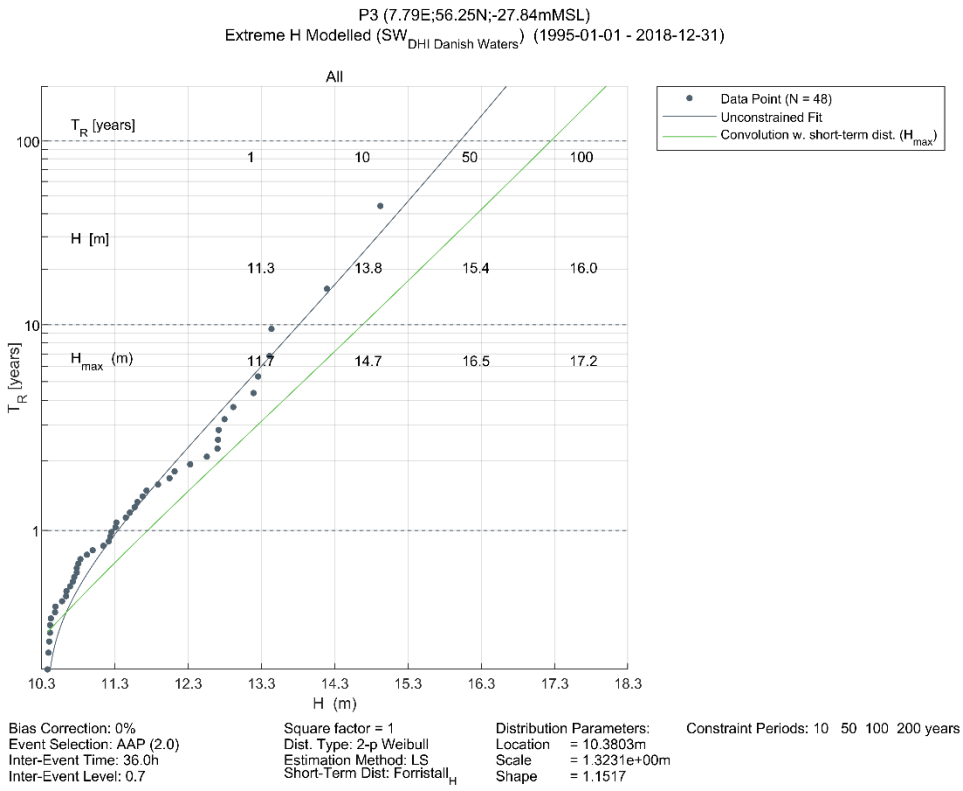

Figure B. 30

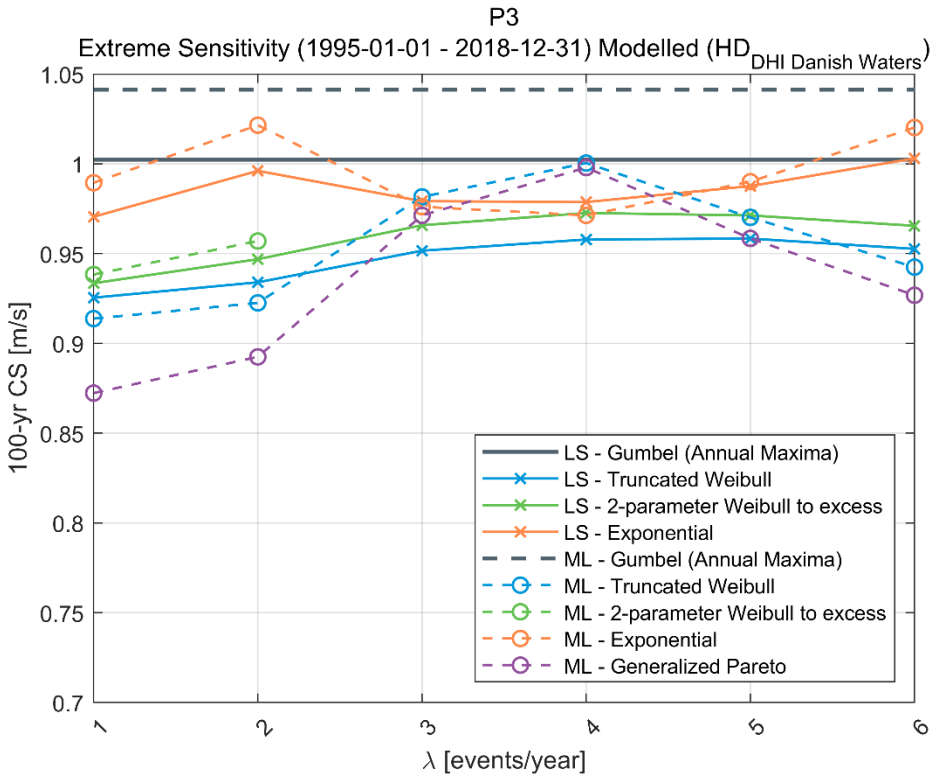

Figure B. 31

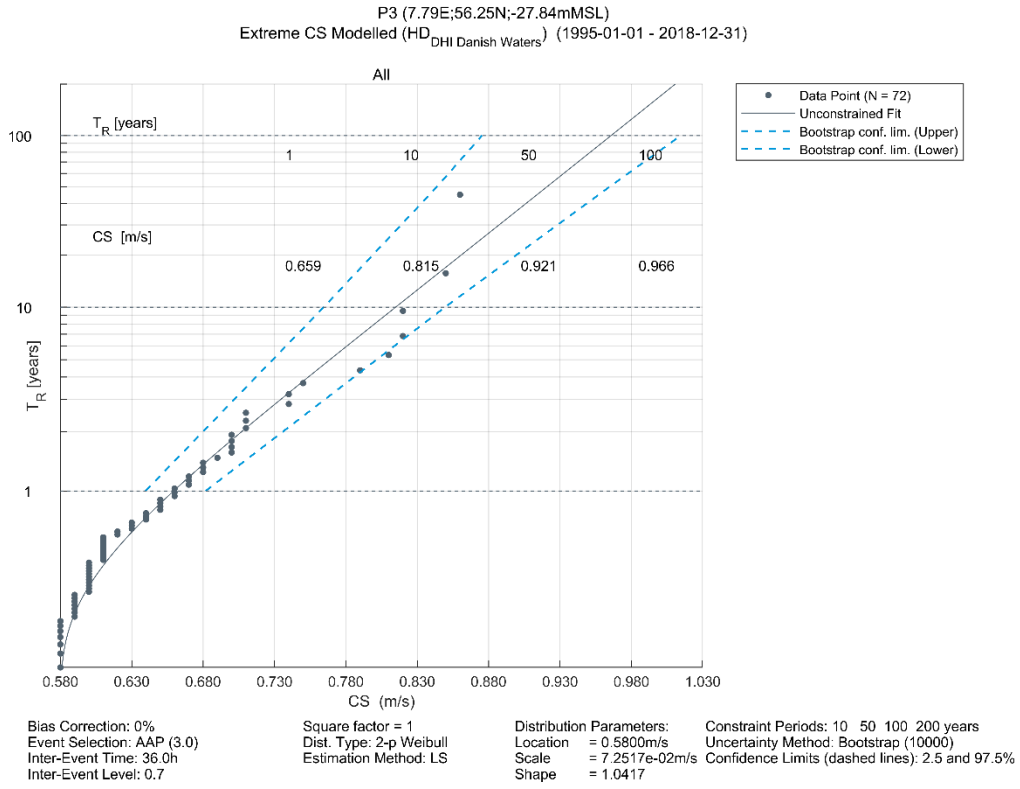

Figure B. 32

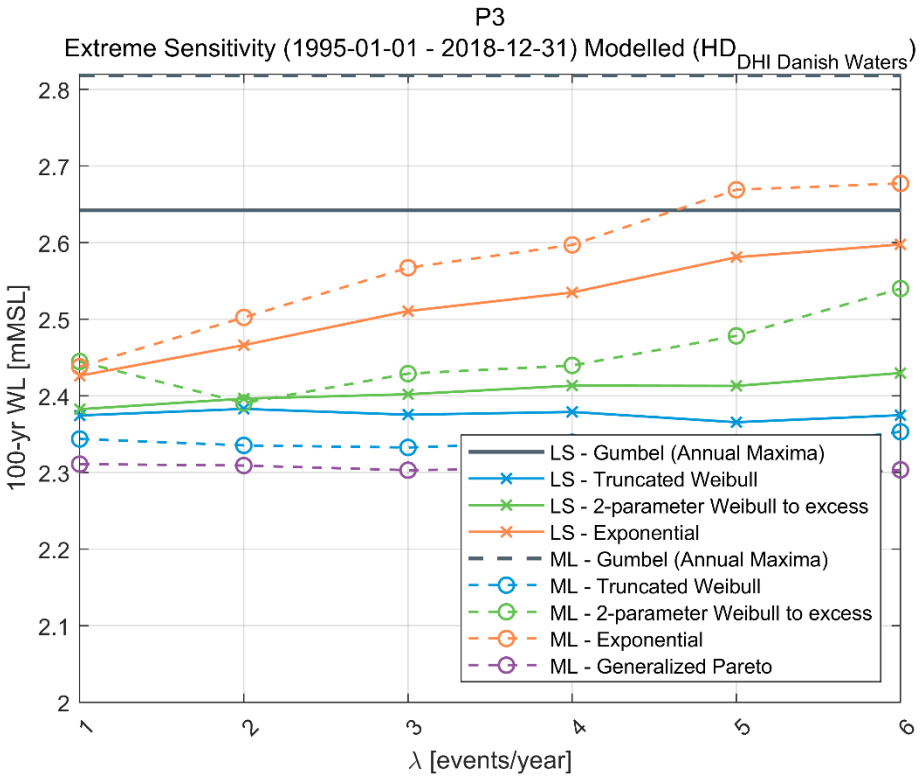

Figure B. 33

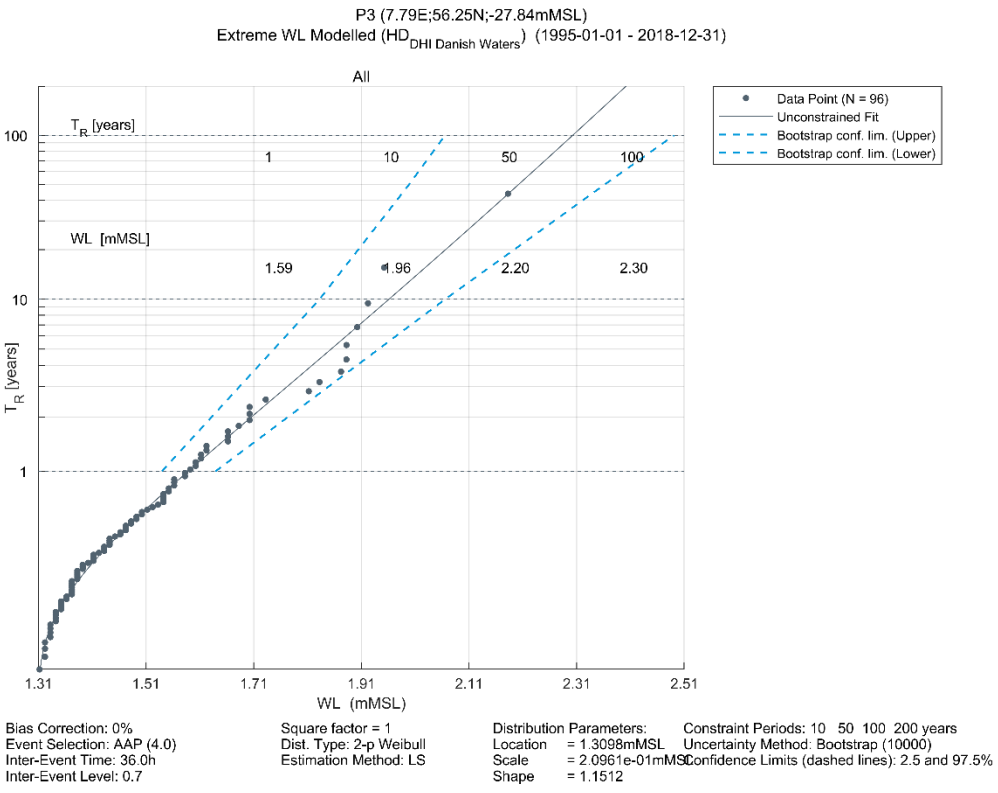

Figure B. 34

Appendix C – Extreme Analysis Methodologies

C Extreme Value Analysis Methodologies

C.1 General

Extreme values with associated long return periods are estimated by fitting a probability distribution to historical data. Several distributions, data selection and fitting techniques are available for estimation of extremes, and the estimated extremes are often rather sensitive to the choice of method. However, it is not possible to choose a preferred method only on its superior theoretical support or widespread acceptance within the industry. Hence, it is common practice to test a number of approaches and make the final decision based on goodness of fit.

The typical extreme value analyses involved the following steps:

1. Extraction of independent identically distributed events by requiring that events are separated by at least 36 hours, and that the value between events had dropped to below 70% of the minor of two consecutive events.
2. Fitting of extreme value distribution to the extracted events, both omni/all-year and directional/seasonal subsets. Distribution parameters are estimated either by maximum likelihood or least-square methods. The following analysis approaches are used (see Section C.2 for details):
    a) Fitting the Gumbel distribution to annual maxima.
    b) Fitting a distribution to all events above a certain threshold (the Peak-Over-Threshold method). The distribution type can be exponential, truncated Weibull or 2-parameter Weibull to excess.
3. Constraining of subseries to ensure consistency with the omni/all-year distribution; see Section C.6.2 for details.
4. Bootstrapping to estimate the uncertainty due to sampling error; see Section C.6 for details.

C.2 Long-term distributions

The following probability distributions are often used in connection with extreme value estimation:

- 2-parameter Weibull distribution
- Truncated Weibull distribution
- Exponential distribution
- Gumbel distribution

The 2-parameter Weibull distribution is given by: $P(X < x) = 1 - \exp\left(-\left(\frac{x}{\beta}\right)^{\alpha}\right)$ (C.1)

with distribution parameters α (shape) and β (scale). The 2-parameter Weibull distribution used in connection with Peak-Over-Threshold (POT) analysis is fitted to the excess of data above the threshold, ie the threshold value is subtracted from data prior to fitting.

The 2-parameter *truncated* Weibull distribution is given by:

$$P(X < x) = 1 - \frac{1}{P_0}\exp\left(-\left(\frac{x}{\beta}\right)^{\alpha}\right) \quad \text{(C.2)}$$

with distribution parameters α (shape) and β (scale) and the exceedance probability, P_0, at the threshold level, γ, given by:

$$P_0 = \exp\left(-\left(\frac{\gamma}{\beta}\right)^{\alpha}\right) \quad \text{(C.3)}$$

The 2-parameter truncated Weibull distribution is used in connection with Peak-Over-Threshold analysis, and, as opposed to the non-truncated 2-p Weibull, it is fitted directly to data, ie the threshold value is **not** subtracted from data prior to fitting.

The exponential distribution is given by:

$$P(X < x) = 1 - \exp\left(-\left(\frac{x-\mu}{\beta}\right)\right), \quad x \geq \mu \quad \text{(C.4)}$$

with distribution parameters β (scale) and μ (location). Finally, the Gumbel distribution is given by:

$$P(X < x) = \exp\left(-\exp\left(\frac{\mu - x}{\beta}\right)\right) \quad \text{(C.5)}$$

with distribution parameters β (scale) and μ (location).

C.3 Individual wave and crest height

C.3.1 Short-term distributions

The short-term distributions of individual wave heights and crests conditional on H_{m0} are assumed to follow the distributions proposed by Forristall [16]. The Forristall wave height distribution is based on Gulf of Mexico measurements, but experience from the North Sea has shown that these distributions may have a more general applicability. The Forristall wave and crest height distributions are given by:

$$P\left(X > x \,|\, H_{m0}\right) = \exp\left(-\left(\frac{x}{\alpha H_{m0}}\right)^{\beta}\right) \quad \text{(C.6)}$$

where the distribution parameters, α and β, are as follows:

Forristall wave height: α = 0.681
β = 2.126

Forristall crest height (3D): $\alpha = 0.3536 + 0.2568 \cdot S_1 + 0.0800 \cdot Ur$

$\beta = 2 - 1.7912 \cdot S_1 - 0.5302 \cdot Ur + 0.2824 \cdot Ur^2$

$S_1 = \frac{2\pi}{g}\frac{H_{m0}}{T_{01}^2}$ and $U_r = \frac{H \cdot L^2}{d^3}$

For this type of distribution, the distribution of the extremes of a given number of events, N, (waves or crests) converges towards the Gumbel distribution conditional on the most probable value of the extreme event, H_{mp} (or C_{mp} for crests):

$$P\left(h_{\max} \mid H_{mp}\right) = \exp\left(-\exp\left(-\ln N\left(\left(\frac{h_{\max}}{H_{mp}}\right)^{\beta} - 1\right)\right)\right) \tag{C.7}$$

C.3.2 Individual waves (modes)

The extreme individual wave and crest heights are derived using the storm mode approach [14] . The storm modes, or most probable values of the maximum wave or crest in the storm (H_{mp} or C_{mp}), are obtained by integrating the short-term distribution of wave heights conditional on H_{m0} over the entire number of sea states making up the storm. In practice, this is done by following these steps:

1. Storms are identified by peak extraction from the time series of significant wave height. Individual storms are taken as portions of the time series with H_{m0} above 0.7 times the storm peak, H_{m0}.

2. The wave (or crest) height distribution is calculated for each sea state above the threshold in each individual storm. The short-term distribution of H (or C) conditional on H_{m0}, $P(h|H_{m0})$, is assumed to follow the empirical distributions by Forristall (see Section C.3). The wave height probability distribution is then given by the following product over the n sea states making up the storm:

$$P\left(H_{\max} < h\right) = \prod_{j=1}^{n_{seastates}} P\left(h \mid H_{m0,j}\right)^{N_{waves,j}} \tag{C.8}$$

with the number of waves in each sea state, N_{waves}, being estimated by deriving the mean zero-crossing period of the sea state. The most probable maximum wave height (or mode), H_{mp}, of the storm is given by:

$$P\left(H_{\max} < h\right) = \frac{1}{e} \tag{C.9}$$

This produces a database of historical storms each characterised by its most probable maximum individual wave height which is used for further extreme value analysis.

C.3.3 Convolution of short-term variability with long-term storm density

The long-term distribution of individual waves and crests is found by convolution of the long-term distribution of the modes (subscript $_{mp}$ for most probable value) with the distribution of the maximum conditional on the mode given by:

$$\begin{aligned} P\left(H_{\max}\right) &= \int_0^{\infty} P\left(h_{\max} \mid H_{mp}\right) \cdot p\left(H_{mp}\right) dH_{mp} \\ &= \int_0^{\infty} \exp\left(-\exp\left(-\ln N\left(\left(\frac{h}{H_{mp}}\right)^{\beta} - 1\right)\right)\right) \cdot p\left(H_{mp}\right) dH_{mp} \end{aligned} \tag{C.10}$$

The value of N, which goes into this equation, is determined by defining equivalent storm properties for each individual storm. The equivalent storms have constant H_{m0} and duration such that their probability density function of H_{max} or C_{max} matches that of the actual storm. The density functions of the maximum wave in the equivalent storms are given by:

$$p\left(H_{\max} \mid H_{m0,eq}, N_{eq}\right) = \frac{d}{dH}\left[1 - \exp\left(-\left(\frac{H_{\max}}{\alpha \cdot H_{m0,eq}}\right)^{\beta}\right)\right]^{N_{eq}} \tag{C.11}$$

The β parameter in eq. (C.10) comes from the short-term distribution of individual crests, eq. (C.6), and is a function of wave height and wave period. The β parameter (shape factor) was taken as the mean value of β estimated from the individual storms. The number of waves in a storm, N, was conservatively calculated from a linear fit to the modes minus one standard deviation.

C.4 Subset extremes

Estimates of subset (e.g. directional and monthly) extremes are required for a number of parameters. In order to establish these extremes, it is common practice to fit extreme value distributions to data sampled from the population (i.e. the model database) that fulfils the specific requirement e.g. to direction, i.e. the extremes from each direction are extracted and distributions fitted to each set of directional data in turn. By sampling an often relatively small number of values from the data set, each of these directional distributions is subject to uncertainty due to sampling error. This will often lead to the directional distributions being inconsistent with the omnidirectional distribution fitted to the maxima of the entire (omnidirectional) data set. Consistency between directional and omnidirectional distributions is ensured by requiring that the product of the n directional annual non-exceedance probabilities equals the omnidirectional, i.e.:

$$\prod_{i=1}^{n} F_i\left(x, \hat{\theta}_i\right)^{N_i} = F_{omni}\left(x, \hat{\theta}_{omni}\right)^{N_{omni}} \tag{C.12}$$

where N_i is the number of sea states or events for the i'th direction and $\hat{\theta}_i$, the estimated distribution parameter. This is ensured by estimating the distribution parameters for the individual distributions and then minimizing the deviation:

$$\delta = \sum_{x_j}\left[-\ln\left(-N_{omni}\ln F_{omni}\left(x, \hat{\theta}_{omni}\right)\right) + \ln\left(-\sum_{i=1}^{n} N_i \ln F_i\left(x_j, \hat{\theta}_i\right)\right)\right]^2 \tag{C.13}$$

Here x_j are extreme values of the parameter for which the optimization is carried out, ie the product of the directional non-exceedance probabilities is forced to match the omnidirectional for these values of the parameter in question.

The directional extremes presented in this report are given without scaling, that is, a T_{yr} event from direction i will be exceeded once every T years on the average. The same applies for monthly extremes. A T_{yr} monthly event corresponds to the event that is exceeded once (in that month) every T years, which is the same as saying that it is exceeded once every *T*/12 years (on average) of the climate for that particular month.

C.5 Optimized directional extremes

The directional extremes were derived from fits to each subseries data set meaning that a T_R year event from each direction will be exceeded once every T_R years on average. Having eg 8 directions this means that **one** of the directions will be exceeded once every $T_R/8$ years on average. A 100-year event would thus be exceeded once every 100/8 = 12.5 years (on average) from **one** of the directions.

For design application, it is often required that the summed (overall) return period (probability) is T_R years. A simple way of fulfilling this would be to take the return value corresponding to the return period T_R times the number of directions, ie in this case the 8x100 = 800-year event for each direction. However, this is often not optimal since it may lead to very high estimates for the strong sectors, while the weak sectors may still be insignificant.

Therefore, an optimized set of directional extreme values was produced for design purpose in addition to the individual values of directional extremes described above. The optimized values were derived by increasing (scaling) the individual T_R values of the directions to obtain a summed (overall) probability of T_R years, while ensuring that the extreme values of the strong sector(s) become as close to the overall extreme value as possible. In practice, this is done by increasing the T_R of the weak directions more than that of the strong sectors, but ensuring that the sum of the inverse directional T_R's equals the inverse of the targeted return period, i.e.:

$$\sum_{i=1}^{n} \frac{1}{T_{R,i}} = \frac{1}{T_{R,\text{omni}}} \tag{C.14}$$

where n is the number of directional sectors and $T_{R,omni}$ is the targeted overall return period.

C.6 Uncertainty assessment

C.6.1 Sources of uncertainty

The extreme values presented in this report are estimated quantities and therefore all associated with uncertainty. The uncertainty arises from a number of sources:

Measurement/model uncertainty: The contents of the database for the extreme value analysis are associated with uncertainty. This type of uncertainty is preferably mitigated at the source – eg by correction of biased model data and removal of obvious outliers in data series. The model uncertainty can be quantified if simultaneous good quality measurements are available for a reasonably long overlapping period.

True extreme value distribution is unknown: The distribution of extremes is theoretically unknown for levels above the levels contained in the extreme value database. There is no justification for the assumption that a parametric extreme value distribution fitted to observed/modelled data can be extrapolated beyond the observed levels. However, it is common practice to do so, and this obviously is a source of uncertainty in the derived extreme value estimates. This uncertainty, increasing with decreasing occurrence probability of the event in question, is not quantifiable, but the metocean expert may minimize it by using experience and knowledge when deciding on an appropriate extreme value analysis approach. Proper inclusion of other information than direct measurements and model results may also help to minimize this type of uncertainty.

Uncertainty due to sampling error: The number of observed/modelled extreme events is limited. This gives rise to sampling error which can be quantified by statistical methods

such as Monte Carlo simulations or bootstrap resampling. The results of such an analysis are termed the confidence limits. The confidence limits should **not** be mistaken for the total uncertainty in the extreme value estimate.

C.6.2 Confidence limits

The confidence limits of extreme estimates are established from a bootstrap analysis or a Monte Carlo simulation.

The bootstrap analysis estimates the uncertainty due to sampling error. The bootstrap consists of the following steps:

1. Construct a new set of extreme events by sampling randomly with replacement from the original data set of extremes

2. Carry out an extreme value analysis on the new set to estimate T-year events

An empirical distribution of the T-year event is obtained by looping steps 1 and 2 many times. The percentiles are read from the resulting distribution.

In the Monte Carlo simulation, the uncertainty is estimated by randomly generating a large number of samples that have the same statistical distribution as the observed sample.

The Monte Carlo simulation can be summarised in the following steps:

1. Randomly generating a sample consisting of N data points, using the estimated parameters of the original distribution. If the event selection is based on a fixed number of events, N is set equal to the size of original data set of extremes. If the event selection is based on a fixed threshold, the sample size N is assumed to be Poisson distributed.

2. From the generated sample, the parameters of the distribution are estimated and the T-year return estimates are established.

Steps 1 and 2 are looped a large number of times, whereby an empirical distribution of the
T-year event is obtained. The quartiles are read from the resulting distribution.

ften carried out prior to data extraction in order to reduce the influence of phases in the analysis (the fact that the water level may not peak at exactly the same time as the peak wave height for instance).